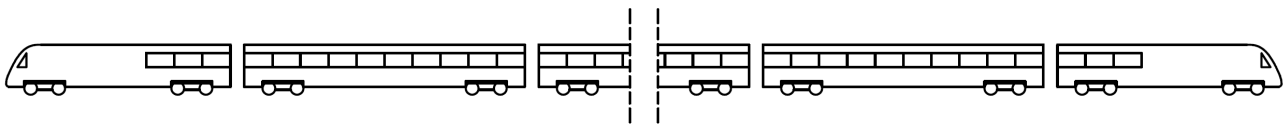




CHALMERS
UNIVERSITY OF TECHNOLOGY



Dynamic bridge-train interaction in high-speed railway design

An evaluation of comfort criteria regulations and analysis methods according to Eurocode

Master's Thesis in the Master's Programme Structural Engineering and Building Technology

MICHAEL ENGBERG
AXEL KRISTENSSON

Department of Civil and Environmental Engineering
Division of Structural Engineering
Concrete Structures
CHALMERS UNIVERSITY OF TECHNOLOGY
Gothenburg, Sweden 2017
Master's Thesis BOMX02-17-22

MASTER'S THESIS BOMX02-17-22

Dynamic bridge-train interaction in high-speed railway design

An evaluation of comfort criteria regulations and analysis methods according to Eurocode

Master's Thesis in the Master's Programme Structural Engineering and Building Technology

MICHAEL ENGBERG
AXEL KRISTENSSON

Department of Civil and Environmental Engineering
Division of Structural Engineering
Concrete Structures
CHALMERS UNIVERSITY OF TECHNOLOGY
Gothenburg, Sweden 2017

Dynamic bridge-train interaction in high-speed railway design
An evaluation of comfort criteria regulations and analysis methods according to Eurocode
MICHAEL ENGBERG
AXEL KRISTENSSON

© MICHAEL ENGBERG, AXEL KRISTENSSON, 2017

Master's Thesis BOMX02-17-22
ISSN 1652-8557
Department of Civil and Environmental Engineering
Division of Structural Engineering
Concrete Structures
Chalmers University of Technology
SE-412 96 Gothenburg
Sweden
Telephone: +46 (0)31-772 1000

Cover:
Visualization of an ICE 2 full-train set analyzed in this thesis.

Gothenburg, Sweden 2017

Dynamic bridge-train interaction in high-speed railway design

An evaluation of comfort criteria regulations and analysis methods according to Eurocode

Master's Thesis in the Master's Programme Structural Engineering and Building Technology

MICHAEL ENGBERG

AXEL KRISTENSSON

Department of Civil and Environmental Engineering

Division of Structural Engineering

Concrete Structures

Chalmers University of Technology

ABSTRACT

High speed railway is being introduced in Sweden through the East Link Project. Eurocode specifies how railway bridges should be designed and analyzed for these types of vehicles. When it comes to vehicle comfort due to vertical accelerations two methods are proposed. The first is a simplified approach based on the static load model LM71 and the second approach is a fully dynamic vehicle bridge interaction model. This thesis aims to compare these two methods using a finite element approach with modelling and analysis in MATLAB and ABAQUS.

Results indicate that that some bridge configurations designed using the simplified approach for the design speed of 350 km/h might yield unconservative results with regards to vertical vehicle accelerations for an ICE 2 train. Critical designs were obtained for simply supported bridges with two and three spans where the fundamental eigenfrequency was critical and continuous bridges with two spans where the second eigenfrequency was critical. The passenger trailers had consistently lower accelerations than the heavier and stiffer motorcars. The resonant peaks of the system was determined by the length of the trailer combined with the eigenmodes of the bridges. The highest response was reached where the design speed is close to a resonant speed of the system.

Finally, the conclusion may be drawn that the simplified vehicle comfort analysis seems to be on the unsafe side for the ICE 2 train evaluated. An updated method in order to determine improved static limits is proposed, however basing a dynamic vehicle comfort on a static model does not accurately represent the real behaviour. Ideally, a better indicator of the dynamic vehicle response should be investigated. For instance, HSLM models specified by Eurocode could be a viable option.

Keywords: Structural dynamics, High-speed railway, Bridge interaction design, Comfort criteria, Eurocode

Dynamiska bro-tåg interaktioner i dimensionering av höghastighetsjärnväg
En utvärdering av komfortkriterier och analysmetoder enligt Eurocode
Examensarbete inom masterprogrammet Structural Engineering and Building Technology

MICHAEL ENGBERG

AXEL KRISTENSSON

Institutionen för Bygg- och miljöteknik
Avdelningen för konstruktionsteknik
Betongbyggnad
Chalmers tekniska högskola

SAMMANFATTNING

Höghastighetståg kommer att introduceras i Sverige genom Ostlänken. Eurokod specificerar hur järnvägsbroar ska dimensioneras och analyseras på denna typ av fordon. När det kommer till fordonskomfort med avseende på vertikala accelerationer presenteras två metoder. Den första är en förenklad analys baserad på den statiska lastmodellen LM71 och den andra är en dynamisk interaktionsmodell med tåg och bro. Denna rapport ämnar till att jämföra dessa två metoder med hjälp av finita elementmodellering och analys i MATLAB och ABAQUS.

Resultat indikerar att vissa brokonfigurationer dimensionerade enligt den förenklade metoden för designhastigheten 350 km/h kan generera icke-konservativa resultat med avseende på vertikala fordonssaccelerationer i ett ICE 2 tåg. Kritiska fall hittades för fritt upplagda broar med två och tre span då den fundamentala egenfrekvensen var avgörande samt för kontinuerliga broar med två span då den sekundära egenfrekvensen var avgörande. Passagerarvagnarna hade konstant lägre accelerationer än de tyngre och styvare lokomotiven. Resonanta toppar i systemet avgjordes av längden på en passagerarvagn kombinerat med egenmoderna för bron. Den högsta responsen uppnåddes då designhastigheten var nära den resonanta hastigheten för systemet.

Till sist kan slutsatsen dras att den förenklade fordonskomfort-analysen verkar vara på den osäkra sidan för den undersökta ICE 2 tåget. En uppdaterad metod för att förbättra de statiska gränserna föreslås, dock verkar inte det vara helt realistiskt att basera dynamisk fordonskomfort på en statisk modell. Helst skulle en mer passande indikator av den dynamiska responsen undersökas. Förslagsvis skulle HSLM modeller enligt Eurokod vara ett lämpligt alternativ.

Nyckelord: Strukturdynamik, Höghastighetståg, Dimensionering med brointeraktioner, Komfortkriterier, Eurokod

CONTENTS

Abstract	i
Sammanfattning	ii
Contents	iii
Preface	xi
Acronyms	xiii
Glossary	xiii
Nomenclature	xiv
1 Introduction	1
1.1 Background	1
1.2 Aim and objective	1
1.3 Limitations	2
1.4 Specification of problem statement	3
1.5 Method	4
2 Theory	5
2.1 High speed railway	5
2.1.1 Operating speeds	5
2.1.2 Train parameters	5
2.1.3 Rail standards and parameters	8
2.2 Reinforced concrete slab bridge	9
2.2.1 Boundary conditions	9
2.3 Regulations according to Eurocode	11
2.3.1 Bridge regulations	11
2.3.2 Simplified vehicle comfort analysis	12
2.3.3 Dynamic vehicle comfort analysis	13
2.3.4 LM71 model	13
2.3.5 Bridge damping parameters	13
2.4 General dynamic theory	14
2.4.1 Equation of motion for a SDOF system	14
2.4.2 Equation of motion for a MDOF system	17
2.4.3 Harmonic excitation and resonance	18
2.4.4 Vibration of Euler-Bernoulli beams	19
2.4.5 Moving load on Euler-Bernoulli beam	23
2.4.6 Timoshenko beam theory	24

2.4.7	Critical velocity	25
2.4.8	Dynamic eigenvalue problems	26
2.4.9	Rayleigh damping	26
2.5	FE-analysis	28
2.5.1	Beam formulations	28
2.5.2	FE-software	30
2.6	Numerical integration methods	31
2.6.1	Newmark- β method	31
2.6.2	Central Difference Method	31
2.6.3	Digital signal processing	32
2.6.4	Nyquist sampling theorem	32
2.7	Interaction theory	33
2.7.1	Contact modelling	33
2.7.2	Rail imperfections	34
2.7.3	Wheel imperfections	34
3	Model development	36
3.1	Bridge model	36
3.1.1	Single layer bridge model	36
3.1.2	Two layer bridge model	40
3.2	Vehicle model	40
3.2.1	Single moving point load	42
3.2.2	Single moving wheel system	46
3.2.3	Single moving wheel-bogie system	50
4	Dynamic bridge analysis using final model	54
4.1	ABAQUS model	54
4.2	Convergence study	58
4.3	Bridge frequency analysis	61
4.4	Vehicle frequency analysis	64
4.5	Analysis scope	66
5	Results	67
5.1	Simply supported bridges	67
5.1.1	Single Span	68
5.1.2	Double Span	71
5.1.3	Triple Span	74
5.2	Continuous bridges	77
5.2.1	Double Span	77
5.2.2	Triple Span	80

6 Discussion	83
6.1 Evaluation of results	83
6.2 Thesis scope	83
6.3 Method choice	84
6.3.1 Preliminary study	86
6.3.2 Search method	86
6.3.3 Section design method	86
6.4 Input parameters	87
6.4.1 Train parameters	87
6.5 Modelling choices	87
6.5.1 Analysis method	87
6.5.2 Number of cars	87
6.5.3 Vehicle lateral instability	88
6.5.4 Computational limitations	88
7 Conclusions	89
8 Further studies	90
References	91
Appendix A Mode Shapes for Continuous Beams	93

List of Figures

2.1	Visualization of an ICE 2 full-train set.	5
2.2	Geometrical measurement of the ICE train according to Lei (2017).	6
2.3	A schematic view of the vehicle model with dynamic components and properties highlighted.	7
2.4	A schematic view of the bridge model with dynamic components and properties highlighted.	8
2.5	Deck cross-section being evaluated in this analysis displayed along with reinforced concrete sleepers and standard UIC 60 rail.	9
2.6	The deflection behaviour of a simply supported multi-span bridge.	10
2.7	The deflection behaviour of a continuous multi-span bridge.	10
2.8	Maximum deflection in the deck in order to meet the comfort regulations in the vehicle according to SS-EN 1990, Figure A2.3. Factors are span length L , deflection δ and speed v	12
2.9	LM71 train model from Eurocode.	13
2.10	Figure depicting a simple mass m on wheels connected to a fixed point by a spring of stiffness k and influenced by a force $p(t)$	14
2.11	Figure depicting a simple mass m on wheels connected to a fixed point by a spring of stiffness k a damper with coefficient c and influenced by a force $p(t)$	16
2.12	Figure depicting a simple mass m on wheels connected to a fixed point by a spring of stiffness k a damper with coefficient c and influenced by a force $p(t)$	17
2.13	Steady-state magnification factor for various forcing frequencies at different level of dampning.	19
2.14	Simply supported E-B beam loaded with an arbitrary load $p_y(x, t)$, with length L and with sectional constants E, I, A and ρ	20
2.15	First longitudinal bending mode of a simply supported beam.	21
2.16	Second longitudinal bending mode of a simply supported beam.	21
2.17	Third longitudinal bending mode of a simply supported beam.	21
2.18	Fourth longitudinal bending mode of a simply supported beam.	21
2.19	First longitudinal bending mode of a continuous beam with two spans.	22
2.20	Second longitudinal bending mode of a continuous beam with two spans.	22
2.21	Third longitudinal bending mode of a continuous beam with two spans.	22
2.22	Fourth longitudinal bending mode of a continuous beam with two spans.	22
2.23	First longitudinal bending mode of a continuous beam with three spans.	22
2.24	Second longitudinal bending mode of a continuous beam with three spans.	22
2.25	Third longitudinal bending mode of a continuous beam with three spans.	23
2.26	Fourth longitudinal bending mode of a continuous beam with three spans.	23
2.27	Single moving point load applied on a homogeneous E-B beam.	23
2.28	A sequence of point loads moving across a bridge.	25
2.29	6-DOF plane-frame Euler Bernoulli beam.	28
2.30	Low-pass Butterworth filter with a cut-off frequency of 39.473 Hz.	32
3.1	Single simply supported Euler Bernoulli beam	37
3.2	MATLAB algorithm for design of section height according to SS-EN 1990 A2.4.4.3.2.	38

3.3	Two layer bridge model. This model is much more refined than the simple one-layer bridge model. It incorporates sleepers as discrete inertia points connected with a vertical spring-dashpot system to the bridge and rail beam elements. The subsoil is assumed to be completely fixed and the bridge is modelled with immovable supports.	40
3.4	Single vehicle models ranging from a single point load to a single wheel and finally a single bogie.	40
3.5	MATLAB algorithm for vehicle model evaluation.	41
3.6	ABAQUS/Explicit algorithm for vehicle-bridge model evaluation.	43
3.7	Single moving point load applied on a homogeneous E-B beam.	44
3.8	Deflection in the middle of a E-B beam subjected to a moving load equal to the weight of a wheel-bogie-system.	44
3.9	Acceleration in the middle of a E-B beam subjected to a moving load equal to the weight of a wheel-bogie-system.	44
3.10	Midpoint deflection envelope for a moving load at various speeds.	45
3.11	Midpoint acceleration envelope for a moving load at various speeds.	45
3.12	Single moving wheel applied on a homogeneous E-B beam.	46
3.13	Deck deflection envelope for various speeds for Hertzian and linearized contact models of the single wheel system.	47
3.14	Deck acceleration envelope for various speeds for Hertzian and linearized contact models of the single wheel system.	47
3.15	Deck deflection for various beam formulations for a single moving wheel with linearized contact and no imperfections.	48
3.16	Deck acceleration for various beam formulations for a single moving wheel with linearized contact and no imperfections.	48
3.17	Wheel deflection envelopes for various imperfection models.	48
3.18	Wheel acceleration envelopes for various imperfection models.	49
3.19	Single moving wheel-bogie system applied on a homogeneous E-B beam.	50
3.20	Wheel deflection in bogie-vehicle envelopes for various imperfection models.	50
3.21	Wheel acceleration in bogie-vehicle envelopes for various imperfection models.	51
3.22	Bogie deflection envelopes for various imperfection models.	51
3.23	Bogie acceleration envelopes for various imperfection models.	51
3.24	Deck deflection for final wheel model compared to point load model.	52
3.25	Deck acceleration for final wheel model compared to point load model.	52
3.26	Deflection envelopes for various bridge models.	53
3.27	Acceleration envelopes for various bridge models.	53
4.1	A schematic view of the final assembled model with dynamic components and properties highlighted.	54
4.2	A schematic view of the final assembled model with degrees of freedom visualized.	55
4.3	Small region of bridge deck with boundary conditions applied.	55
4.4	Small region of bridge deck with interactions and inertias.	56
4.5	Boundary conditions and loads acting on the vehicle.	56
4.6	Detail of interaction system of a single motorcar bogie.	57
4.7	Spring-dashpot and contact interactions in a vehicle.	57
4.8	Convergence of trailer accelerations with regard to number of vehicles used in the analysis.	58

4.9	Convergence of bridge deflection with regard to number of vehicles used in the analysis.	58
4.10	Convergence of trailer accelerations with regard to number of vehicles used in the analysis.	59
4.11	Convergence of bridge deck deflection with regard to number of vehicles used in the analysis.	59
4.12	Convergence of trailer accelerations with regard to number of spans used in the analysis.	59
4.13	Convergence of bridge deck deflection with regard to number of spans used in the analysis.	59
4.14	Convergence of motorcar accelerations with regards to sample rate.	60
4.15	Convergence of trailer accelerations with regards to sample rate.	60
4.16	Convergence of deck accelerations with regards to sample rate.	60
4.17	Convergence of deck deflections with regards to sample rate.	60
4.18	Eigenfrequencies from ABAQUS and Analytic solutions for various span lengths for a simply supported bridge of one span.	62
4.19	Eigenfrequencies from ABAQUS and Analytic solutions for various span lengths for a continuous double span bridge.	63
4.20	Eigenfrequencies from ABAQUS and Analytic solutions for various span lengths for a continuous triple span bridge.	64
4.21	Undeformed trailer in frequency analysis.	64
4.22	Undeformed motorcar in frequency analysis.	64
5.1	Vertical trailer acceleration envelopes for simply supported single span bridges designed for speeds up to 350 km/h.	68
5.2	Vertical motorcar acceleration envelopes for simply supported single span bridges designed for speeds up to 350 km/h.	68
5.3	Contour plot of trailer acceleration envelopes for simple supported single span bridges.	69
5.4	Contour plot of motorcar acceleration envelopes for simple supported single span bridges. Resonant velocities for each span length is indicated with dashed line.	69
5.5	Maximum vertical vehicle acceleration from each envelope for simply supported single span bridges. Each envelope is represented by a single point in the figure.	70
5.6	The speed at which the maximum trailer acceleration is reached is plotted versus the analytic resonant speed and the maximum speed in the analysis.	70
5.7	Trailer acceleration envelopes for various simply supported double span bridges. Each line represents a single unique bridge.	71
5.8	Motorcar acceleration envelopes for various simply supported double span bridges.	71
5.9	Trailer acceleration contour plots for various simply supported double span bridges. Fundamental resonant speeds are indicated with dashed line.	72
5.10	Motorcar acceleration contour plots for various simply supported double span bridges.	72
5.11	The maximum values of each envelope for various simply supported double span bridges are plotted against the acceleration limit of 1 m/s ² . Cases exceeding this comfort limit are indicated with a red box.	73
5.12	The speed at which maximum response is obtained are visualized for simply supported double span bridges. Resonant speeds for various spans are indicated and correlation is prominent.	73
5.13	Trailer acceleration envelopes for various simply supported triple span bridges. Each line represents a single unique bridge.	74
5.14	Motorcar acceleration envelopes for various simply supported triple span bridges.	74

5.15	Trailer acceleration contour plots for various simply supported triple span bridges. Fundamental resonant speeds are indicated with dashed line.	75
5.16	Motorcar acceleration contour plots for various simply supported triple span bridges.	75
5.17	The maximum values of each envelope for various simply supported triple span bridges are plotted against the acceleration limit of 1 m/s ² . Cases exceeding this comfort limit are indicated with a red box.	76
5.18	The speed at which maximum response is obtained are visualized for simply supported triple span bridges. Resonant speeds for various spans are indicated and correlation is prominent.	76
5.19	Trailer acceleration envelopes for various continuous double span bridges. Each line represents a single unique bridge.	77
5.20	Motorcar acceleration envelopes for various continuous double span bridges.	77
5.21	Trailer acceleration contour plots for various continuous double span bridges. Fundamental and second resonant speeds are indicated with dashed line.	78
5.22	Motorcar acceleration contour plots for various continuous double span bridges.	78
5.23	The maximum values of each envelope for various continuous double span bridges are plotted against the acceleration limit of 1 m/s ² . Cases exceeding this comfort limit are indicated with a red box.	79
5.24	The speed at which maximum response is obtained are visualized for continuous double span bridges. Resonant speeds corresponding to the fundamental and second eigenmode for various spans are indicated and correlation is prominent.	79
5.25	Trailer acceleration envelopes for various continuous triple span bridges. Each line represents a single unique bridge.	80
5.26	Motorcar acceleration envelopes for various continuous triple span bridges.	80
5.27	Trailer acceleration contour plots for various continuous triple span bridges. Fundamental, second and third resonant speeds are indicated with dashed line.	81
5.28	Motorcar acceleration contour plots for various continuous triple span bridges.	81
5.29	The maximum values of each envelope for various continuous triple span bridges are plotted against the acceleration limit of 1 m/s ² . Cases exceeding this comfort limit are indicated with a red box.	82
5.30	The speed at which maximum response is obtained are visualized for continuous double span bridges. Resonant speeds corresponding to the fundamental, second and third eigenmode for various spans are indicated and correlation is prominent.	82
6.1	Alternative ABAQUS/Explicit algorithm for optimization of simplified comfort analysis.	85

List of Tables

2.1	Geometrical vehicle parameters used for the ICE motor car and trailers respectively as provided by Lei (2017).	6
2.2	Dynamic vehicle parameters used for the ICE motorcar and trailer as provided by Lei (2017).	7
2.3	Rail, sleeper and pad parameters.	8

2.4	Frequency parameter, β_n , for the first five modes for continuous beams derived by Talukdar (2016).	22
3.1	Bridge geometric properties for single layer model	37
3.2	Bridge material properties for single layer model	37
3.3	Eigenfrequencies and accumulative modal mass in y-direction for each eigenmode below 200 Hz. Total effective modal mass is displayed as part of total mass.	39
4.1	Eigenfrequency comparison between analytic solution and two-layer FE-model for a simply supported single 19.53 m span bridge.	61
4.2	Eigenfrequency comparison between analytic solution and two-layer FE-model for a continuous double 19.53 m span bridge.	62
4.3	Eigenfrequency comparison between analytic solution and two-layer FE-model for a continuous triple 19.53 m span bridge.	63
4.4	Eigenfrequencies and corresponding mode shapes for trailer vehicle.	65
4.5	Eigenfrequencies and corresponding mode shapes for motorcar vehicle.	65
4.6	Example of sectional heights for the simply supported single span bridges designed for the maximum speed of 350 km/h.	66
A.1	Frequency parameter β_{nr} for different span and mode numbers.	93

PREFACE

This master thesis in structural engineering was produced during the spring of 2017 at COWI AB in cooperation with Chalmers University of Technology. We would like to thank our examiner Joosef Leppänen, supervisor Peter Möller at Chalmers and supervisors Magnus Bäckström, Niclas Karlsson and Marcus Hjelm at COWI for guidance and support throughout the project. Furthermore we would like to thank our opponents Josefin Panarelli and Angelica Henriksson for great feedback, discussion and inspiration.

Enjoy your reading.

Michael Engberg & Axel Kristensson

Gothenburg, June 2017

Acronyms

- API** Application Programming Interface. 30
- CDM** Central Difference Method. 40
- DOF** Degree of Freedom. 17, 50
- DSP** Digital Signal Processing. 32
- E-B** Euler–Bernoulli. 19
- FEA** Finite Element Analysis. 12, 30
- FEM** Finite Element Method. 28
- HSLM** High Speed Load Model. 30, 90
- ICE** Intercity-Express. 2, 4–6, 90
- LM71** Load Model 71. 1, 11, 13, 90
- MDOF** Multiple Degrees of Freedom. 17, 18, 26, 31
- SDOF** Single Degree of Freedom. 14
- SLS** Serviceability Limit State. 11, 35
- TGV** Train à Grande Vitesse. 90
- ULS** Ultimate Limit State. 11, 35, 86

Glossary

- dashpot** A damper. 2, 50, 55
- East Link project** The introduction of high speed railway in Sweden. 1, 2, 5, 6, 90
- effective modal mass** The mass of the dynamic system that is activated by a certain mode in a certain direction. 37, 39
- eigenmode** The shape of the structure for a given eigenfrequency. 2

Eurocode The European building standard for structural design. 1

Hertzian contact Nonlinear contact definition based on theory by Hertz (1881). 3

Hunting oscillation Oscillation that occur in the bogie at certain speeds due to the cone-shape of the wheels. 2, 88

interaction The interplay of dynamic systems with rigid-bodies, springs and dampers. 1

Rayleigh damping Damping proportional to mass and stiffness.. 23

wheelflats Imperfection due to wheel lock during braking that cause wheel defects. 34

Nomenclature

Greek letters

α	Rayleigh damping coefficient [-]
β	Newmark- β constant [-]
β	Rayleigh damping coefficient [-]
β_n	Frequency parameter [-]
δ	Deflection [m]
$\delta(x - vt)$	Dirac delta function
γ	Newmark- β constant [-]
Γ_{ai}	Modal participation factor
γ_{df}	Maximum vertical bridge acceleration for unballasted track [m/s ²]
κ	Shear correction factor [-]
ν	Poisson's ratio [-]
Ω	Excitation frequency [rad/s]
ω_d	Damped natural frequency [rad/s]
ω_i	Circular eigenfrequency for mode i [rad/s]
ω_n	Undamped natural frequency [rad/s]
ω_{max}	Maximum eigenfrequency [Hz]
Φ	Dynamic factor dependant on determinant length and maintenance level [-]
Φ_2	Dynamic factor for a well maintained track [-]
ϕ_i	Eigenvector for mode i
ρ	Density [kg/m ³]
φ''	Dynamic enhancement due to imperfections [-]
φ'_{dyn}	Dynamic enhancement factor [-]

ζ Damping factor, expressed as a ratio of critical damping [-]

Roman lower case letters

\ddot{u}	Acceleration of an object [m]
$\ddot{\mathbf{u}}$	DOF accelerations vector [m/s ²]
$\dot{\mathbf{u}}$	DOF velocities vector [m/s]
$\mathbf{p}(t)$	External force vector [N]
\mathbf{u}	DOF displacements vector [m]
a_x	Acceleration of an object in x-direction [m/s ²]
b_v	Maximum vertical train acceleration for comfort analysis [m/s ²]
c	Coefficient of viscous damping [Ns/m]
c_e	External damping coefficient [Ns/m]
c_i	Internal damping coefficient [Ns/m]
c_{cr}	Critical viscous damping [Ns/m]
c_{pad}	Vertical damping of pads [Ns/m]
c_{pri}	Vertical damping of primary suspension [Ns/m]
c_{sec}	Vertical damping of secondary suspension [Ns/m]
c_{slp}	Vertical damping of sleepers [Ns/m]
cc_{slp}	Sleeper spacing [m]
f_c	Highest signal frequency [Hz]
f_n	Eigenfrequency of mode n [Hz]
f_s	Sampling frequency [Hz]

f_s	Spring force [N]
f_d	Driving frequency [Hz]
h	Height deck [m]
h	Time step [s]
h_1	Distance between bogie center and wheelset center [m]
h_2	Distance between bogie center and secondary suspension point [m]
h_3	Distance between vehicle center and secondary suspension point [m]
h_{crit}	Critical time step [s]
k	Spring stiffness [N/m]
k_H	Nonlinear Hertzian spring parameter
k_{lin}	Linearized contact stiffness [N/m]
k_{pad}	Vertical stiffness of pads [N/m]
k_{pri}	Vertical stiffness of primary suspension [N/m]
k_{sec}	Vertical stiffness of secondary suspension [N/m]
k_{slp}	Vertical stiffness of sleepers [N/m]
l_{car}	Total vehicle length [m]
m	Mass of an object [kg]
m_r	Rail mass [kg/m]
m_w	Wheelset mass [kg]
m_{ai}^{eff}	Effective modal mass [kg]
m_α	Generalized mass [kg]
m_{bog}	Bogie mass [kg]
m_{car}	Car body mass [kg]
m_{slp}	Sleeper mass [kg]
p	Point load [N]
$p(t)$	Time-dependant excitation force [N]
$p_y(x, t)$	Transverse load acting on a beam [N/m]
r	Ratio between frequency of excitation and free vibration [-]
$r(x)$	Rail imperfection profile
r_w	Wheel radius [m]
t	Time [s]
u	Displacement of an object [m]
u_0	Initial displacement [m]

v	Velocity [m/s ²]
w	Width deck [m]
x	Coordinate in x-direction [m]
x_1	Position of first axis [m]
x_2	Position of second axis [m]
x_3	Position of third axis [m]
x_4	Position of fourth axis [m]

Miscellaneous

\bullet'	First-order space derivative
\bullet''	Second-order space derivative
\bullet^T	Transpose
$\ddot{\bullet}$	Second-order time derivative
$\dot{\bullet}$	First-order time derivative
$\frac{\partial^n}{\partial t^n}(\bullet)$	n th -order time derivative
$\frac{\partial^n}{\partial x^n}(\bullet)$	n th -order space derivative

Roman capital letters

C	Viscous damping matrix
K	Stiffness matrix
K_{le}	Local element stiffness matrix
M	Mass matrix
M_{le}	Local element mass matrix
T	Element transformation matrix
T_i	Influence magnitude matrix in direction i
A	Cross-sectional area [m ²]
D_s(r)	Dynamic magnification factor [-]
E	Young's Modulus [Pa]
EI_r	Rail bending stiffness [Nm ²]
F_x	Force acting in x-direction [N]
G	Shear Modulus [Pa]
I	Second moment of inertia [m ⁴]
J_{bog}	Bogie pitch inertia moment [kgm ²]
J_{car}	Car body pitch inertia moment [kgm ²]
L	Span length [m]
L_r	Maximum roughness level spectrum
L_φ	Determinant length [-]
U(r)	Dynamic displacement at frequency ratio r [m]
U₀	Static displacement [m]

1 Introduction

This master's thesis was written in order to expand the knowledge of dynamic bridge-train systems for high-speed railway design, especially with regards to comfort in the train carriages and the evaluation of these effects.

1.1 Background

In Sweden, there is an interest to develop and establish a high-speed railway network in south and central parts of the country connecting the major cities. The first step in this initiative, Ostlänken (East Link project), connecting Järna south of Stockholm to Linköping is currently in the investigative phase. The proposed system would have an operating speed of 320 km/h. It is estimated that this 150 km stretch will require the construction of roughly 130 new railway bridges.

As of today there is limited knowledge in Sweden regarding the reliability of simplified methods presented in Eurocode used to estimate dynamic interaction effects on bridge structures subjected to high-speed train loading. Therefore, this is an area of interest for further investigation in order to build more efficient bridge structures in the future. COWI is interested in investigating the dynamic interaction between bridge construction, rails and train cars for high-speed railway bridges. This study was a continuation of the master's thesis of Hjelm and Karlsson (2016), also produced at COWI.

CEN (2010a) states that in order to achieve *Very high* level of comfort in the train the vertical vehicle acceleration must not exceed $b_v = 1.0 \text{ m/s}^2$. This analysis could either be performed using a simplified approach based on the static load model LM71 multiplied by a dynamic factor, Φ . That load case however does not completely resemble the characteristics of a high speed train, therefore Eurocode proposes an alternative method based on a dynamic bridge-train interaction model. It would be preferable to know how the results of these methods differ and whether or not it is safe to always use the simplified approach.

1.2 Aim and objective

This master's thesis aims to investigate the vertical acceleration in a high-speed railway train by studying a dynamic interaction system of a bridge deck, railway and vehicle. Firstly, a preliminary study was performed where the impact of modelling parameters was evaluated in order to be able to construct a realistic model. The final model was then evaluated for a range of scenarios with varying span amounts, span lengths, boundary conditions and vehicle speeds. The results obtained were compared to simplified vehicle comfort models and regulations presented in Eurocode in order to determine the accuracy of said models and whether this simplified approach is applicable for all examined bridge configurations.

1.3 Limitations

Interaction was modelled using a vehicle model based on a bogie-carbody system built using springs and dashpots. The specific train set used in this analysis was the German Intercity-Express (ICE). The bridge-rail system includes rail, sleepers, pads and bridge deck. The track was assumed to be ballast-free, as this is the configuration deemed most likely to be used for the proposed East Link project. The model was evaluated for speeds ranging from 120 km/h to 350 km/h as this is the range covered in Eurocodes simplified vehicle comfort analysis. The vehicle accelerations are evaluated in the center-point of each carbody.

Furthermore, the bridge type was restricted to solely reinforced concrete slab bridges. Bridges were not designed from scratch, but rather models were adapted from real-life examples with some modifications in section heights. Bridge cross-sections were approximated as homogeneous rectangular cross-sections of fixed section width and sufficient section height to achieve a desired sectional stiffness. The span lengths of the bridges investigated in the analysis were in the range of 10-50 m, as this interval was deemed to include a the most common examples of real-life railway bridges.

Contact between wheel and rail was defined as frictionless in its tangential behaviour. Furthermore no loss of contact was investigated, thus uncoupled deflections are not allowed for these interfaces. There was, however, a desire to investigate the effects of track irregularities. Consequently, this phenomenon was investigated during the preliminary study. The study did not intend to take geotechnical aspects into consideration and abutments were assumed to be fixed, that is soil elasticity was not taken into account. Furthermore, no settlement of the rail was assumed to take place.

Modelling took place in 2D-space and did therefore not include any lateral movement of the vehicle due to effects such as Hunting oscillation in the bogies. Plate eigenmodes were neglected as they are not prominent for concrete slab structures as opposed to for other bridge types. The vehicle was assumed to move with constant velocity along the center-line of the bridge and no acceleration or deceleration was assumed to occur in the longitudinal direction of the bridge. The analysis put focus on the superstructure and did therefore not include substructure elements such as columns or foundations.

Alternative rail transportation modes such as magnetic levitation trains have not been included in this thesis. Although the method proposed could be applied to analyze the response of these types of vehicles as well.

1.4 Specification of problem statement

A key aspect in the design of the dynamic vehicle-bridge model is determining how its degree of complexity affects the dynamic response. The following parameters were deemed especially interesting and were thus chosen for evaluation in the preliminary analysis:

1. Vehicle complexity
 - (a) Single point load
 - (b) Single wheel vehicle
 - (c) Single wheel-bogie vehicle
2. Bridge complexity
 - (a) Simple single layer bridge model
 - (b) Two layer bridge model including sleepers, pads and rail
3. Contact complexity
 - (a) Nonlinear Hertzian contact definition
 - (b) Linearized contact definition
4. Imperfection complexity
 - (a) No imperfections
 - (b) Corrugation imperfections

How is the vertical acceleration in train locomotive and trailer respectively affected by the following parameters for an complex vehicle model and how does the results from a dynamic vehicle-bridge model compare to the simplified vehicle comfort criteria specified in Eurocode?

1. Analysis parameters
 - (a) Train speed
 - (b) Span lengths
 - (c) Number of spans
 - (d) Number of vehicles
2. Eurocode regulations
 - (a) Are the simplified model on the safe side for all speed and span configurations?
 - (b) Is there a possibility to improve the simplified approach stated in Eurocode to be more accurate?

1.5 Method

Initially, a preliminary study was performed aimed at investigating available literature connected the subject of dynamic interaction for gathering of valuable knowledge. Of special interest was the knowledge as to how damped dynamic systems may be modelled in a realistic manner. Furthermore, sufficient material and component data was gathered in order to correctly represent structural components within the dynamic bridge-vehicle interaction model.

The initial model was created using MATLAB (2016a) in order to have full control of the dynamic behaviour and the parameters affecting the results. This model incorporated a single layer bridge model with a vehicle consisting of a single wheel or a single wheel-bogie. Multiple parameters were evaluated such as contact definition, rail imperfections, beam formulation and change of vehicle complexity. These results formed the basis for the final model which will be used in the dynamic comfort evaluation.

The evaluation process of the simplified method for comfort analysis was performed using ABAQUS/Explicit by DASSAULT SYSTEMS (2017). Models were generated according to Eurocode regulations and evaluated for an ICE traversing at a specified speed. In order to optimize this work flow, a python scripting approach was chosen which allowed for many analyses to be run by a single script. Results were captured and finally evaluated in MATLAB (2016a).

2 Theory

This chapter will introduce essential concepts for performing and understanding the method and results presented in this thesis. Most of the sources are obtained from Chalmers Library. Vectors are indicated using lowercase bold symbols (\mathbf{v}) while matrices are uppercase bold symbols (\mathbf{M}).

2.1 High speed railway

High speed railway is the next generation of railway transportation with trains reaching speeds much higher than previously. This increase does however result in dynamic effects such as resonance that could prove to be critical for the design of railway bridges. In order to obtain an efficient design it is therefore essential that the dynamic properties is analyzed. This section will cover some of the main dynamic parameters for a high speed railway vehicle and parameters regarding the rail-sleeper system.

2.1.1 Operating speeds

Currently in Sweden, the maximum train speed is about 200 km/h for the X2000-trains according to Nielsen, Ekberg, and Lundén (2005). Eurail (2017) specifies that the German Intercity-Express (ICE) High-speed trains are able to reach speeds up towards 300 km/h. At the time of writing this thesis it has not been specified what train will be used in the East Link project. Therefore as an upper bound, the speed of 350 km/h was chosen.

2.1.2 Train parameters

This section contains ICE train parameters obtained from Lei (2017). This set of parameters are sufficient to create a 2D dynamic train model, however the original data included parameters for a fully 3D model. Table 2.1 states geometrical data related to Figure 2.2. Table 2.2 presents dynamic properties such as suspension stiffness, damping and rotary inertia of the multiple vehicle bodies. The model in Figure 2.3 schematically shows the physical representation of each property. A limitation of this data is that the exact train model is not disclosed, however by comparing geometrical data it is most likely an ICE 2 train. According to manufacturer Siemens (2017) there are two possible car configurations possible for this train type. Firstly, the train could be run as a half-train with one motorcar and seven passenger trailers. Secondly, it could be run as a full-train consisting of two motorcars and 14 passenger trailers, as seen in Figure 2.1. The second configuration would be the most critical with regards to resonant effects in a bridge analysis.

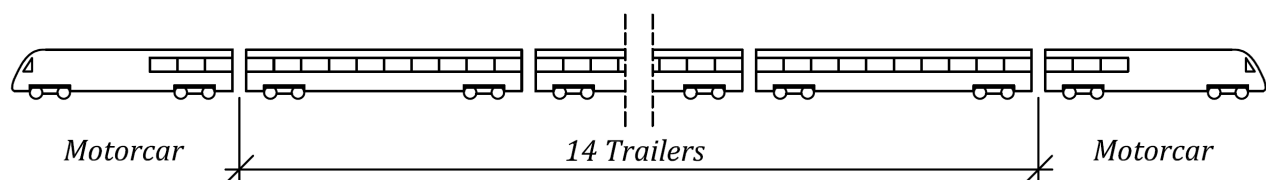


Figure 2.1: Visualization of an ICE 2 full-train set.

Alternative train data is presented by Wanming Zhai (2009). The vehicle here is a chinese high-speed train called *Chinese Star* which is a prototype train no longer in use. This train had a configuration of two motorcars and 9 passenger cars and the parameters seem to correspond roughly with the ICE data. However, the final data used in this thesis was based on the ICE-train since this is a train set more likely to be implemented in the East Link project.

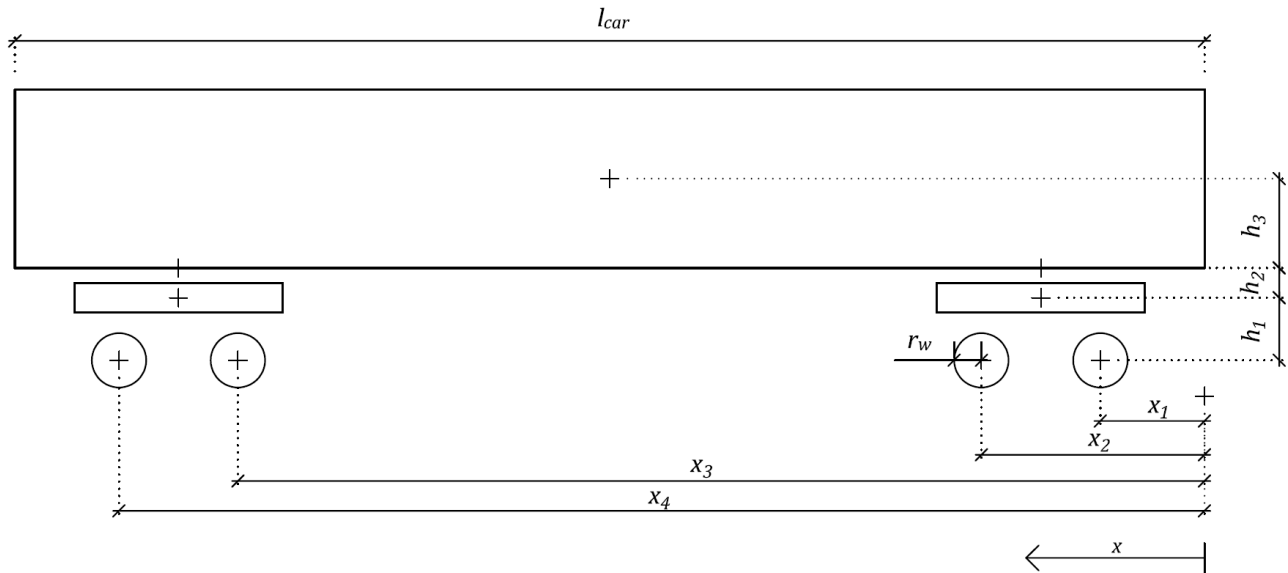


Figure 2.2: Geometrical measurement of the ICE train according to Lei (2017).

Table 2.1: Geometrical vehicle parameters used for the ICE motor car and trailers respectively as provided by Lei (2017).

Parameter	Description	Motor car	Trailer
r_w	Wheel radius [m]	0.460	0.460
h_1	Distance between bogie and wheelset [m]	0.100	0.100
h_2	Distance between bogie and secondary suspension point [m]	0.451	0.451
h_3	Distance between vehicle center and secondary suspension point [m]	0.900	0.900
l_{car}	Total vehicle length [m]	20.160	24.340
x_1	Position of first axis [m]	3.700	2.270
x_2	Position of second axis [m]	6.700	5.070
x_3	Position of third axis [m]	15.160	19.270
x_4	Position of fourth axis [m]	18.160	22.070

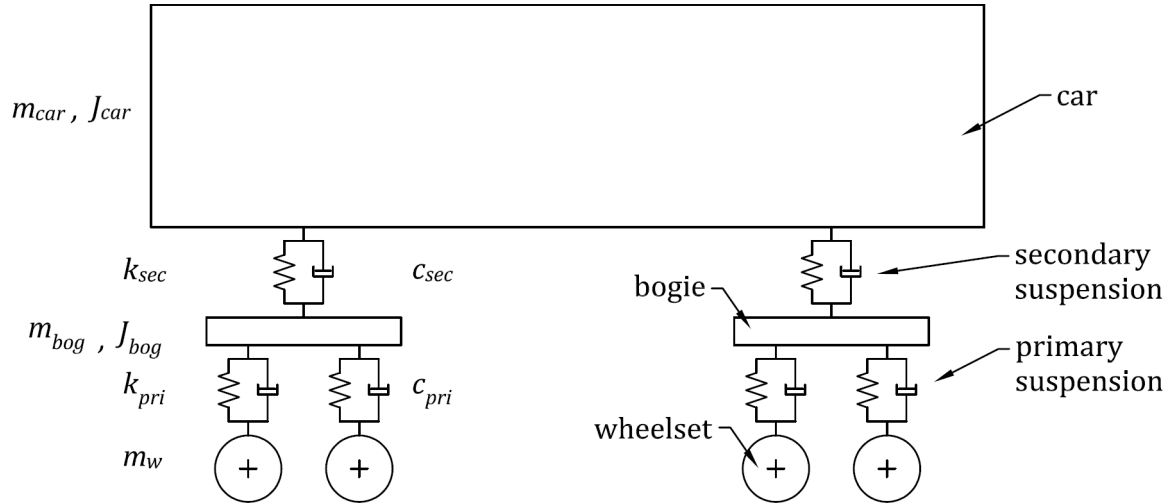


Figure 2.3: A schematic view of the vehicle model with dynamic components and properties highlighted.

Table 2.2: Dynamic vehicle parameters used for the ICE motorcar and trailer as provided by Lei (2017).

Parameter	Description	Motorcar	Trailer
m_{car}	Car body mass [kg]	$58.8 \cdot 10^3$	$45.5 \cdot 10^3$
m_{bog}	Bogie mass [kg]	$5.35 \cdot 10^3$	$3.09 \cdot 10^3$
m_w	Wheelset mass [kg]	$2.20 \cdot 10^3$	$1.56 \cdot 10^3$
J_{car}	Car body pitch inertia moment [kgm^2]	$3.089 \cdot 10^6$	$2.391 \cdot 10^6$
J_{bog}	Bogie pitch inertia moment [kgm^2]	$0.546 \cdot 10^3$	$0.499 \cdot 10^3$
k_{pri}	Vertical stiffness of primary suspension [N/m]	$2.418 \cdot 10^6$	$2.820 \cdot 10^6$
c_{pri}	Vertical damping of primary suspension [Ns/m]	$30.0 \cdot 10^3$	$21.9 \cdot 10^3$
k_{sec}	Vertical stiffness of secondary suspension [N/m]	$1.520 \cdot 10^6$	$0.324 \cdot 10^6$
c_{sec}	Vertical damping of secondary suspension [Ns/m]	$90.0 \cdot 10^3$	$29.2 \cdot 10^3$

2.1.3 Rail standards and parameters

For modern high-speed railway on bridges, UIC60 rail with prestressed concrete sleepers are frequently used. Rail, sleeper and pad data presented in Table 2.3 is gathered from Nielsen and Igeland (1995) and Lei (2017). The model in Figure 2.4 schematically shows the physical representation of each property. The maintenance level should be specified for each project and the structural design is dependent on that parameter. If nothing else is specified, a well maintained rail is assumed.

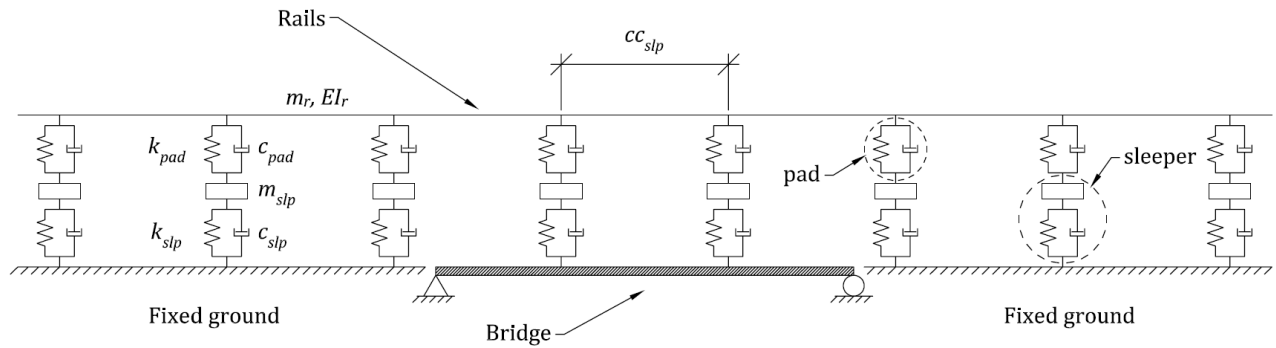


Figure 2.4: A schematic view of the bridge model with dynamic components and properties highlighted.

Table 2.3: Rail, sleeper and pad parameters.

Parameter	Description	Value
m_r	Rail mass [kg/m]	60
EI_r	Rail bending stiffness [Nm ²]	$6.4 \cdot 10^6$
m_{slp}	Sleeper mass [kg]	340
cc_{slp}	Sleeper spacing [m]	0.630
k_{pad}	Vertical stiffness of pads [N/m]	$100.0 \cdot 10^6$
c_{pad}	Vertical damping of pads [Ns/m]	$79.5 \cdot 10^3$
k_{slp}	Vertical stiffness of sleepers [N/m]	$80.0 \cdot 10^6$
c_{slp}	Vertical damping of sleepers [Ns/m]	$50.0 \cdot 10^3$

2.2 Reinforced concrete slab bridge

There are many possible structural choices to be made when constructing a reinforced concrete slab bridge, e.g. material, reinforcement strategy, section layout etc. As a basis for analysis in this thesis a solid rectangular bridge section similar to the one used by Hjelm and Karlsson (2016) is implemented. The bridge has a fixed width of 6.8 m and the height is variable in order to adjust the stiffness for different span lengths, see Figure 2.5. Any effects due to the stiffness of the substructure has been neglected. Furthermore a positive vertical camber is assumed so that the deck is completely horizontal when subjected to self-weight.

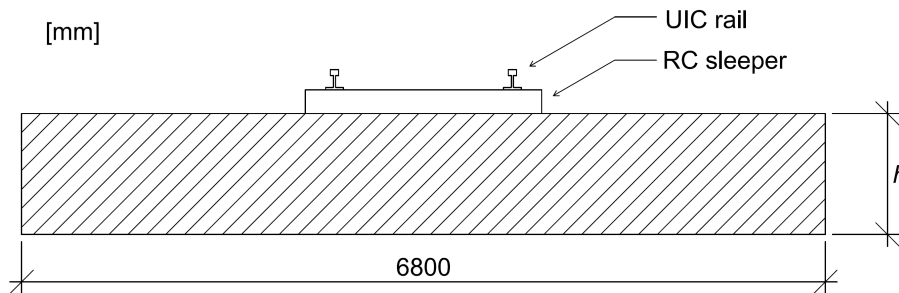


Figure 2.5: Deck cross-section being evaluated in this analysis displayed along with reinforced concrete sleepers and standard UIC 60 rail.

A concrete slab bridge carries transverse load through beam action to its supports in longitudinal direction. More specifically, as it deflects a tensile and compressive zone is formed internally in the structure Lundh (2007). With the bending resistance of the cross-section, a resisting moment is mobilized which makes it possible for the bridge to attain equilibrium under the design load. In field sections, most reinforcement is concentrated to the bottom fibres of the girder while in support sections, the opposite is true. This is to best utilize the tensile capabilities of the reinforcement steel. Boundary conditions play an important role in the design of concrete girder bridges, as it decides the moment distribution which is the basis for the reinforcement configuration. The following section will investigate different such conditions.

2.2.1 Boundary conditions

Simply supported bridges are bridges in which each span acts independently from neighbouring spans. Boundary conditions are such that free rotation is allowed over each support, meaning that support moments are zero (or close to zero in real structures). Furthermore, this causes rotations to be discontinuous along the length of the bridge, as each span deflects independently, see Figure 2.6. These bridges require larger field sections and more tensile field reinforcement in comparison to their continuous counterparts to carry the larger field moment.

Simply supported bridges may be assembled span by span, with each section shipped into place separately. For bridges spanning across rivers or sea straits, this may be done conveniently with the use of barges.

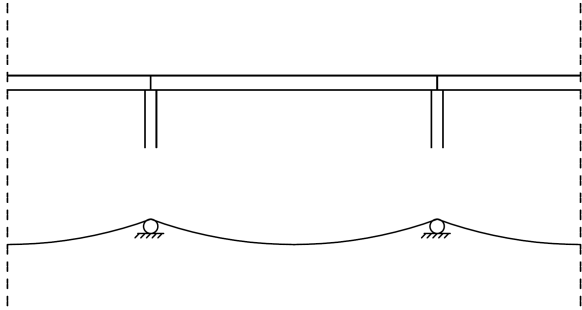


Figure 2.6: The deflection behaviour of a simply supported multi-span bridge.

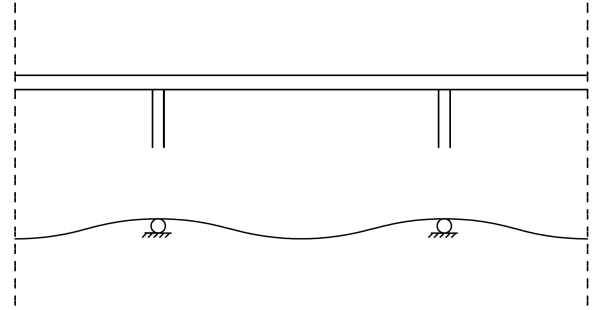


Figure 2.7: The deflection behaviour of a continuous multi-span bridge.

Continuous bridges are, as they sound, continuous in their nature. This means that any load effect affecting one span will propagate into the neighbouring spans. Moments over mid supports are non-zero, requiring flexural tension reinforcement in the top fibres of the bridge deck. The major benefit of this setup is the deflection behaviour of such a structure. Due to the fact that multiple spans cooperate in taking the load, each span becomes more stiff and thus deflections are greatly limited in comparison to simply supported structures, see Figure 2.7. Another benefit is the possibility for construction of more slender cross sections, as the moment is more evenly distributed between span and field sections. A common method employed for construction of continuous bridges is launching, whereby the bridge is continuously slid into place from the abutments.

2.3 Regulations according to Eurocode

The performance of a bridge should be evaluated for Ultimate Limit State (ULS) and Serviceability Limit State (SLS) according to Section 2.3.1. For design with regards to vehicle comfort criteria a simplified method based on the static load model LM71 is presented as seen in Section 2.3.2. As an alternative approach, a dynamic analysis could be performed according to Section 2.3.3.

2.3.1 Bridge regulations

According to CEN (2010b) the most unfavourable effect of Eqs. (2.1) or (2.2) should be used in design of the bridge.

$$\left(1 + \varphi'_{dyn} + \frac{\varphi''}{2}\right) \cdot \begin{pmatrix} \text{HSLM} \\ \text{or} \\ \text{Real Train} \end{pmatrix} \quad (2.1)$$

$$\Phi \cdot (\text{LM71} + \text{SW}/0) \quad (2.2)$$

Where:

φ'_{dyn}	= max ($y_{dyn}/y_{stat} - 1$)	Dynamic enhancement factor from analysis
φ''		Dynamic response due to imperfections in the rail-wheel system
Φ		Dynamic factor dependent on determinant length and maintenance level

The maximum allowable deflection for railway bridges according to Trafikverket (2011) is $L/800$. The vertical acceleration of the bridge deck should, for unballasted track, be limited to $\gamma_{df} = 5 \text{ m/s}^2$ according to CEN (2010b). This is to ensure sufficient contact force between wheel and rail. The frequencies at which this check is to be performed shall be determined as the largest of the following for each structural member:

- 30 Hz
- $1.5 \times$ fundamental frequency
- Frequency of third mode of longitudinal bending

For the dynamic analysis, loading shall be determined using *Real Trains*. According to Eurocode, *Real Trains* are defined as every possible train configuration (i.e. axle loads, axle spacing etc.) which could cross the bridge at speeds of over 200 km/h CEN (2010b). *Real Trains* may be chosen specifically for an individual project, as deemed appropriate by the design team.

The speeds to be included in the dynamic ultimate limit state analysis should be chosen such that the maximum speed is 120% of the intended maximum speed at the site of interest according to CEN (2010b). Subsequently, at least $320 \cdot 1.2 = 384 \text{ km/h}$ should be included in the analysis of bridges on the East Link project. However since the focus of this thesis is comfort criteria under service state, this addition can be

neglected. A recommended lower speed limit for dynamic analysis is set at 40 m/s = 144 km/h. Any identified resonant speeds within the above stated range are to be checked more carefully; a reasonable approach would be to take finer velocity steps in these regions.

2.3.2 Simplified vehicle comfort analysis

In order to obtain *Very high* comfort level within the train cabin, it is recommended in CEN (2006) that vertical acceleration of the train car is kept below 1 m/s² at all times. The governing parameters are bridge span length, number of spans, boundary conditions and the speed at which trains are travelling. Fulfillment of this criteria may be determined either using a simplified approach based on the static deflection δ [m] in combination with train speed according to Figure 2.8 or by performing a dynamic interaction analysis on the train-bridge system e.g. using FEA-software.

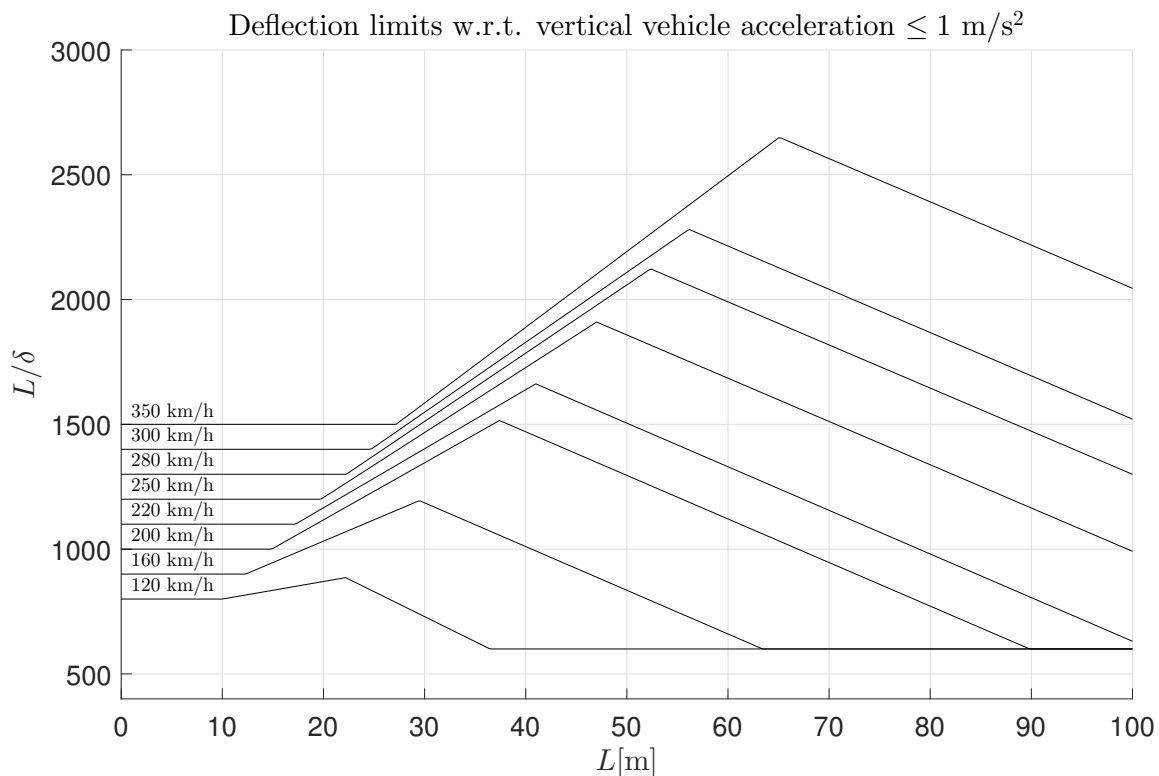


Figure 2.8: Maximum deflection in the deck in order to meet the comfort regulations in the vehicle according to SS-EN 1990, Figure A2.3. Factors are span length L , deflection δ and speed v .

The values for L/δ in Figure 2.8 apply to bridges with three or more simply supported spans. For bridges with one or two simply supported or continuous spans, L/δ should be multiplied with 0.7. For continuous bridges with three or more spans, L/δ should be multiplied with 0.9. When applying these factors the value of L/δ should never be less than 600.

2.3.3 Dynamic vehicle comfort analysis

When considering passenger comfort for the dynamic bridge-vehicle system there are certain factors that should be considered according to CEN (2006). These are expressed as follows.

- A series of vehicle speeds up to the highest specified speed.
- Vehicle loads according to real trains specified for the current project.
- The dynamic interaction between masses in the real train and the framework.
- Damping and stiffness properties in the vehicle.
- Sufficient number of vehicles to cause maximum load effect in the longest span.
- Sufficient number of spans in multiple span bridges, to cause resonance in the vehicle suspension.

A model adopting these factors will be presented in Chapter 4 after the preliminary studies of Chapter 3 are complete. Convergence study of sufficient number of vehicles and spans are presented in Section 4.2.

2.3.4 LM71 model

LM71 as seen in Figure 2.9 is a static train load model according to Eurocode. When considering this model in dynamic analysis it should be multiplied with a dynamic factor Φ which is determined using Eq. (2.3) for a carefully maintained track. L_Φ is the determinant length and is dependent on the bridge.

$$\Phi_2 = \frac{1.44}{\sqrt{L_\Phi} - 0.2} + 0.82 \quad 1.0 \leq \Phi_2 \leq 1.67 \quad (2.3)$$

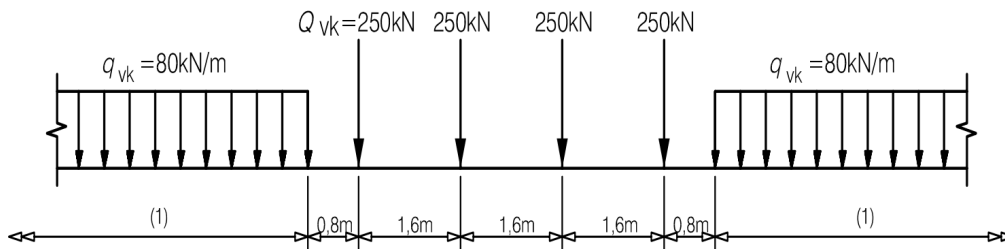


Figure 2.9: LM71 train model from Eurocode.

2.3.5 Bridge damping parameters

The structural damping, ξ , of a reinforced concrete bridge can be obtained from Section 6.4.6.3.1 Table 6.6 in CEN (2010b). This value represents the lower limit of percentage of critical damping. Additional damping $\Delta\xi$ has been neglected in this analysis since Arvidsson (2014) found that using that factor can yield unconservative results.

$$\xi = \begin{cases} 1.5 & \text{if span } L \geq 20 \text{ m} \\ 1.5 + 0.07(20 - L) & \text{if span } L < 20 \text{ m} \end{cases}$$

2.4 General dynamic theory

Structural dynamic theory is the basis for evaluating the vibrations and dynamic effects such as resonance in a structure. This chapter will cover some of the main theory regarding bridge design and dynamic loading from trains.

2.4.1 Equation of motion for a SDOF system

When treating the theory laying the groundwork for the calculation of dynamic systems, it is convenient to start at the most basic level. A common representation of a simple dynamic system is a spring-connected point-mass affected by some transient force $p(t)$, see Figure 2.10. This is a typical example of a Single Degree of Freedom (SDOF) system. By employing Newton's second law, see Eq. (2.4), it is possible to establish an equation of motion for this dynamic system, Craig Jr. and Kurdila (2006).

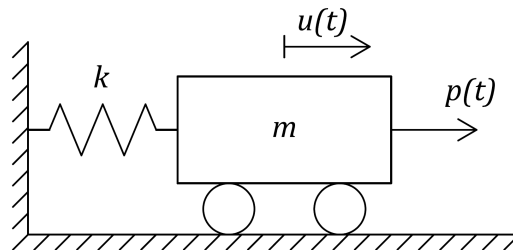


Figure 2.10: Figure depicting a simple mass m on wheels connected to a fixed point by a spring of stiffness k and influenced by a force $p(t)$.

$$\sum F_x = ma_x \quad (2.4)$$

where:

F_x	Forces acting in x -direction [N].
m	Mass of the object [kg].
a_x	Acceleration in x -direction [m/s^2].

For the case of Figure 2.10 this would yield Eq. (2.5)

$$-f_s + p(t) = m\ddot{u} \quad (2.5)$$

where:

$f_s = ku$	Spring force dependent on spring stiffness constant, k [N/m].
$p(t)$	Time-dependent excitation force [N].
u	Displacement of the mass, m [m].
\ddot{u}	Acceleration of the mass, m [m/s^2].

Eq. (2.5) may be conveniently rewritten Eq. (2.6).

$$m\ddot{u} + ku = p(t) \quad (2.6)$$

Free vibration is said to occur for the case when $p(t) \equiv 0$. For this case, the general solution is simply the homogeneous solution to the second order differential equation seen in Eq. (2.7).

$$m\ddot{u} + ku = 0 \quad (2.7)$$

Consequently, the general solution may be stated as Eq. (2.8)

$$u = A_1 \cos(\omega_n t) + A_2 \sin(\omega_n t) \quad (2.8)$$

where constants A_1 and A_2 are chosen such that the applicable initial conditions are fulfilled. For this case, the undamped circular frequency, ω_n [rad/s], may be determined according to Eq. (2.9).

$$\omega_n = \sqrt{\frac{k}{m}} \quad (2.9)$$

For non-zero excitational force, $p(t)$, i.e. when the mass undergoes forced vibration, a particular solution is required to solve the differential equation. The total solution is then the sum of the homogeneous, $u_c(t)$, and the particular, $u_p(t)$, solutions. This corresponds to the equation seen in Eq. (2.10).

$$u(t) = u_c(t) + u_p(t) \quad (2.10)$$

The nature of u_p is heavily influenced by the nature of the excitation force $p(t)$. This thesis will focus on harmonic excitational forces, which may be expressed in general terms as Eq. (2.11)

$$p(t) = p_0 \cos(\Omega t) \quad (2.11)$$

where:

p_0	is the excitation force amplitude [kN].
Ω	is the forcing frequency [rad/s].

The explicit particular solution to this type of problem will be examined further in Section 2.4.3, however first and foremost, there is a need to introduce the concept of damping. In reality, there is a certain degree of energy loss in a dynamic system; the vibrations cannot perpetuate with the same magnitude for an infinite amount of time without influx of energy. A damping factor c may be introduced to represent the damping that occurs naturally in the system which will ultimately lead to dissipation of energy and a steadily decreasing vibrational amplitude. The previous schematic model is then then expanded into the model shown in Figure 2.11.

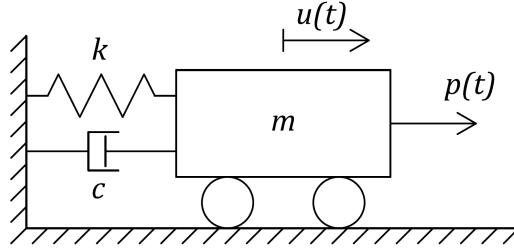


Figure 2.11: Figure depicting a simple mass m on wheels connected to a fixed point by a spring of stiffness k a damper with coefficient c and influenced by a force $p(t)$.

For the case where a damper is present, the equation of motion instead becomes the one seen in Eq. (2.12).

$$m\ddot{u} + c\dot{u} + ku = p(t) \quad (2.12)$$

This equation is then, for convenience, rewritten as in Eq. (2.13)

$$\ddot{u} + 2\zeta\omega_n\dot{u} + \omega_n^2u = \omega_n^2\frac{p(t)}{k} \quad (2.13)$$

where:

$\zeta = \frac{c}{c_{cr}}$	is the damping ratio [-].
c	is the viscous damping coefficient [Ns/m].
$c_{cr} = 2m\omega_n = 2\sqrt{km}$	is the critical viscous damping coefficient [Ns/m].
$\omega_n = \sqrt{\frac{k}{m}}$	is the undamped circular frequency [rad/s].

This system has a damped natural frequency, ω_d [rad/s], defined as seen in Eq. (2.14).

$$\omega_d = \omega_n\sqrt{1 - \zeta^2} \quad (2.14)$$

The solution to the equation of motion has the form seen in Eq. (2.15)

$$u(t) = e^{-\zeta\omega_n t} \left(u_0 \cos(\omega_d t) + \frac{v_0 + \zeta\omega_n u_0}{\omega_n} \sin(\omega_d t) \right) \quad (2.15)$$

which may be written as in Eq. (2.16)

$$u(t) = U e^{-\zeta\omega_n t} \cos(\omega_d t - \alpha) \quad (2.16)$$

where α [rad] is the phase lag. The response solution requires initial conditions in the form of initial displacement, $u_0 = u(0)$, and initial velocity, $v_0 = \dot{u}_0 = \dot{u}(0)$ in order to be solved.

2.4.2 Equation of motion for a MDOF system

For systems with more than one Degree of Freedom (DOF), multiple equations of motion will be formed. These systems are thus named Multiple Degrees of Freedom (MDOF) systems. For example a damped 2-DOF system as the one shown in Figure 2.12 has the equation of motion stated in Eq. (2.17). By introducing a matrix notation the general equation of motion can be expressed as Eq. (2.18)

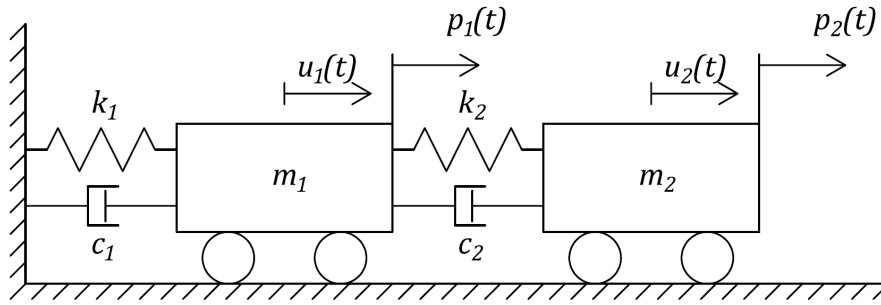


Figure 2.12: Figure depicting a simple mass m on wheels connected to a fixed point by a spring of stiffness k a damper with coefficient c and influenced by a force $p(t)$.

$$\underbrace{\begin{bmatrix} m_1 & 0 \\ 0 & m_2 \end{bmatrix}}_{\mathbf{M}} \underbrace{\begin{bmatrix} \ddot{u}_1 \\ \ddot{u}_2 \end{bmatrix}}_{\ddot{\mathbf{u}}} + \underbrace{\begin{bmatrix} c_1 + c_2 & -c_2 \\ -c_2 & c_2 \end{bmatrix}}_{\mathbf{C}} \underbrace{\begin{bmatrix} \dot{u}_1 \\ \dot{u}_2 \end{bmatrix}}_{\dot{\mathbf{u}}} + \underbrace{\begin{bmatrix} k_1 + k_2 & -k_2 \\ -k_2 & k_2 \end{bmatrix}}_{\mathbf{K}} \underbrace{\begin{bmatrix} u_1 \\ u_2 \end{bmatrix}}_{\mathbf{u}} = \underbrace{\begin{bmatrix} p_1(t) \\ p_2(t) \end{bmatrix}}_{\mathbf{p}(t)} \quad (2.17)$$

$$\mathbf{M}\ddot{\mathbf{u}} + \mathbf{C}\dot{\mathbf{u}} + \mathbf{K}\mathbf{u} = \mathbf{p}(t) \quad (2.18)$$

where the notations are as presented in Eq.(2.19) for a dynamic system of n degrees of freedom. \mathbf{M} is the mass matrix, \mathbf{C} is the viscous damping matrix, \mathbf{K} is the stiffness matrix and $\mathbf{p}(t)$ is the force vector. In the case of the 2-DOF system presented in Figure 2.12 the masses will form a diagonal lumped mass matrix. However this is not always the case, especially when modelling more complex elements such as beams. For a beam it is common to apply a consistent mass matrix formulation which distributes the mass over the whole element, see Section 2.5.1. In order to obtain the eigenmodes and eigenvectors of a MDOF system such as the one shown in Figure 2.12, the associated eigenproblem must be solved as described in Section 2.4.8.

$$\mathbf{M} = \begin{bmatrix} m_{11} & \dots & m_{1n} \\ \vdots & \ddots & \vdots \\ m_{n1} & \dots & m_{nn} \end{bmatrix} \quad \mathbf{C} = \begin{bmatrix} c_{11} & \dots & c_{1n} \\ \vdots & \ddots & \vdots \\ c_{n1} & \dots & c_{nn} \end{bmatrix} \quad \mathbf{K} = \begin{bmatrix} k_{11} & \dots & k_{1n} \\ \vdots & \ddots & \vdots \\ k_{n1} & \dots & k_{nn} \end{bmatrix} \quad \mathbf{p}(t) = \begin{bmatrix} p_1(t) \\ \vdots \\ p_n(t) \end{bmatrix} \quad (2.19)$$

\mathbf{u} , $\dot{\mathbf{u}}$ and $\ddot{\mathbf{u}}$ are the displacement, velocity and acceleration vectors respectively, having the appearance as stated in Eq. (2.20).

$$\mathbf{u} = \begin{bmatrix} u_1 \\ \vdots \\ u_n \end{bmatrix} \quad \dot{\mathbf{u}} = \begin{bmatrix} \dot{u}_1 \\ \vdots \\ \dot{u}_n \end{bmatrix} \quad \ddot{\mathbf{u}} = \begin{bmatrix} \ddot{u}_1 \\ \vdots \\ \ddot{u}_n \end{bmatrix} \quad (2.20)$$

Generally, there are three approaches commonly employed to solve MDOF systems:

- Mode superposition with real modes from the undamped system
- Mode superposition with complex modes from the damped system
- Directly integrating the coupled equations of motion

2.4.3 Harmonic excitation and resonance

Resonance is an important phenomenon in structural dynamics. It occurs when the frequency at which a structure is forced to vibrate approaches one of its eigenfrequencies. This leads to rapid escalation of the amplitude of the activated vibrational mode. Without sufficient damping, this might cause excessive deformation of the structure with severe structural damage or even collapse as a consequence. Resonance may occur when a dynamic structural system is subjected to a harmonic force. This corresponds to the following equation of motion provided by Craig Jr. and Kurdila (2006):

$$m\ddot{u} + c\dot{u} + ku = p_0 \cos(\Omega t) \quad (2.21)$$

The corresponding solution to this equation is on the form:

$$u(t) = \frac{U_0}{\sqrt{(1-r^2)^2 + (2\zeta r)^2}} \cos(\Omega t - \alpha) + e^{-\zeta\omega_n t} (A_1 \cos(\omega_d t) + A_2 \sin(\omega_d t)) \quad (2.22)$$

Where $r = \Omega/\omega_n$ is the frequency ratio. It is evident that the amplitude of the steady-state response is not only dependent on the force magnitude, but also on the damping factor ζ and the frequency ratio r . An important feature of this system is the so called steady-state magnification factor, D_s , defined as stated in Eq. (2.23) and visualized in Figure 2.13

$$D_s(r) = \frac{U(r)}{U_0} = \frac{1}{\sqrt{(1-r^2)^2 + (2\zeta r)^2}} \quad (2.23)$$

where:

$$\begin{array}{ll} U_0 = p_0/k & \text{is the static displacement.} \\ U(r) & \text{is the dynamic displacement at frequency ratio } r. \end{array}$$

As the excitation frequency approaches the natural frequency circular frequency of the system, the frequency response of the system shows an increase of excitation amplitude for each load cycle. When

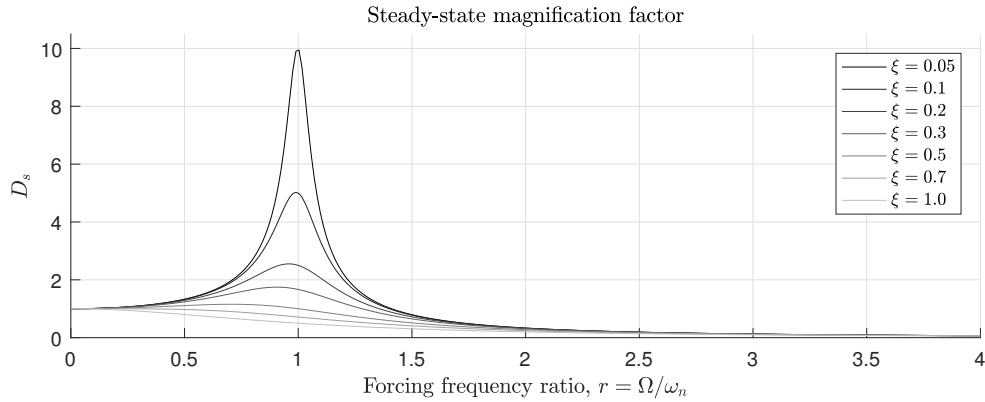


Figure 2.13: Steady-state magnification factor for various forcing frequencies at different level of damping.

the system attains this frequency, resonance is said to occur in the structure. The only factor limiting the dynamic amplification of the deformations is the damping, ζ . For most structural systems this factor is usually in the range of 0.5 – 5%.

2.4.4 Vibration of Euler-Bernoulli beams

The governing equation of an Euler–Bernoulli (E-B) beam loaded with a transverse load, $p_y(x, t)$ may be stated as:

$$\frac{\partial^2}{\partial x^2} \left(EI \frac{\partial^2 u}{\partial x^2} \right) + \rho A \frac{\partial^2 u}{\partial t^2} = p_y(x, t) \quad (2.24)$$

where:

E	is the Young's modulus [Pa]
I	is the second moment of area about the z-axis [m ⁴].
ρ	is the density [kg/m ³].
A	is the cross-sectional area [m ²].

For the purpose of this thesis, the unloaded case will be studied in order to obtain the eigenfrequencies of the E-B beam along with accompanying mode shapes. That is, the case where $p_y(x, t) \equiv 0$. Assuming harmonic motion according to Eq. (2.25) is an important step toward finding the eigenmodes and eigenfrequencies of the beam.

$$u(x, t) = U(x) \cos(\omega t - \alpha) \quad (2.25)$$

If free vibration occurs for a uniform, unloaded beam, the equation may then be written as stated in Eq. (2.26).

$$\frac{d^4 U}{dx^4} - \lambda^4 = 0 \quad (2.26)$$

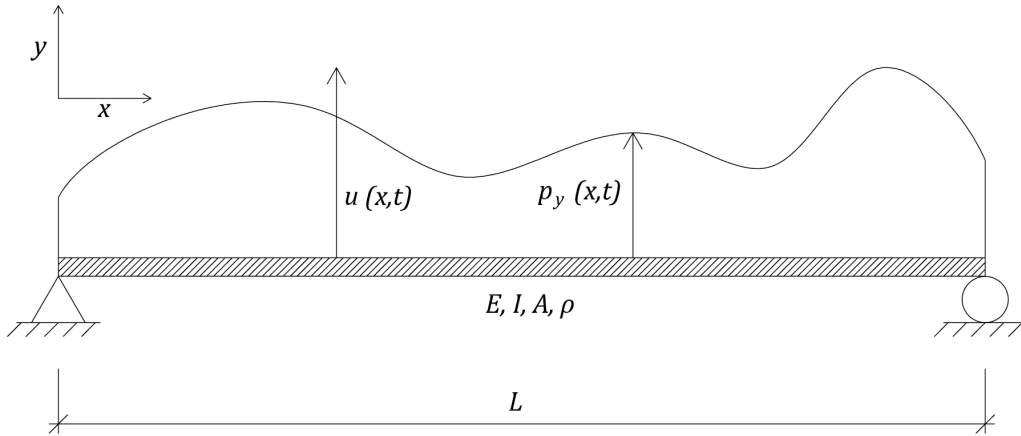


Figure 2.14: Simply supported E-B beam loaded with an arbitrary load $p_y(x,t)$, with length L and with sectional constants E, I, A and ρ .

where the term λ^4 is defined as Eq.(2.27).

$$\lambda^4 = \omega^2 \frac{\rho A}{EI} \quad (2.27)$$

This in turn yields a solution to the 4th-order ordinary differential equation as may be seen in Eq. (2.28).

$$U(x) = C_1 \sinh(\lambda x) + C_2 \cosh(\lambda x) + C_3 \sin(\lambda x) + C_4 \cos(\lambda x) \quad (2.28)$$

There are four constants $C_1 - C_4$ of which three may be determined from boundary conditions along with the eigenvalue λ , while the fourth one is arbitrary. The properties of $U(x)$ presented in Eqs.(2.29)-(2.31) are true for each boundary condition respectively.

– For a fixed end:

$$U = \frac{dU}{dx} = 0 \quad (2.29)$$

– For a pinned end:

$$U = \frac{d^2U}{dx^2} = 0 \quad (2.30)$$

– For a free end:

$$\frac{d^2U}{dx^2} = \frac{d^3U}{dx^3} = 0 \quad (2.31)$$

For the most easily solvable case of a simply supported beam, boundary conditions inserted into Eq. (2.28) result in a system of equations ultimately leading to Eq. (2.32).

$$\sinh(\lambda L) \sin(\lambda L) = 0 \quad (2.32)$$

Non-trivial solutions to this equation are found when the sine term is zero, thus solving Eq. (2.33) for the eigenvalues λ .

$$\sin(\lambda L) = 0 \quad (2.33)$$

This way, the solutions λ_n may be stated as Eq. (2.34), where n is a positive integer.

$$\lambda_n = \frac{n\pi}{L} \quad (2.34)$$

Consequently, the natural frequencies of the simply supported beam is found by insertion into Eq. (2.27), giving Eq. (2.35). Furthermore, the mode functions defining the shape of the eigenmodes is given by backwards substitution into the original system of equations arising from boundary conditions. If normalized by setting the amplitude to unity, the mode functions $\phi_n(x)$ are given by Eq. (2.36).

$$\omega_n = \left(\frac{n\pi}{L}\right)^2 \sqrt{\frac{EI}{\rho A}} \quad (2.35)$$

$$\phi_n(x) = \sin \frac{n\pi x}{L} \quad (2.36)$$

The four first longitudinal bending modes of a simply supported beam thus have shapes as shown in Figures 2.15 - 2.18.



Figure 2.15: First longitudinal bending mode of a simply supported beam.

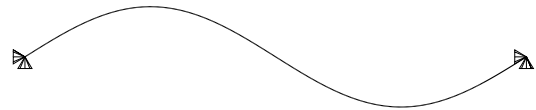


Figure 2.16: Second longitudinal bending mode of a simply supported beam.

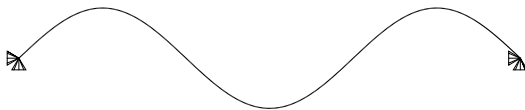


Figure 2.17: Third longitudinal bending mode of a simply supported beam.



Figure 2.18: Fourth longitudinal bending mode of a simply supported beam.

By applying coupling conditions, eigenfrequencies and modes can be solved for continuous systems. Eigenfrequencies can be found using Eq. (2.37) with the appropriate frequency parameter β_n according to Table 2.4. Corresponding mode shape functions are stated in Appendix A.

$$\omega_n = \left(\frac{\beta_n}{L}\right)^2 \sqrt{\frac{EI}{\rho A}} \quad (2.37)$$

Table 2.4: Frequency parameter, β_n , for the first five modes for continuous beams derived by Talukdar (2016).

Number of spans	Mode 1	Mode 2	Mode 3	Mode 4	Mode 5
1	π	2π	3π	4π	5π
2	π	3.9272	2π	7.0686	3π
3	π	3.5500	4.3040	2π	6.6920

The corresponding mode shapes are visualized in Figures 2.19 - 2.22 for the two span beams and Figures 2.23 - 2.26 for the three span beams.

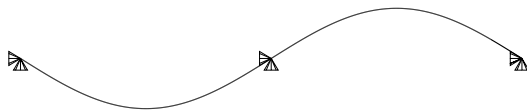


Figure 2.19: First longitudinal bending mode of a continuous beam with two spans.



Figure 2.20: Second longitudinal bending mode of a continuous beam with two spans.

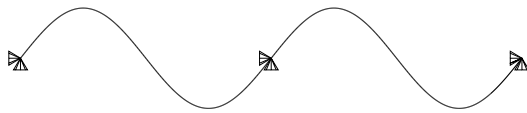


Figure 2.21: Third longitudinal bending mode of a continuous beam with two spans.



Figure 2.22: Fourth longitudinal bending mode of a continuous beam with two spans.

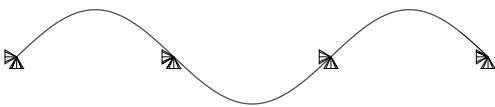


Figure 2.23: First longitudinal bending mode of a continuous beam with three spans.



Figure 2.24: Second longitudinal bending mode of a continuous beam with three spans.



Figure 2.25: Third longitudinal bending mode of a continuous beam with three spans.

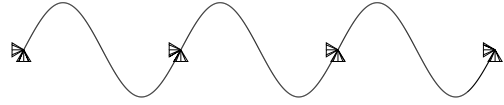


Figure 2.26: Fourth longitudinal bending mode of a continuous beam with three spans.

2.4.5 Moving load on Euler-Bernoulli beam

Consider a simply supported homogeneous Euler-Bernoulli beam subjected to a single point load, p , moving at a constant speed, v , according to Figure 2.27. The structure is assumed to have Rayleigh damping applied, with a damping factor of $\xi = 1.5\%$.

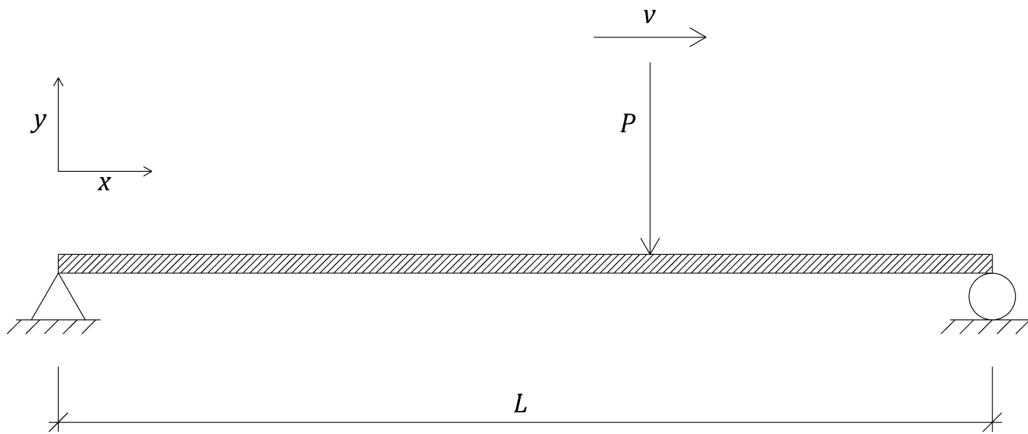


Figure 2.27: Single moving point load applied on a homogeneous E-B beam.

As shown by Wu, Yau, and Yang (2004) the equation of motion for this system can be derived as Eq. (2.38) using the Dirac delta function, δ , as defined by its properties as an integrand, see Eq. (2.39).

$$m \frac{\partial^2 u}{\partial t^2} + c_e \frac{\partial u}{\partial t} + c_i I \frac{\partial^5 u}{\partial t \partial x^4} + EI \frac{\partial^4 u}{\partial x^4} = p \delta(x - vt), \quad 0 \leq vt \leq L \quad (2.38)$$

$$\int_a^b f(t) \delta(t - t_0) dt = \begin{cases} f(t_0) & \text{if } a < t_0 < b \\ 0 & \text{otherwise} \end{cases} \quad (2.39)$$

Here c_e and c_i represent the external and internal damping coefficients. m is the mass per unit length for the beam. Note that the deflection $u(x, t)$ is a function of time t and coordinate x . By applying simply supported boundary conditions and assuming that initially the whole beam is at rest the governing

equation of motion can be solved for $u(x, t)$ which finally yields Eq. (2.40).

$$\begin{aligned}
u(x, t) = & \sum_{n=1}^{\infty} \frac{2pL^3 / (EI n^4 \pi^4)}{(1 - r^2)^2 + (2\xi_n r)^2} \\
& \times \left\{ (1 - r^2) \sin(\Omega_n t) - 2\xi_n r \cos(\Omega_n t) + e^{-\xi_n \omega_n t} \right. \\
& \times \left[2\xi_n r \cos(\omega_d t) + \frac{r}{\sqrt{1 - \xi_n^2}} (2\xi_n^2 + r^2 - 1) \sin(\omega_d t) \right] \left. \right\} \\
& \times \sin\left(\frac{n\pi x}{L}\right)
\end{aligned} \tag{2.40}$$

where:

$\omega_n = \frac{n^2 \pi^2}{L^2} \sqrt{\frac{EI}{m}}$	Natural frequency for mode n [-]
$\xi_n = \frac{1}{2} \left(\frac{\alpha}{\omega_n} + \beta \omega_n \right)$	Rayleigh damping expressed by choosing $c_e = \alpha m$ and $c_i = \beta E$ [%]
$\omega_d = \omega_n \sqrt{1 - \xi_n^2}$	Damped frequency of vibration for mode n [rad/s]
$\Omega_n = \frac{n\pi v}{L}$	Exciting frequency from the moving point load [rad/s]
$r = \frac{\Omega_n}{\omega_n}$	Ratio between the frequency of excitation and free vibration [-]

2.4.6 Timoshenko beam theory

Unlike Euler Bernoulli beam theory presented in Section 2.4.4, Timoshenko beam theory considers shear deformation and rotatory inertia effects. For a linear elastic isotropic homogeneous beam with a constant cross section a single equation of motion can be stated as Eq. (2.41) according to Craig Jr. and Kurdila (2006).

$$\begin{aligned}
& \underbrace{EI \frac{\partial^4 u}{\partial x^4} - \left(p_y - \rho A \frac{\partial^2 u}{\partial t^2} \right)}_{\text{Euler Bernoulli theory}} \quad \underbrace{-\rho I \frac{\partial^4 u}{\partial x^2 \partial t^2}}_{\text{Principal rotatory inertia}} \\
& + \underbrace{\frac{EI}{\kappa GA} \frac{\partial^2}{\partial x^2} \left(p_y - \rho A \frac{\partial^2 u}{\partial t^2} \right)}_{\text{Principal shear deformation}} \quad \underbrace{-\frac{\rho I}{\kappa GA} \frac{\partial^2}{\partial t^2} \left(p_y - \rho A \frac{\partial^2 u}{\partial t^2} \right)}_{\text{Combined rotatory inertia and shear deformation}} = 0
\end{aligned} \tag{2.41}$$

Where:

$G = \frac{E}{2(1+\nu)}$	Shear modulus for a homogeneous isotropic elastic material [N/m ²]
$\kappa = \frac{5(1+\nu)}{6+5\nu}$	Shear correction factor by Timoshenko (1922) [-]

Similar as for the Euler beam in Section 2.4.5, a moving point load could be applied on a Timoshenko beam. Mackertich (1990) showed that the the rotary inertia and shear deformation effect may be significant for the dynamic moving load problem. Therefore it is critical to evaluate this effect later in the analysis. A finite element formulation of this beam theory will be presented in Section 2.5.

2.4.7 Critical velocity

Considering a sequence of moving loads with roughly equal spacing moving across a beam, there exist a number of critical velocities at which the beam is excited in its eigenfrequency. As stated by Mao and Lu (2013), the repeated loading may be expressed as in Eq. (2.42).

$$P(t) = \sum_j^{N_c} f_c(t)\delta(t - jt_c) \quad (2.42)$$

Where t_c is the time L_c/v it takes between one load impulse and the next. Here L_c is the length between the sequential loads (in the case of train loading this would be roughly equal to car length) and v is naturally the speed of the loads (train velocity). A schematic view of the load model is seen in Figure 2.28. N_c represents the number of loads in the consecutive sequence of loads of equal magnitude.

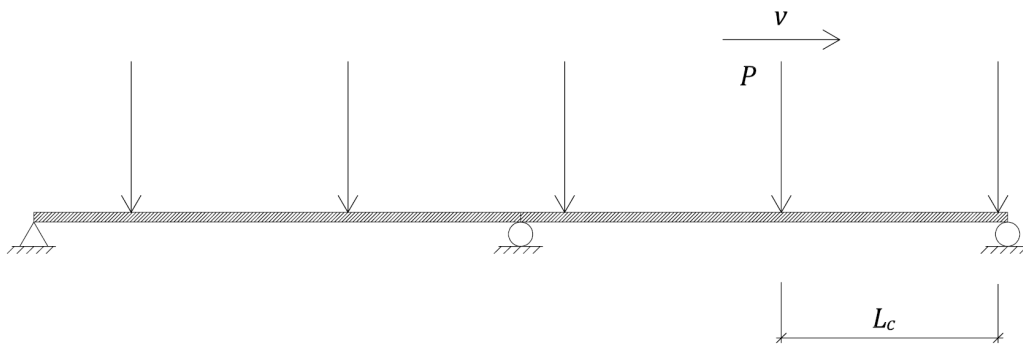


Figure 2.28: A sequence of point loads moving across a bridge.

It can be shown that for a bridge loaded with sequential point loads, there arise a number of apparent driving frequencies, f_d , at which the bridge is excited for a given speed. The car length of the studied vehicles along with the speed of the loads are of great importance, as they determine at what rate the bridge is excited. The expression presented in Eq. (2.43) corresponds to the driving frequencies caused by the moving consecutive point loads.

$$f_d = n \frac{v}{L_c} \quad (2.43)$$

where n is a positive integer. When these driving frequencies approach the bridge eigenfrequencies, f_n , resonance effects may start to occur. This was verified to some degree by Mao and Lu (2013) for the case of a simply supported, single-span bridge. Inserting this criterion into Eq. (2.43) yields an expression for the critical resonant velocities v_r , as seen in Eq. (2.44)

$$v_r = \frac{f_n L_c}{n} \quad (2.44)$$

It should be noted, however, that the bridge fundamental frequency could be misleading if the mass of the train is large in relation to the mass of the bridge. For the remainder of this report, vehicle mass is considered to be negligible in this respect.

2.4.8 Dynamic eigenvalue problems

When studying MDOF FE-models it is often of interest to find the eigenfrequencies and eigenmodes of the system. In this case it is useful to rewrite the governing equations of motion into a generalized eigenvalue problem as stated in Eq. (2.45).

$$(\mathbf{K} - \omega_i^2 \mathbf{M})\phi_i = \mathbf{0} \quad (2.45)$$

where:

ω_i	Circular eigenfrequency for mode i [rad/s]
ϕ_i	Eigenvector for mode i

Polynomial root finding is one technique for solving this equation. Using this method, ω_i^2 is solved by taking the determinant on the left-hand expression of Eq. (2.45) according to Craig Jr. and Kurdila (2006) which yield Eq. (2.46).

$$\det(\mathbf{K} - \omega_i^2 \mathbf{M}) = 0 \quad (2.46)$$

2.4.9 Rayleigh damping

An approach to introduce damping in a structure is to adopt Rayleigh damping. This type of damping is also called proportional damping since it is proportional to the mass matrix and stiffness matrix of a dynamic system as presented in Eq. (2.47), according to Craig Jr. and Kurdila (2006).

$$\mathbf{C} = \alpha \mathbf{M} + \beta \mathbf{K} \quad (2.47)$$

Due to orthogonality it can be seen that the damping ξ_r for mode r is equal to Eq. (2.48).

$$\xi_r = \frac{1}{2} \left(\frac{\alpha}{\omega_r} + \beta \omega_r \right) \quad (2.48)$$

The constants α and β can now easily be solved by choosing ζ_r for two known eigenfrequencies of the structure. For the case where $\xi_i = \xi_j = \xi$ the constants can be determined from Eq. (2.49) and Eq. (2.50).

$$\alpha = \frac{2\omega_i\omega_j\xi}{\omega_i + \omega_j} \quad (2.49)$$

$$\beta = \frac{2\xi}{\omega_i + \omega_j} \quad (2.50)$$

The choice of modes where to apply the Rayleigh damping is dependent on the structure being analyzed. In a dynamic analysis of a 3D shell-element bridge Qin and Lou (2000) considered eigenfrequencies up to the limit of 50 Hz by taking $\omega_i = \omega_1$ and $\omega_j = (\omega_2 + \omega_{\text{end}})/2$. This approach can be used with regulations according to Eurocode specified in Section 2.3.1.

Another approach for determining which modes to use, is to study the effective mass participation factor for each mode and include all modes up to a certain limit. The American building code ASCE 7-05 (2005)

specifies that a sufficient number of modes shall be chosen so that the accumulated modal mass participation exceeds 90% of the actual mass of the structure. This section however refers to seismic analysis although it is comparable to dynamic train loading. Abaqus (2005) states that the effective modal mass, m_{ai}^{eff} , is defined as Eq. (2.51) for mode $\alpha = 1, 2, \dots$ in the kinematic direction $i = x, y, z, rx, ry, rz$.

$$m_{ai}^{eff} = (\Gamma_{ai})^2 m_{\alpha} \quad (2.51)$$

where m_{α} is the generalized mass according to Eq. (2.52) and Γ_{ai} is the modal participation factor as expressed by Eq. (2.53)

$$m_{\alpha} = \phi_{\alpha}^T \mathbf{M} \phi_{\alpha} \quad (2.52)$$

$$\Gamma_{\alpha} = \frac{1}{m_{\alpha}} \phi_{ai}^T \mathbf{M} \mathbf{T}_i \quad (2.53)$$

\mathbf{M} is the mass matrix of the finite element system, ϕ_{α} is the eigenvector for mode α and \mathbf{T}_i defines the influence magnitude for each degree of freedom for a rigid body motion in the kinematic direction i .

2.5 FE-analysis

The Finite Element Method (FEM) introduces a powerful toolbox for solving complex static and dynamic problems numerically. This section will briefly cover the variations in beam formulation for a Euler-Bernoulli and a Timoshenko beam.

2.5.1 Beam formulations

The matrix formulations for a 6-DOF plane-frame Euler Bernoulli beam as specified by Ottosen and Petersson (1992) and implemented in CALFEM (2004) are displayed in Figure 2.29. The damping matrix is given by Eq. (2.48) assuming Rayleigh damping. Eq. (2.54) represents the local element stiffness matrix and Eq. (2.55) represents the local consistent mass matrix

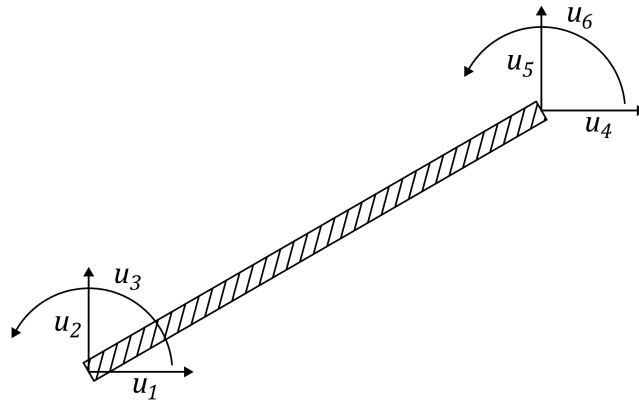


Figure 2.29: 6-DOF plane-frame Euler Bernoulli beam.

$$\mathbf{K}_{le} = E \begin{bmatrix} \frac{A}{L} & 0 & 0 & -\frac{A}{L} & 0 & 0 \\ 0 & \frac{12I}{L^3} & \frac{6I}{L^2} & 0 & -\frac{12I}{L^3} & \frac{6I}{L^2} \\ 0 & \frac{6I}{L^2} & \frac{4I}{L} & 0 & -\frac{6I}{L^2} & \frac{2I}{L} \\ -\frac{A}{L} & 0 & 0 & \frac{A}{L} & 0 & 0 \\ 0 & -\frac{12I}{L^3} & -\frac{6I}{L^2} & 0 & \frac{12I}{L^3} & -\frac{6I}{L^2} \\ 0 & \frac{6I}{L^2} & \frac{2I}{L} & 0 & -\frac{6I}{L^2} & \frac{4I}{L} \end{bmatrix} \quad (2.54)$$

$$\mathbf{M}_{le} = \frac{\rho AL}{420} \begin{bmatrix} 140 & 0 & 0 & 70 & 0 & 0 \\ 0 & 156 & 22L & 0 & 54 & -13L \\ 0 & 22L & 4L^2 & 0 & 13L & -3L^2 \\ 70 & 0 & 0 & 140 & 0 & 0 \\ 0 & 54 & 13L & 0 & 156 & -22L \\ 0 & -13L & -3L^2 & 0 & -22L & 4L^2 \end{bmatrix} \quad (2.55)$$

where:

E	Young's Modulus
A	Sectional Area
I	Sectional second moment of inertia
L	Element length
ρ	Sectional density

When constructing the global model these matrices has to be transformed from local space to global space. Eq. (2.56) is the element stiffness matrix in global space and Eq. (2.57) is the element mass matrix in global space.

$$\mathbf{K}_e = \mathbf{T}^T \mathbf{K}_{le} \mathbf{T}; \quad (2.56)$$

$$\mathbf{M}_e = \mathbf{T}^T \mathbf{M}_{le} \mathbf{T}; \quad (2.57)$$

where \mathbf{T} is the element transformation matrix as specified in Eq. (2.58).

$$\mathbf{T} = \begin{bmatrix} \cos(\theta) & \sin(\theta) & 0 & 0 & 0 & 0 \\ -\sin(\theta) & \cos(\theta) & 0 & 0 & 0 & 0 \\ 0 & 0 & 1 & 0 & 0 & 0 \\ 0 & 0 & 0 & \cos(\theta) & \sin(\theta) & 0 \\ 0 & 0 & 0 & -\sin(\theta) & \cos(\theta) & 0 \\ 0 & 0 & 0 & 0 & 0 & 1 \end{bmatrix} \quad (2.58)$$

The main difference implementing a Timoshenko beam compared to a Euler beam is the introduction of shear deformation and rotary inertia a can be seen in the element stiffness matrix, Eq. (2.59)

$$\mathbf{K}_{le} = \frac{E}{1+m} \begin{bmatrix} \frac{A(1+m)}{L} & 0 & 0 & \frac{-A(1+m)}{L} & 0 & 0 \\ 0 & \frac{12I}{L^3} & \frac{6I}{L^2} & 0 & -\frac{12I}{L^3} & \frac{6I}{L^2} \\ 0 & \frac{6I}{L^2} & \frac{4I(1+m/4)}{L} & 0 & -\frac{6I}{L^2} & \frac{2I(1-m/2)}{L} \\ -\frac{A(1+m)}{L} & 0 & 0 & \frac{A(1+m)}{L} & 0 & 0 \\ 0 & -\frac{12I}{L^3} & -\frac{6I}{L^2} & 0 & \frac{12I}{L^3} & -\frac{6I}{L^2} \\ 0 & \frac{6I}{L^2} & \frac{2I(1-m/2)}{L} & 0 & -\frac{6I}{L^2} & \frac{4I(1+m/4)}{L} \end{bmatrix} \quad (2.59)$$

where:

m	$= (12/L^2) \cdot \frac{EI}{GA\kappa}$	Sectional constant
κ		Shear correction factor
G		Shear modulus

2.5.2 FE-software

There are a wide range of commercially available finite element software applicable for different types of problems and level of complexity. This section will cover some alternatives and their applicability to this thesis.

MATLAB (2017) is a user friendly and modular script environment for working quickly with vectors and matrices. In conjunction with the finite element toolbox CALFEM (2004), models can be created and analyzed with relative ease. Common CALFEM (2004)-functions are `beam2d` which is used to generate element matrices and `assem` which assembles all element matrices into global matrices. Due to the modularity of MATLAB, a numerical integration scheme for both explicit and implicit analysis can be implemented.

ABAQUS by DASSAULT SYSTEMS (2017) is a commercial Finite Element Analysis (FEA) program for static and dynamic problems. Very large models can easily be created and analyzed quickly with multithreading capabilities. ABAQUS/Explicit is particularly powerful when analyzing highly discontinuous problems. Models can be created using the user interface or by the flexible scripting Application Programming Interface (API). This feature allows Python code to run within the ABAQUS-environment. Scripting is very useful when parameters need to be modified frequently as in this thesis or any other parametric study.

BRIGADE/Plus by Scanscot (2017) is a FEA-software built as an extension of ABAQUS. One powerful feature is that it includes High Speed Load Model (HSLM) train models and a very intuitive way to apply these for dynamic bridge analysis. Explicit analysis is not available in this software which could be a limitation when loss of contact and large movements should be analyzed.

2.6 Numerical integration methods

The governing equation of motion for a MDOF system can be expressed as Eq. (2.18). This is the basis for any numerical integration of a dynamic MDOF system. This section will present to different methods that could be applied during analysis.

2.6.1 Newmark- β method

A common technique for integration of second-order MDOF systems is the implicit Newmark- β method. In each time increment, h , the accelerations, $\ddot{\mathbf{u}}$, are solved from the equations of motion as described in Eq. (2.60) according to Craig Jr. and Kurdila (2006).

$$\mathbf{M}\ddot{\mathbf{u}}_{n+1} + \mathbf{C}\dot{\mathbf{u}}_{n+1} + \mathbf{K}\mathbf{u}_{n+1} = \mathbf{p}_{n+1} \quad (2.60)$$

where \mathbf{u} and $\dot{\mathbf{u}}$ is approximated using a generalized Taylor as seen in Eqs. (2.61) and (2.62)

$$\dot{\mathbf{u}}_{n+1} = \dot{\mathbf{u}}_n + ((1 - \gamma)\ddot{\mathbf{u}}_n + \gamma\ddot{\mathbf{u}}_{n+1})h \quad (2.61)$$

$$\mathbf{u}_{n+1} = \mathbf{u}_n + \dot{\mathbf{u}}_nh + ((1 - 2\beta)\ddot{\mathbf{u}}_n + 2\beta\ddot{\mathbf{u}}_{n+1})\frac{h^2}{2} \quad (2.62)$$

The Newmark- β method is unconditionally stable for constants $\gamma = \frac{1}{2}$ and $\beta = \frac{1}{4}$. Each iteration could be very time consuming for large MDOF systems. However, the time-step can be quite large in comparison with an explicit approach.

2.6.2 Central Difference Method

As explained by Craig Jr. and Kurdila (2006), The Central Difference Method (CDM) is an explicit numerical method well suited for solving second-order MDOF systems. This method is based on the finite-difference expression specified in Eq. (2.63) and (2.64)

$$\dot{\mathbf{u}}_n = \frac{\mathbf{u}_{n+1} - \mathbf{u}_{n-1}}{2h} \quad (2.63)$$

$$\ddot{\mathbf{u}}_n = \frac{\mathbf{u}_{n+1} - 2\mathbf{u}_n + \mathbf{u}_{n-1}}{h^2} \quad (2.64)$$

Substituting these expressions into the governing equation on motion, Eq. (2.18), gives the solution scheme as Eq. (2.65). Using this equation the next time-step \mathbf{u}_{n+1} can easily be solved using \mathbf{u}_n and \mathbf{u}_{n-1} from the current and previous time-step.

$$\left(\frac{1}{h^2}\mathbf{M} + \frac{1}{2h}\mathbf{C}\right)\mathbf{u}_{n+1} + \left(\mathbf{K} - \frac{2}{h^2}\mathbf{M}\right)\mathbf{u}_n + \left(\frac{1}{h^2}\mathbf{M} - \frac{1}{2h}\mathbf{C}\right)\mathbf{u}_{n-1} = \mathbf{p}_n \quad (2.65)$$

In order to ensure stability in the solution a sufficiently small time step, h , has to be chosen. For an undamped structure the maximum allowed time step, h_{crit} , can be expressed as Eq. (2.66).

$$h_{crit} = \frac{2}{\omega_{max}} \quad (2.66)$$

where ω_{max} is the highest eigenfrequency of the structure found by solving $\det(\mathbf{K} - \omega^2\mathbf{M}) = 0$. Applying damping to the structure reduces the maximum allowed time step as seen in Eq. (2.67) according to Abaqus (2005).

$$h_{crit} = \frac{2}{\omega_{max}} \left(\sqrt{1 + \xi^2} - \xi \right) \quad (2.67)$$

2.6.3 Digital signal processing

Numerical methods might produce noisy results which are difficult to analyze. Digital Signal Processing (DSP) is a method adopted in order to reduce this noise by applying a low-pass filter to the sampled data. A Butterworth low-pass filter, as seen in Figure 2.30, with a specified cutoff frequency and order of magnitude is one of multiple filters that could be applied. Diehl, Carroll, and Nagaraj (1999) show how DSP significantly can increase the quality of results from ABAQUS/Explicit analysis, however the Butterworth filter in ABAQUS is limited to order two which might not be ideal for all kinds of data. Therefore, in addition to the ABAQUS approach data could also be filtered in MATLAB using a higher order Butterworth filter MATLAB (2016b). Usage of this technique can be seen in Section 3.2. A comparison between multiple filtering techniques is beyond the scope of this thesis.

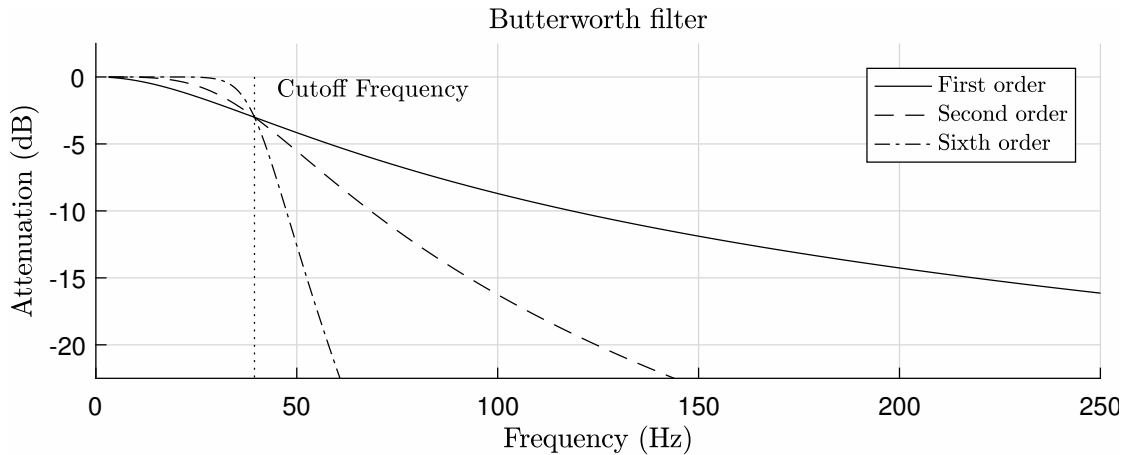


Figure 2.30: Low-pass Butterworth filter with a cut-off frequency of 39.473 Hz.

2.6.4 Nyquist sampling theorem

When sampling any signal it is critical that sufficient level of detail is adopted in order to avoid loss of information. The Nyquist sampling theorem states that the sampling frequency, f_s , must be at least twice the highest signal frequency, f_c , according to Eq. (2.68) as explained by Nyquist (1928).

$$f_s \geq 2f_c \quad (2.68)$$

2.7 Interaction theory

Previous theory is based on an analytic approach which might not be completely realistic in all cases. This section will focus on some parameters that are critical for modelling of a discontinuous model where the bridge and vehicle is two separate systems.

2.7.1 Contact modelling

There are many techniques for modelling contact between rigid and elastic bodies. A common approach is to implement a very stiff spring between the colliding parts, this however can be done in multiple ways. The most basic model would be an elastic spring that does not take contact loss into consideration. The contact force would in this case become Eq. (2.69) where F is the force, k is the spring stiffness and δ is the overclosure of the interference zone.

$$F = k\delta \quad (2.69)$$

A quick improvement to this model would be to set the spring stiffness to zero when there is contact loss, i.e. when $\delta < 0$. A spring stiffness of zero would result in a contact force of zero according to Eq. (2.70).

$$F = \begin{cases} 0, & \delta \leq 0 \\ k\delta, & \delta > 0 \end{cases} \quad (2.70)$$

Finding the correct spring stiffness k is difficult due to the nonlinear geometric properties of the wheel and the rail. Another approach is to model contact according to theory by Hertz (1881) in combination with loss of contact, as done similarly by Zhou (2011) and Chatterjee (1997)

$$F = \begin{cases} 0, & \delta \leq 0 \\ k_H \delta^{3/2}, & \delta > 0 \end{cases} \quad (2.71)$$

The Hertzian spring parameter, k_H can be determined using the equivalent Young's modulus and the radius of the colliding materials. For wheel-rail interaction of a single wheel with identical materials it can be formulated as Eq. (2.72) according to Nielsen, Pieringer, and Kropp (2014). Here E is the Young's modulus, ν is Poissons ratio and r_w is the wheel radius.

$$k_H = \frac{2}{3} \frac{E}{1 - \nu^2} r_w^{1/2} \quad (2.72)$$

The Hertzian contact has a nonlinear response, however the contact stiffness could be linearized around a small interval near static deflection and therefore function as a good approximation for the linear contact models. The linearized Hertzian contact stiffness can be calculated as in Eq. (2.73) according to Esveld (2001).

$$k_{lin} = \frac{dF}{d\delta} = \frac{3}{2} k_H \delta^{1/2} = \frac{3}{2} k_H^{2/3} F^{1/3} \quad (2.73)$$

where $\delta = (F/k_H)^{2/3}$ is the overclosure derived from Eq. (2.71) and the load $F = mg$ is determined from the static load of a single wheel in the vehicle system. The nonlinear Hertzian stiffness k_H is obtained from Eq. (2.72).

2.7.2 Rail imperfections

Surface imperfections due to corrugation can be modelled in many ways. Usually an periodic sinusoid function is implemented where the wavelength is chosen so that it is critical for the current vehicle model and velocity being analysed. Eq. (2.74) has been proposed by Nielsen and Igeland (1995) and Eq. (2.75) by Bogacz and Kowalska (2001) where r is the roughness profile for coordinates x along the rail.

$$r_{\text{Nielsen \& Igeland}} = 20 \cdot 10^{-6} \cdot \sin\left(\frac{2\pi}{0.060} \cdot x\right) \quad (2.74)$$

$$r_{\text{Bogacz \& Kowalska}} = -10 \cdot 10^{-6} \cdot \left(\cos\left(\frac{2\pi}{0.050} \cdot x\right) + 1\right) \quad (2.75)$$

Another approach to determine the imperfection profile is by studying the maximum roughness level spectrum in one-third octave bands L_r as defined in Eq. (2.76) by the Swedish National Rail Administration according to Nielsen et al. (2005) with $r_{\text{ref}} = 1 \mu\text{m}$.

$$L_r = 10 \cdot \log_{10}\left(\frac{r^2}{r_{\text{ref}}^2}\right) \quad [\text{dB re 1 m}] \quad (2.76)$$

For the European Norm prEN 3095 the roughness limit spectrum is defined by Eq. (2.77) according to Grassie (2012). L is the roughness limit in dB and λ is the wavelength in millimetres.

$$L_{\text{ISO 3095:2005}} = \begin{cases} -9.7 + 18.5 \log_{10}\left(\frac{\lambda}{10}\right) & \text{for } \lambda \geq 10 \\ -9.7 & \text{for } 10 > \lambda \geq 3 \end{cases} \quad (2.77)$$

Using Eq. (2.76) and Eq. (2.77) and evaluating the roughness at one-third octave bands from the lower wavelength limit of $\lambda = 3.15 \text{ mm}$ to the upper limit of $\lambda = 630 \text{ mm}$ results in a series of sinusoidal functions which together represents the roughness profile. Additionally, a random shift in phase is introduced in order to offset each spectrum band. The roughness profile is stated in Eq. (2.78) where r_i is the roughness amplitude corresponding to a particular wavelength λ_i with a phase shift ϕ_i for a spectrum band i .

$$r_{\text{ISO 3095:2005}} = \sum \left(r_i \cdot \sin\left(\frac{2\pi}{\lambda_i} \cdot x + \phi_i\right) \right) \quad (2.78)$$

Note that the ISO3095-profile will vary depending on the random phase applied to each spectrum band. The ISO3095 approach is also most common when evaluating the acoustic performance of the track and might not be suited for dynamic vehicle analysis where periodic profiles could be more critical. Out of the three profiles presented the one by Nielsen and Igeland (1995) seems to be critical with regards to dynamic resonance effects.

2.7.3 Wheel imperfections

Apart from rail imperfections, there also exist imperfections in the wheel surface to some extent. One common type of imperfection is a phenomenon called wheel flats. These occur as the train wheels lock during braking, causing the wheel tread to get ground by friction. These are however to be considered

defects and their occurrence should be limited with proper maintenance routines. Any effects arising from this phenomenon would stem from faulty maintenance and thus fall under accidental load, which is considered in ULS. Furthermore, Nielsen and Igeland (1995) demonstrates that these effects are most prominent in speed ranges far below the operating speeds of conventional high speed trains. Since this thesis deals with high speed and SLS conditions, wheel imperfections are considered to fall outside the scope of this report and will hereafter be neglected.

3 Model development

In order to perform dynamic analysis including a realistic vehicle model it is critical that the modelling choices are well-examined. The dynamic interaction behaviour will be modelled in 2D for computational efficiency reasons, as the main area of interest is vertical deflections and accelerations. This chapter explain the algorithms used for the models of different complexity, which parameters are critical for accurate results and the final model used in further analysis.

Arvidsson (2014) showed that modeling the bridge-vehicle interaction system instead of using a traditional axle load approach could reduce the bridge accelerations up towards 20 % for bridges with spans shorter than 30 m. Therefore is it critical to consider this approach when evaluating the vehicle comfort criteria. The reduction will not be as apperant in this chapter since only single loads will be applied to the bridges, however the impact will be greater in Chapter 4 where a multi-point vehicle will be applied.

3.1 Bridge model

The bridge type being evaluated is a reinforced concrete slab bridge as seen in Figure 2.5. There are multiple ways to model this system in commercially available FEM-software. The element type used in the model could be 3D solids of high order which would give an accurate simulation with regards to localized effects and plate eigenmodes, however this approach is computationally costly and therefore not ideal for this thesis where a large amount of bridge configurations will be evaluated. Another option would be to use 3D shell elements since they also can describe plate eigenmodes but are much more performant. The final approach would be to use 2D beam elements which are very fast but can only describe vertical bending and axial eigenmodes. Since plate modes are not as predominant for solid slab sections as for more slender hollow box or girder structures, the 2D beam element type was chosen to be used in later analysis.

The section is assumed to remain uncracked during loading. Since reinforcement has little impact on the sectional stiffness in uncracked state reinforcement has been omitted from the FEM-models. Furthermore all materials are assumed linear elastic and sections are homogeneous isotropic with a constant cross section.

3.1.1 Single layer bridge model

Initially the bridge deck is modelled as a single simply supported 2D Euler Bernoulli beam as seen in Figure 3.1. This model is used as a basis for evaluation of the vehicles models in Section 3.2. The bridge data used in the development phase is listed below in Tables 3.1 and 3.2. As a comparison a Timoshenko beam approach was also evaluated which explains the included shear deformation factors in the data table.



Figure 3.1: Single simply supported Euler Bernoulli beam

Table 3.1: Bridge geometric properties for single layer model

Parameter	Description	Value
L	Length span [m]	19.53
w	Width deck [m]	6.80
h	Height deck [m]	1.00
A	Area deck [m ²]	6.81
I	Second moment of inertia [m ⁴]	0.570

Table 3.2: Bridge material properties for single layer model

Parameter	Description	Value
E	Young's modulus [GPa]	35.0
ν	Poisson's ratio [-]	0.20
G	Shear modulus [GPa]	21.9
κ	Shear correction factor [-]	0.86
ρ	Density [kg/m ³]	$2.40 \cdot 10^3$
ξ	Damping percentage of critical damping [%]	1.50
α	Rayleigh damping coefficient [-]	0.87
β	Rayleigh damping coefficient [-]	$2.71 \cdot 10^{-5}$

The height of the section is designed using the algorithm presented in Figure 3.2 using the span length of 19.53 m and a maximum vehicle speed of 350 km/h. Using this span length is convenient since it is a multiple of the sleeper spacing of 0.63 m. This algorithm is used to design deck sections that will later be applied in the final model.

In order to determine the damping coefficients presented above, a frequency analysis was performed and the accumulative *effective modal mass* was studied. Notably, when looking at Table 3.3, there exist a number of zero value entries in the column for the effective modal mass. These modes are either axial or symmetrical in the examined vertical direction and thus do not contribute towards the total effective modal mass. When considering eigenmodes up until the 6th mode, a total of over 90% of the bridge mass is covered. This is deemed sufficient for choice of maximum frequency considered in Rayleigh damping model according to guidelines presented in Section 2.4.9.

Design deck section using LM71 train model
and simplified analysis from SS-EN 1990
A2.4.4.3.2

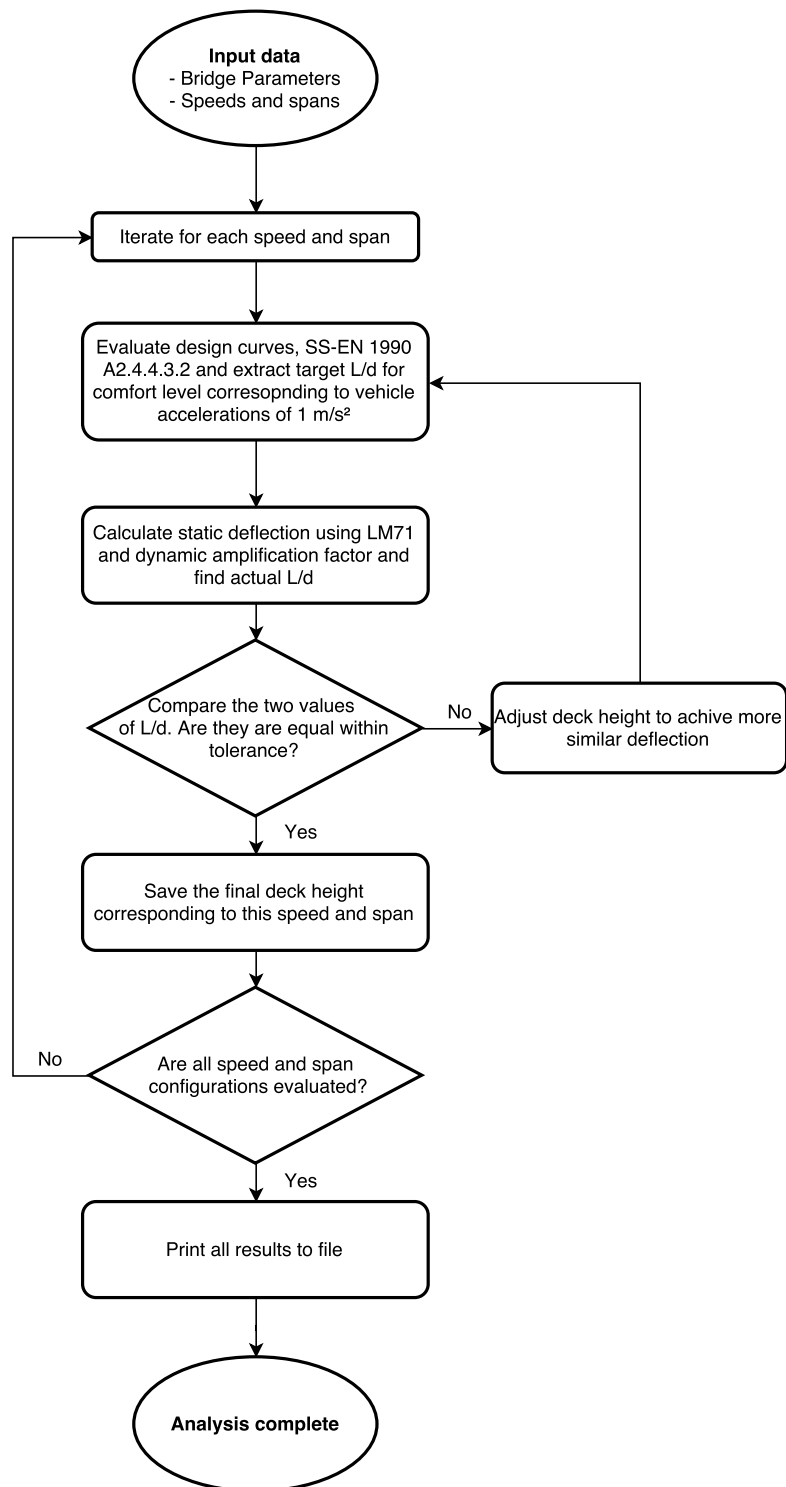











Figure 3.2: MATLAB algorithm for design of section height according to SS-EN 1990 A2.4.4.3.2.

Table 3.3: Eigenfrequencies and accumulative modal mass in y-direction for each eigenmode below 200 Hz. Total effective modal mass is displayed as part of total mass.

Mode	Effective modal mass [kg]	Frequency [Hz]	Total effective modal mass	Mode shapes
1	$2.58 \cdot 10^5$	4.5	80.9%	
2	0	17.9	80.9%	
3	$2.83 \cdot 10^4$	39.5	89.7%	
4	0	68.5	89.7%	
5	0	97.8	89.7%	
6	$9.95 \cdot 10^3$	103.8	92.8%	
7	0	144.5	92.8%	
8	$4.96 \cdot 10^3$	189.6	94.4%	
9	0	195.5	94.4%	

3.1.2 Two layer bridge model

In order to obtain a realistic response in the final analysis a two layer bridge model is introduced, see Figure 3.3. This new model includes inertia effects from the rail and sleepers and the internal stiffness and damping properties of these elements. The rail which is assumed to be of type UIC60 is modeled as an Euler beam and the reinforced concrete sleepers is modeled as discrete point mass elements. Material parameters for this extended model is found in Table 2.3.

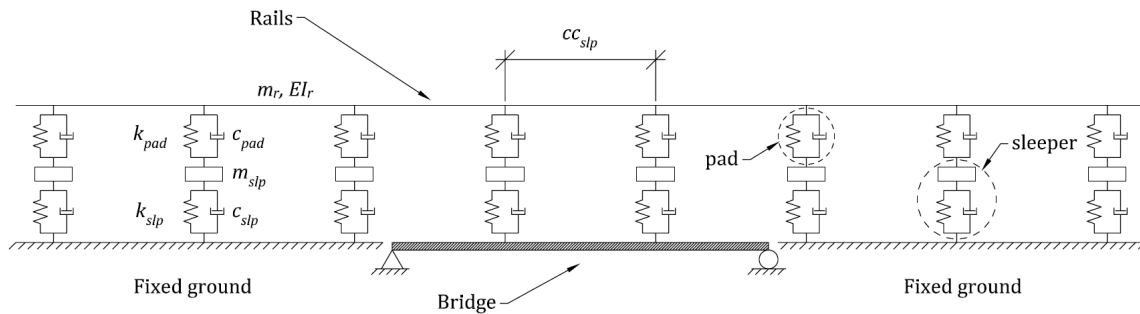


Figure 3.3: Two layer bridge model. This model is much more refined than the simple one-layer bridge model. It incorporates sleepers as discrete inertia points connected with a vertical spring-dashpot system to the bridge and rail beam elements. The subsoil is assumed to be completely fixed and the bridge is modelled with immovable supports.

3.2 Vehicle model

In this part of the vehicle development phase modelling choices for a single point load and wheel will be analyzed and evaluated. A point load model will be compared to a wheel model and a wheel-bogie model as seen in Figure 3.4. The wheel models will be used to evaluate the impact of imperfections, contact modelling and integration method. It is assumed that the bridge are constructed with an upward camber, therefore deflection caused by self-weight of the structure will be neglected.

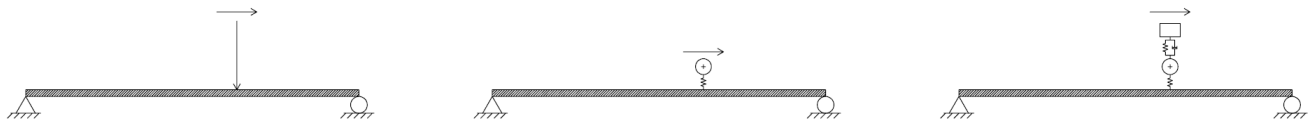


Figure 3.4: Single vehicle models ranging from a single point load to a single wheel and finally a single bogie.

In order to evaluate modeling properties for these interaction models, a MATLAB script was created. The main algorithm of this program can be seen in Figure 3.5. This model is very flexible for evaluation of various dynamic bridge and vehicle parameters such as contact definition of imperfection profile. The model is currently limited to only a single moving wheel or wheel-bogie system however it could be expanded into supporting multiple vehicles. This model was mainly used in the preliminary analysis phase. Results were derived using the explicit Central Difference Method (CDM) in order to be similar

to the numerical integration applied in ABAQUS/Explicit. A further comparison between integration methods is outside the scope of this thesis and will not be performed.

Matlab algorithm - Single point vehicle

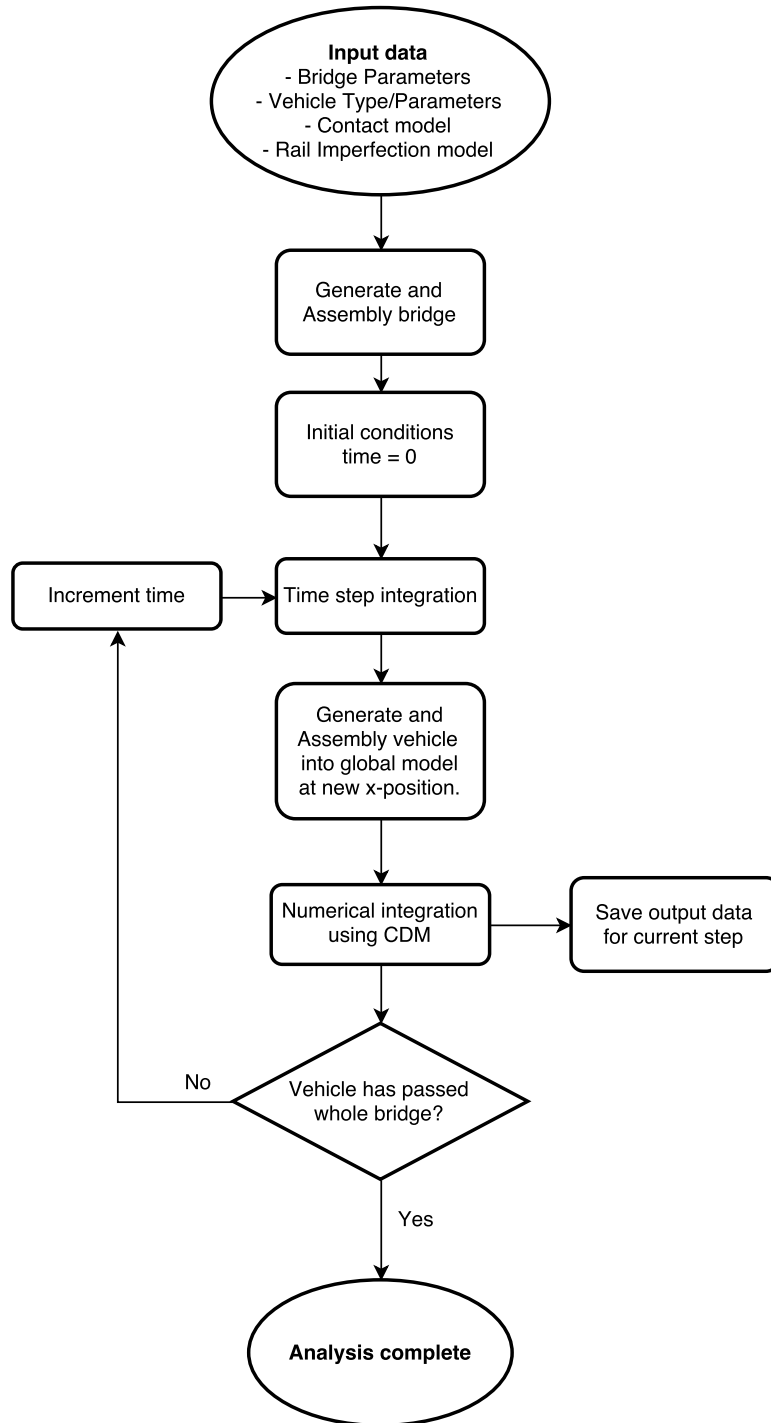


Figure 3.5: MATLAB algorithm for vehicle model evaluation.

Digital signal processing in the form of a Butterworth filter is applied in order to reduce the noise and get more accurate results. The cutoff frequency is determined from the regulations specified in Section 2.3.1. For a simply supported bridge with span length of 19.53 m, a cutoff frequency of 39.473 Hz, which corresponds to the third bending mode, is applied. The shape of the filter can be visualized in Figure 2.30. ABAQUS does only support second order Butterworth filtering, so to be able to higher order filters raw data had to be extracted from ABAQUS into MATLAB where the much more powerful signal processing toolbox could be applied. Acceleration data from MATLAB has been filtered with a sixth order Butterworth filter in order to get a sharper cut-off region than for lower order filters.

As a validation of the MATLAB results, another algorithm which is based on ABAQUS was used. A flowchart describing this algorithm is seen in Figure 3.6. ABAQUS/Explicit has a very flexible and modular contact module which is incorporated into the model instead of a discrete spring as in the MATLAB model. This contact definition does create a lot of high frequency noise into the results which means the same low-pass filter used in the MATLAB approach has to be applied here as well. This algorithm is applied in both the evaluation phase where dynamic parameters are studied as well as in the final analysis where results are compared to the simplified comfort analysis presented in Eurocode.

3.2.1 Single moving point load

The dynamic response for a single moving point load as seen in Figure 3.7 is evaluated using the analytic solution presented in Section 2.4.5 in conjunction with bridge data from the single layer bridge in Section 3.1.1. The point load magnitude has been chosen to be equal to the weight of one wheelset with a bogie. Figure 3.8 shows an example on the midpoint deflection while the moving load moves along the bridge at a velocity of $75 \text{ m/s} = 270 \text{ km/h}$. Figure 3.9 shows the corresponding accelerations.

This dynamic system has been evaluated for multiple speeds in order to create an envelope which is presented in Figures 3.10 and 3.11. These tests will function as a basis of comparison when more complex vehicle models and behaviour are introduced.

Abaqus Algorithm
Advanced bridge-vehicle interaction model

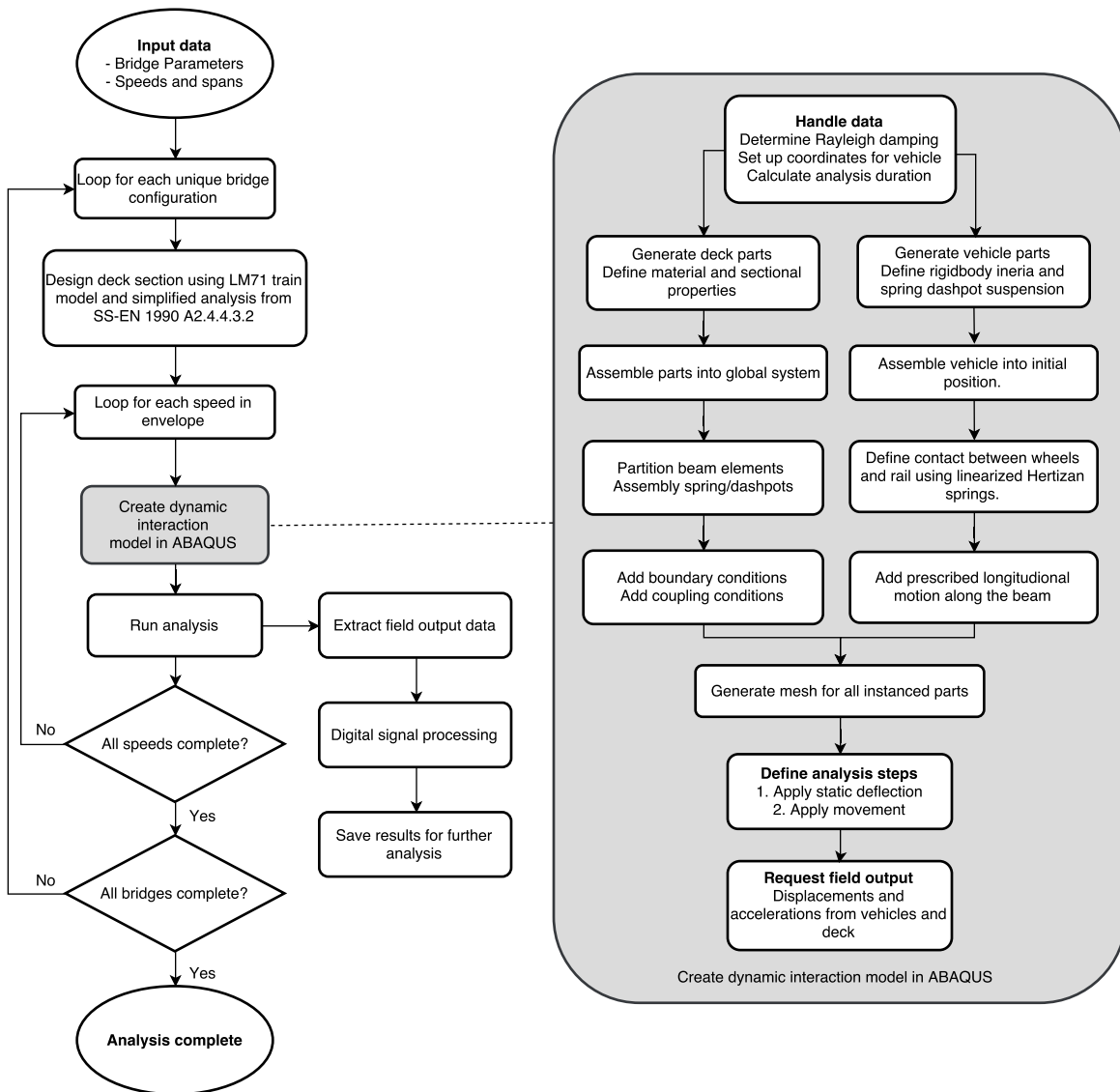


Figure 3.6: ABAQUS/Explicit algorithm for vehicle-bridge model evaluation.

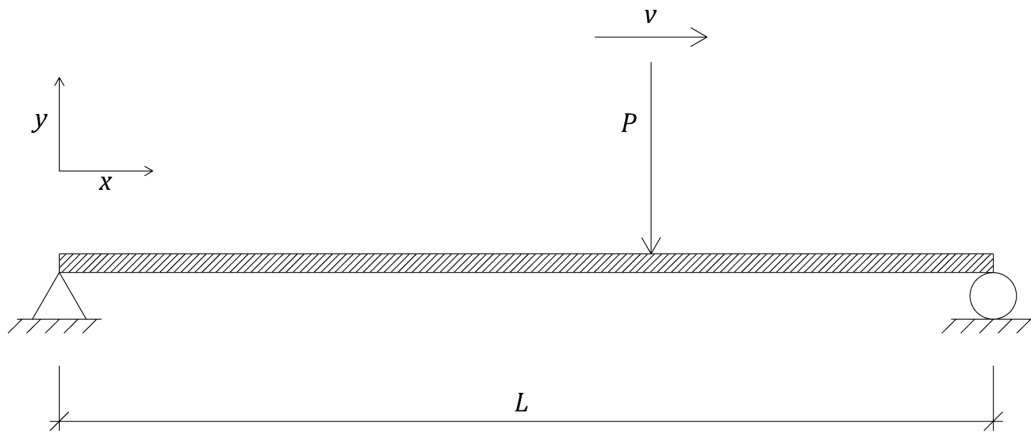


Figure 3.7: Single moving point load applied on a homogeneous E-B beam.

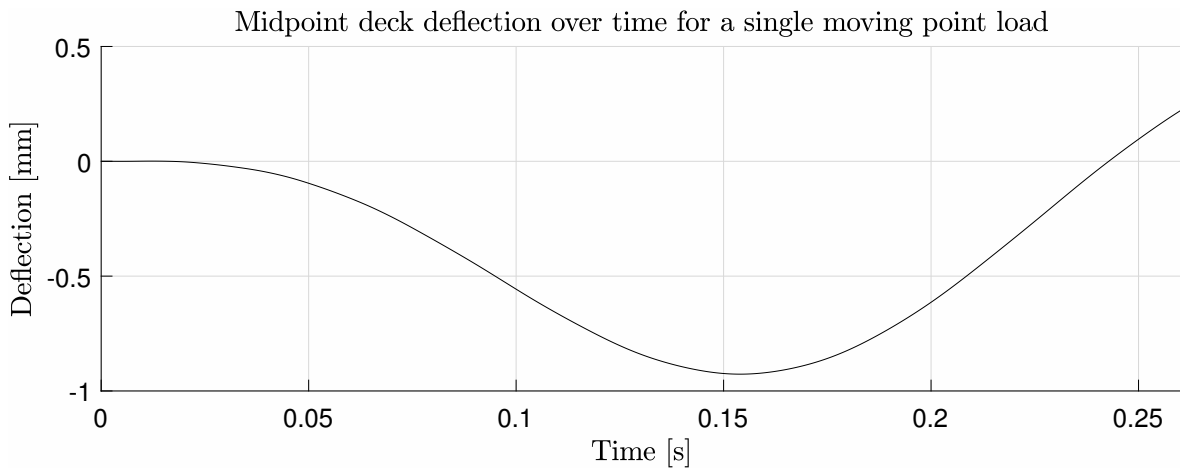


Figure 3.8: Deflection in the middle of a E-B beam subjected to a moving load equal to the weight of a wheel-bogie-system.

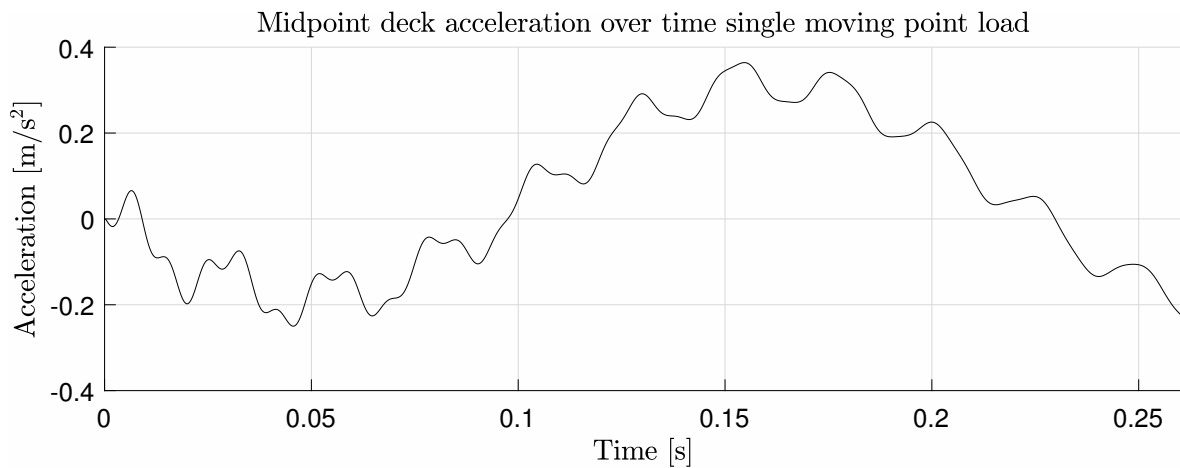


Figure 3.9: Acceleration in the middle of a E-B beam subjected to a moving load equal to the weight of a wheel-bogie-system.

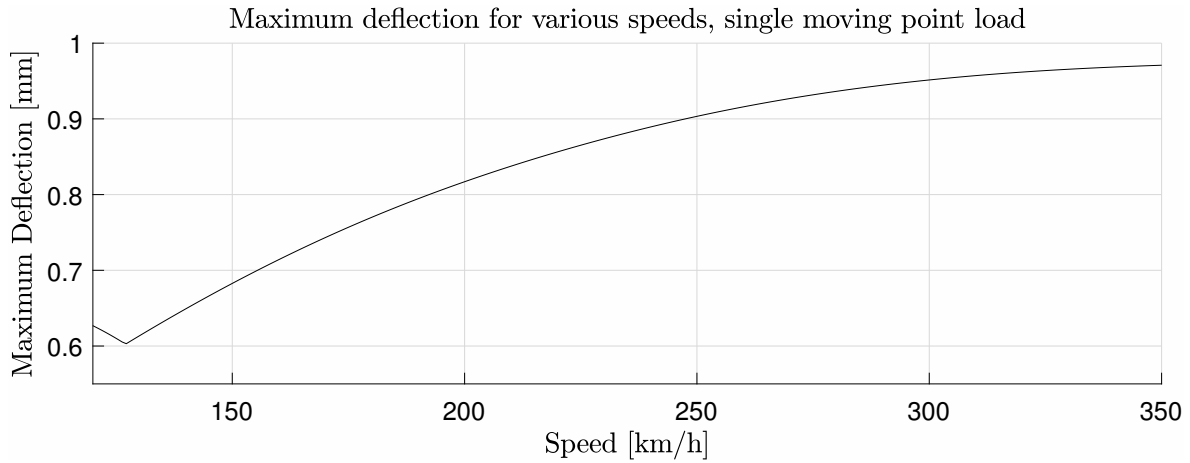


Figure 3.10: Midpoint deflection envelope for a moving load at various speeds.

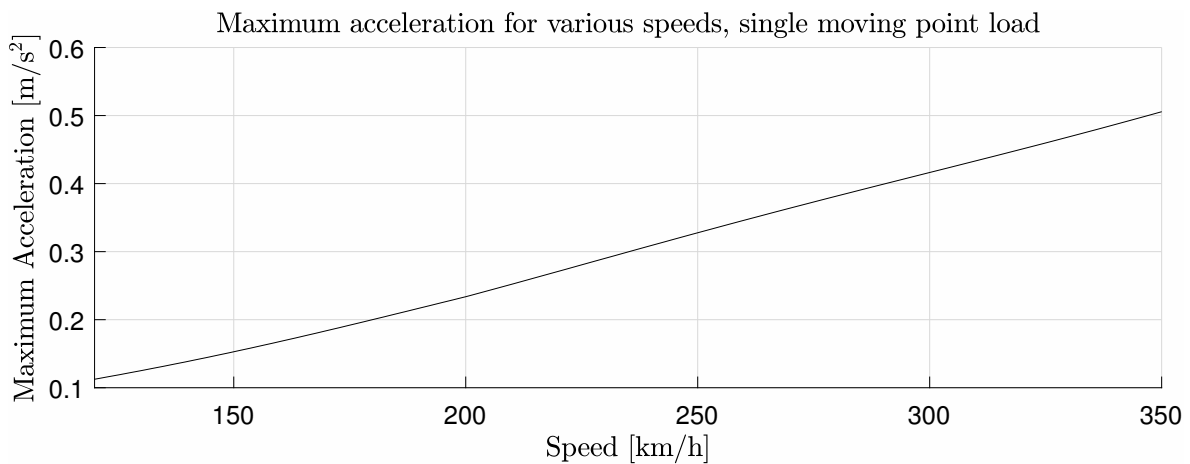


Figure 3.11: Midpoint acceleration envelope for a moving load at various speeds.

3.2.2 Single moving wheel system

For this model, a wheel accompanied by a spring-connected point-mass is introduced instead of the more simple point load approximation. The stiffness of the contact is formulated using a linearized Hertzian spring and a nonlinear Hertzian spring as discussed in Section 2.7.1. The mass, m , of the wheel represents the equivalent mass of a wheel and a bogie in order to be able to compare results between the models. The wheel is free to move vertically and has a prescribed longitudinal motion equal to the velocity, v . The wheel has no rotational degree of freedom and moves without friction. A schematic model may be seen in Figure 3.12.

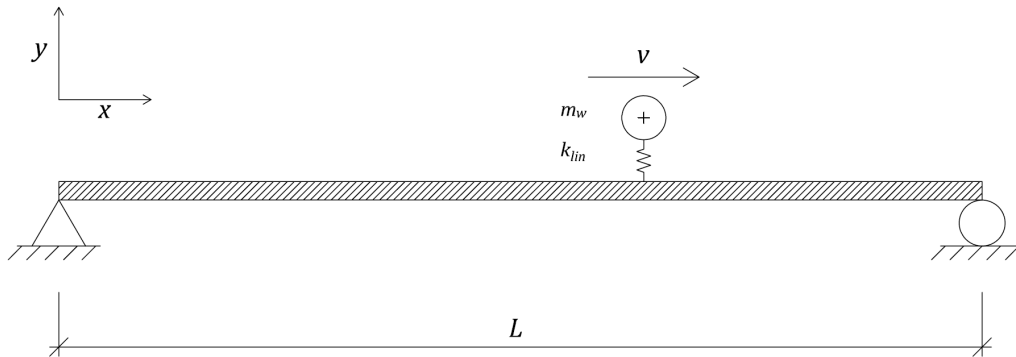


Figure 3.12: Single moving wheel applied on a homogeneous E-B beam.

The system is modelled using the finite-element method Ottosen and Petersson (1992) using a moving element implementation by Lei (2017). The model is created using MATLAB (2017) and the FE-toolbox CALFEM (2004). The problem is solved incrementally using Newmark- β and the Central Difference Method and the results are compared. The solution algorithm used is the one presented in Figure 3.5. Convergence study was performed for mesh density and it was found that a deck element size of 2 m was sufficient for this analysis.

Initial conditions are set so that static deflection of the vehicle is applied and the deck is completely horizontal and at rest. Another approach would be to use step-wise ramping of the external force vector and allowing the system to find static equilibrium. The first approach is preferred over the ramping method since the computational time is reduced drastically.

The contact between the wheel and the beam was modelled as a vertical spring. Using this approach assumes there are no tangential friction or loss of contact between the rail and wheel. In order to simulate loss of contact a linearized spring and a Hertzian spring is implemented in addition to constant stiffness. The linearization is performed using Eq. (2.73) which yields the linearized contact stiffness $k_{lin} = 2.145 \cdot 10^9$ N/m for a single wheelset. The influence of the different contact models can be seen in Figures 3.13 and 3.14. A distinct increase in maximum deflection of the bridge can be seen in the wheel-vehicle model compared to the simple point load model. The difference in bridge response for the single wheel model is very small. Further tests will therefore be performed using the linearized contact approach, as this is more easily implemented in ABAQUS.

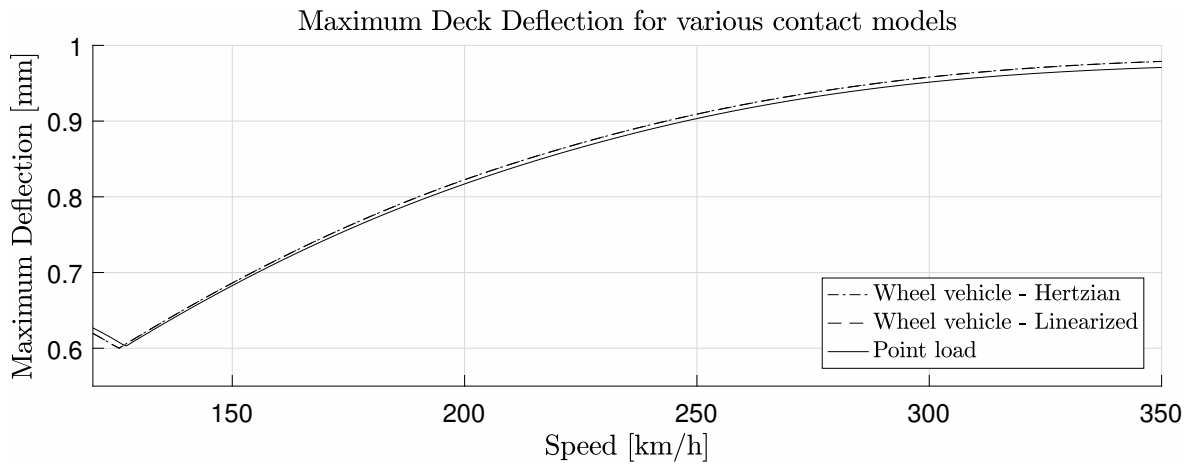


Figure 3.13: Deck deflection envelope for various speeds for Hertzian and linearized contact models of the single wheel system.

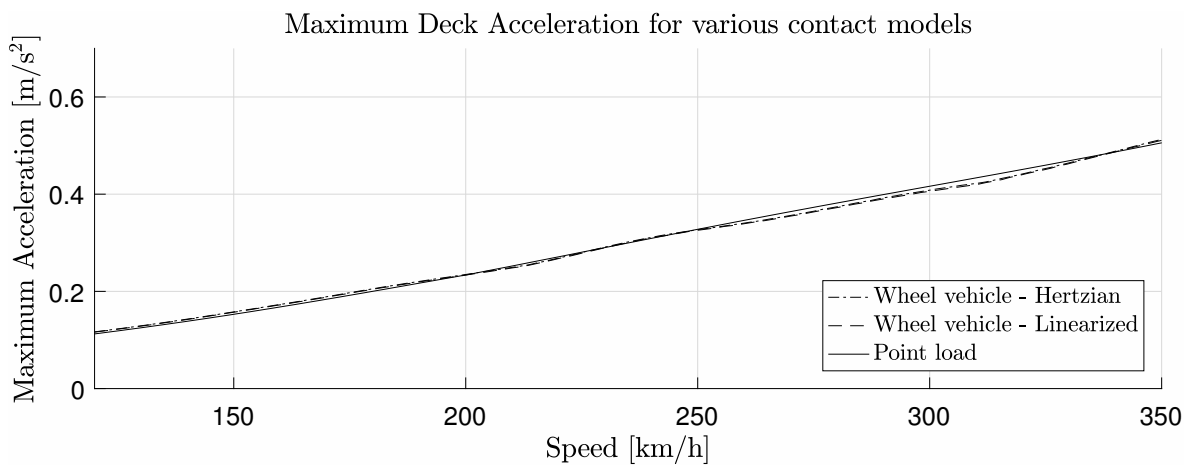


Figure 3.14: Deck acceleration envelope for various speeds for Hertzian and linearized contact models of the single wheel system.

Euler-Bernoulli and Timoshenko beam formulations have been evaluated for the single wheel model with a linearized contact formulation and no imperfections. The influence of beam formulation has been evaluated and results are presented in Figures 3.15 and 3.16. Both yield very similar results for the single layer bridge profile defined in Section 3.1.1.

The impact of rail imperfections due to corrugation on the wheel response has been evaluated and the results are presented in Figures 3.17 and 3.18. For this vehicle model a small variation in the deflection can be seen. The results seem to correspond well with conclusions from Nielsen and Igeland (1995) that stated that loss of contact occur for around and above 100 km/h and resonance appear at very low speeds. This effect will remain in the model until more complex vehicle models are introduced.

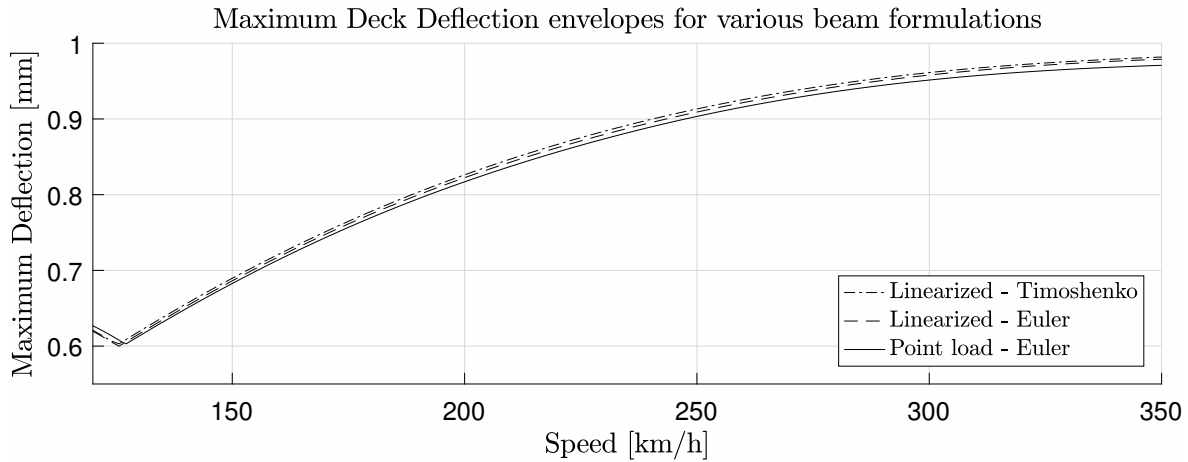


Figure 3.15: Deck deflection for various beam formulations for a single moving wheel with linearized contact and no imperfections.

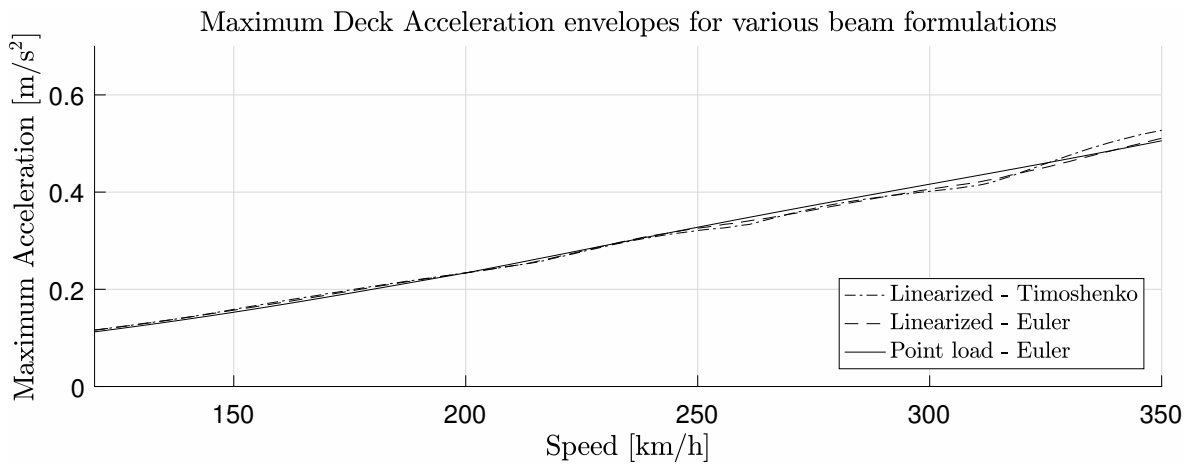


Figure 3.16: Deck acceleration for various beam formulations for a single moving wheel with linearized contact and no imperfections.

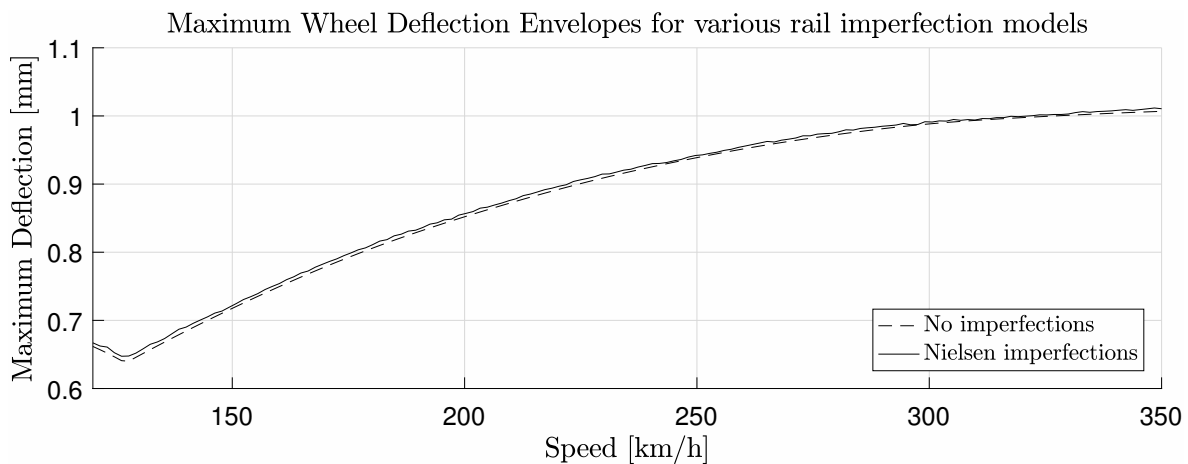


Figure 3.17: Wheel deflection envelopes for various imperfection models.

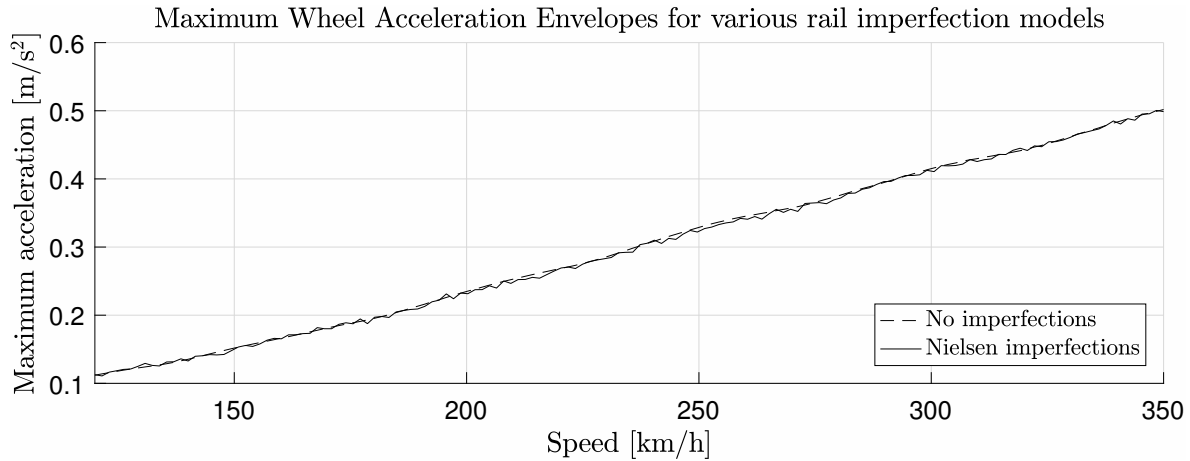


Figure 3.18: Wheel acceleration envelopes for various imperfection models.

This single wheel vehicle evaluation seems to indicate that a model based on a linearized Hertzian contact formulation with rail imperfections moving along an Timoshenko beam is critical with regards to vehicle and bridge response. However, this vehicle isn't very realistic and could easily be expanded by introducing a bogie and internal suspension and damping. Section 3.2.3 will evaluate a slightly more complex vehicle model and the results will form the basis of the final bridge-vehicle interaction model.

3.2.3 Single moving wheel-bogie system

In this case, another layer of complexity is added to the model as seen in Figure 3.19. The system is now expanded to accommodate a wheel connected to a bogie with springs and dashpots. Relative horizontal motion is prevented for the wheel in relation to the bogie, by means of coupling all horizontal vehicle DOFs.

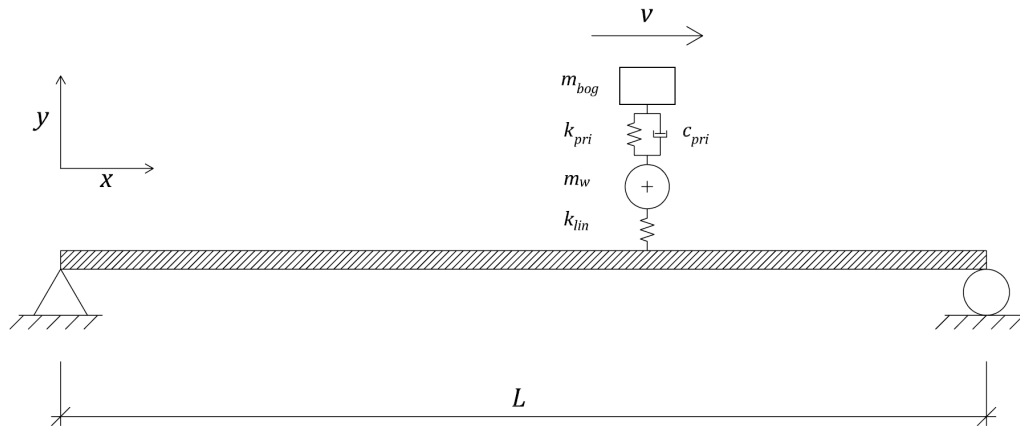


Figure 3.19: Single moving wheel-bogie system applied on a homogeneous E-B beam.

Firstly the importance of imperfections was evaluated for the wheel and bogie response as seen in Figures 3.20, 3.21, 3.22 and 3.23. These results seem to indicate that the influence is most important when considering DOFs close to the imperfection zone. The bogie is not very much affected by this effect due to the internal suspension and damping. Since this thesis aims to focus on the carriage response, which would be an additional level of complexity it is safe to assume that corrugation imperfections has very little impact in this speed range. Imperfections will therefore be neglected in the following evaluations.

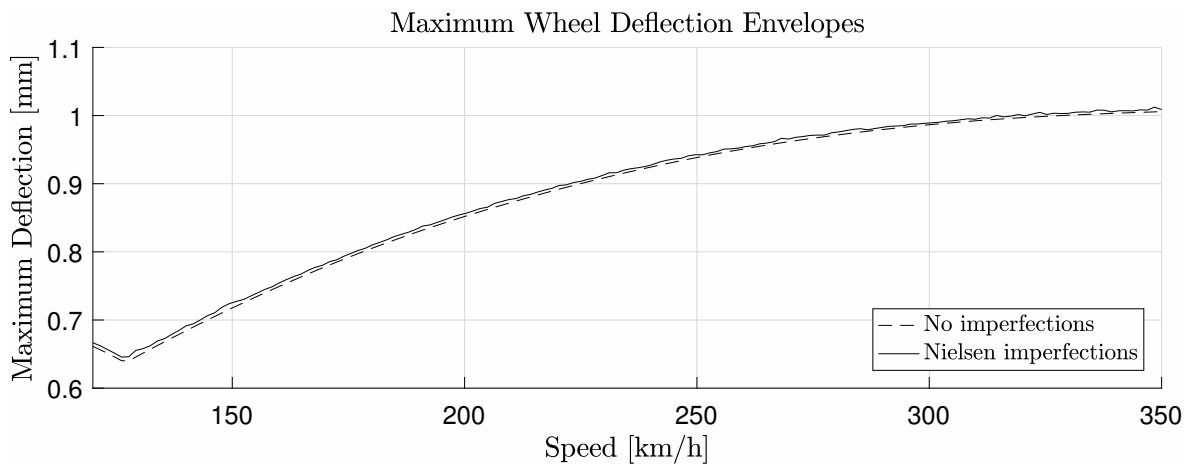


Figure 3.20: Wheel deflection in bogie-vehicle envelopes for various imperfection models.

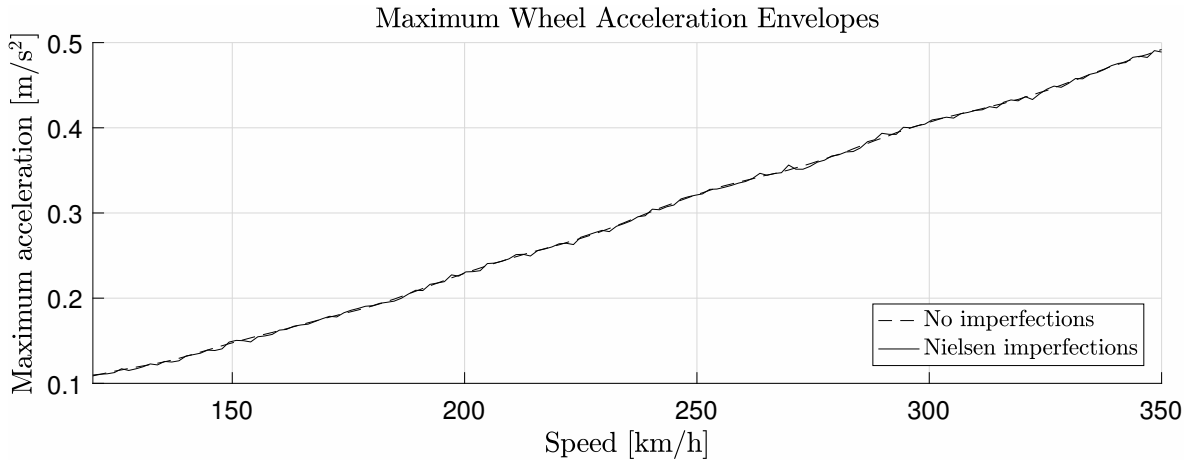


Figure 3.21: Wheel acceleration in bogie-vehicle envelopes for various imperfection models.

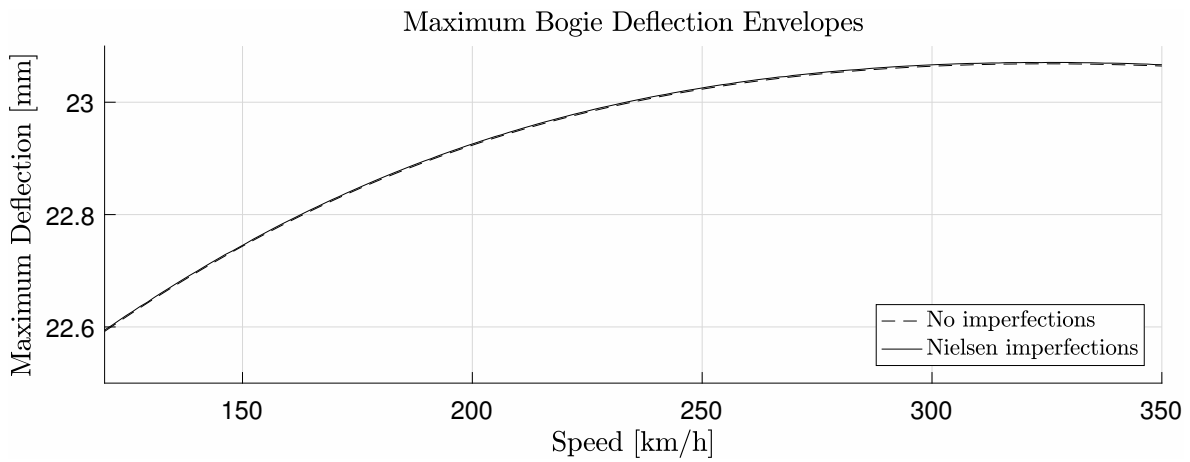


Figure 3.22: Bogie deflection envelopes for various imperfection models.

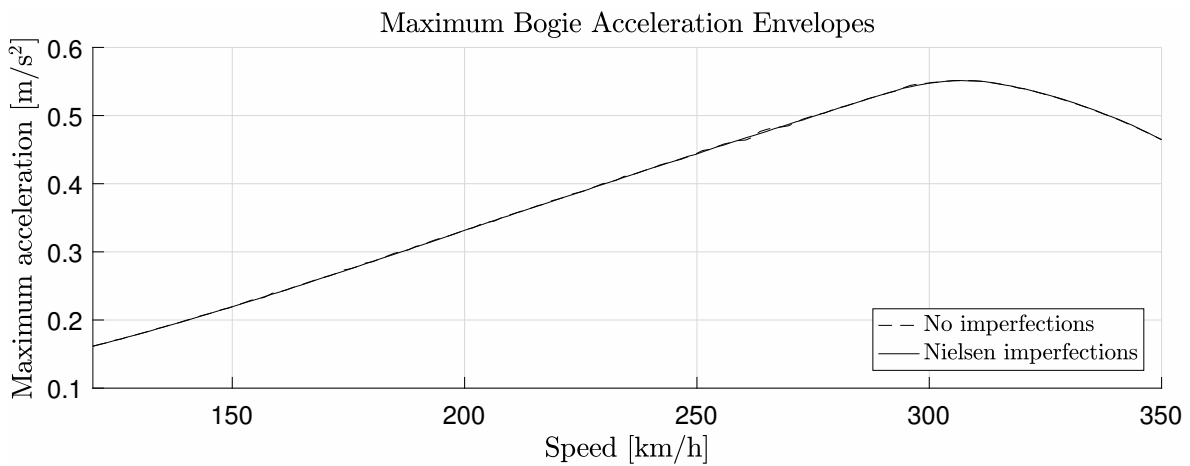


Figure 3.23: Bogie acceleration envelopes for various imperfection models.

The deck deflection and acceleration has been evaluated for the single bogie vehicle and the results are shown in Figures 3.24 and 3.25. The model used is based on results from the single wheel vehicle from Section 3.2.2. Euler-Bernoulli beam formulation is applied, wheel-rail contact is modelled as a linearized Hertzian spring and imperfections are neglected. Furthermore as verification of these results, an ABAQUS model according to Figure 3.6 is also created and analysed. By default, ABAQUS employs a Timoshenko beam formulation however the results should still be comparable according to the results shown in Figures 3.15 and 3.16.

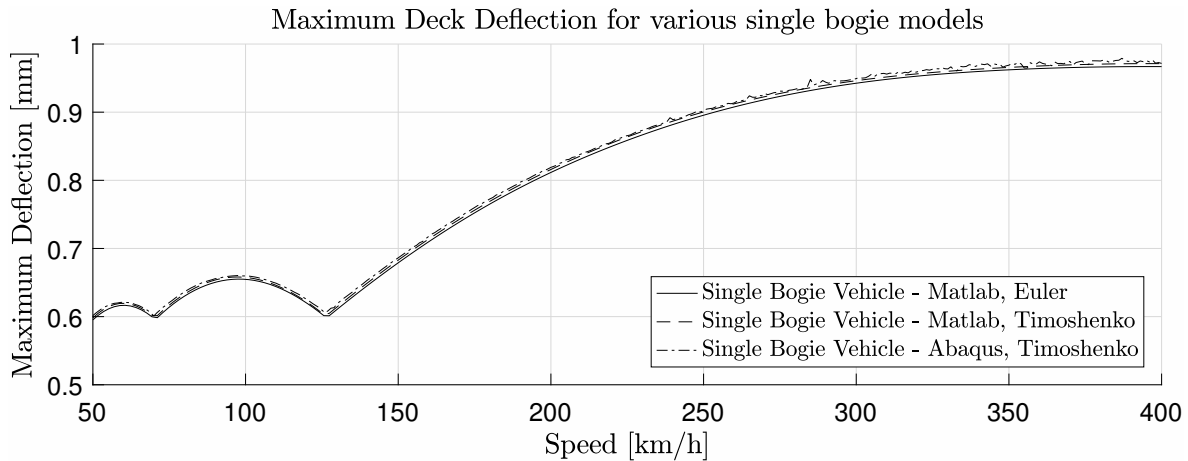


Figure 3.24: Deck deflection for final wheel model compared to point load model.

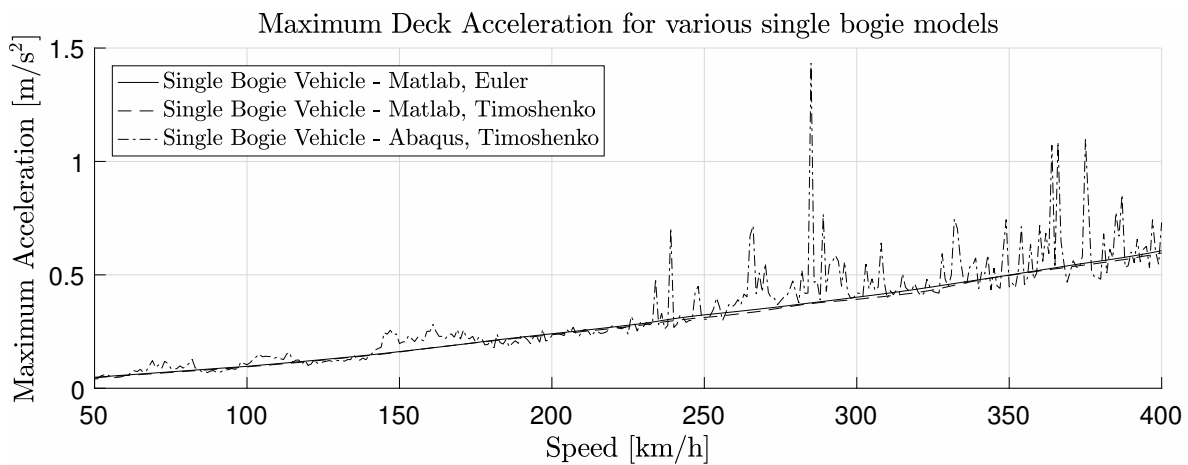


Figure 3.25: Deck acceleration for final wheel model compared to point load model.

The results show very similar response for the deflection however the acceleration is much more noisy from ABAQUS, even though a high order Butterworth filter is applied. The large amount of noise is likely caused by the contact formulation applied in ABAQUS/Explicit. Introducing a two-layer bridge model should result in smoother results of the bridge accelerations. High frequent noise will be located in the rail but not transferred through the sleeper-system to the bridge deck. Results from evaluation of the two-layer bridge is presented in Figures 3.26 and 3.27.

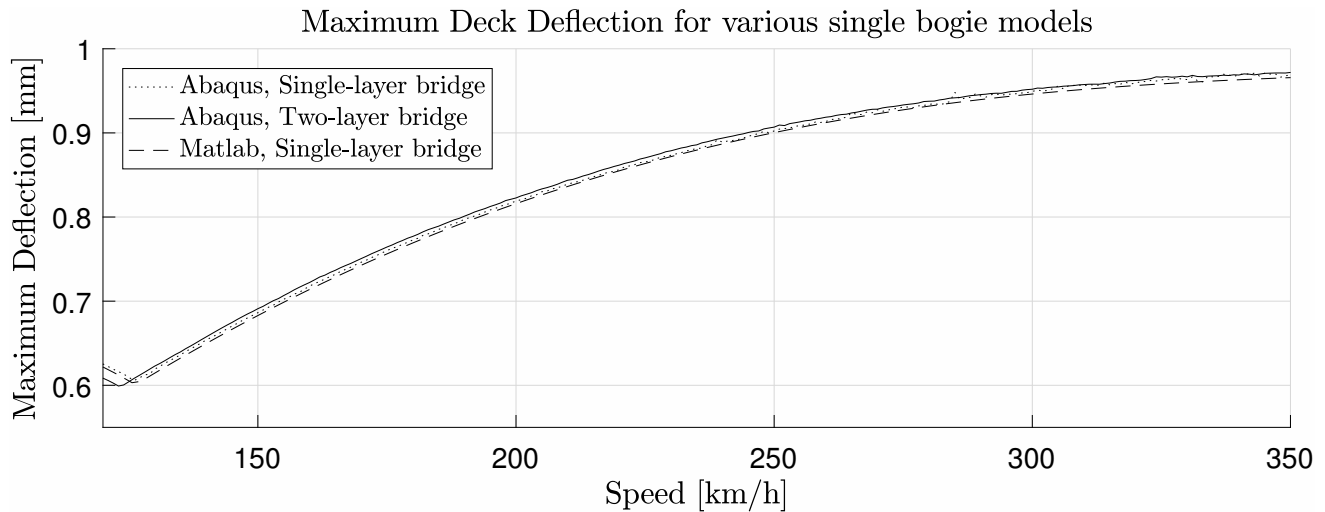


Figure 3.26: Deflection envelopes for various bridge models.

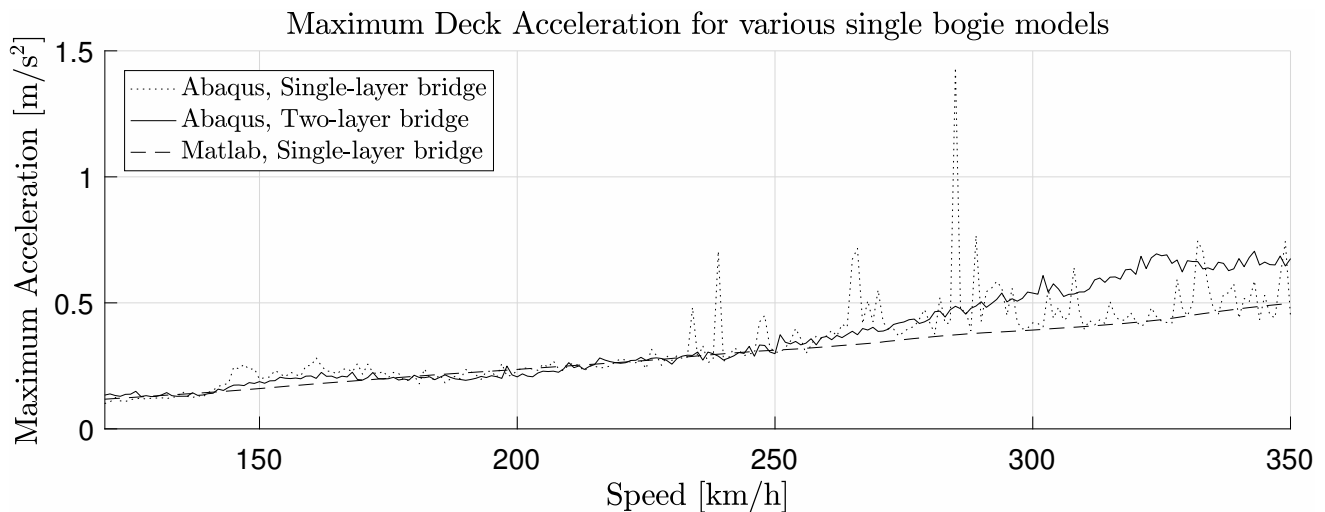


Figure 3.27: Acceleration envelopes for various bridge models.

From these figures the following conclusions can be drawn: firstly, introducing the second layer in the bridge model seems to generate much less noisy data. In order to achieve the results shown in Figure 3.27 the single-layer bridge data had to be filtered with a very high 20th order Butterworth filter while the two-layer only had to be filtered with a 2nd order filter. The internal dynamic bridge-sleeper-rail system seems to act as a natural filter since the wheel is no longer in direct contact with the bridge deck, which is more realistic. Secondly, the two-layer bridge seems to have most impact in the speed range above 250 km/h. Since this is within the range of interest it is crucial that the final evaluation model incorporates this feature.

4 Dynamic bridge analysis using final model

The final model incorporates a two layer bridge model and multiple complex three layer vehicles as seen in Figure 4.1. The internal vehicle suspension parameters are specified according to Section 2.1.2 and the wheelsets adopt a linearized contact formulation. The DOFs of this system are visualized in the schematic Figure 4.2. Most DOFs are limited to the vertical direction however rotary terms are defined for the car-body and bogies.

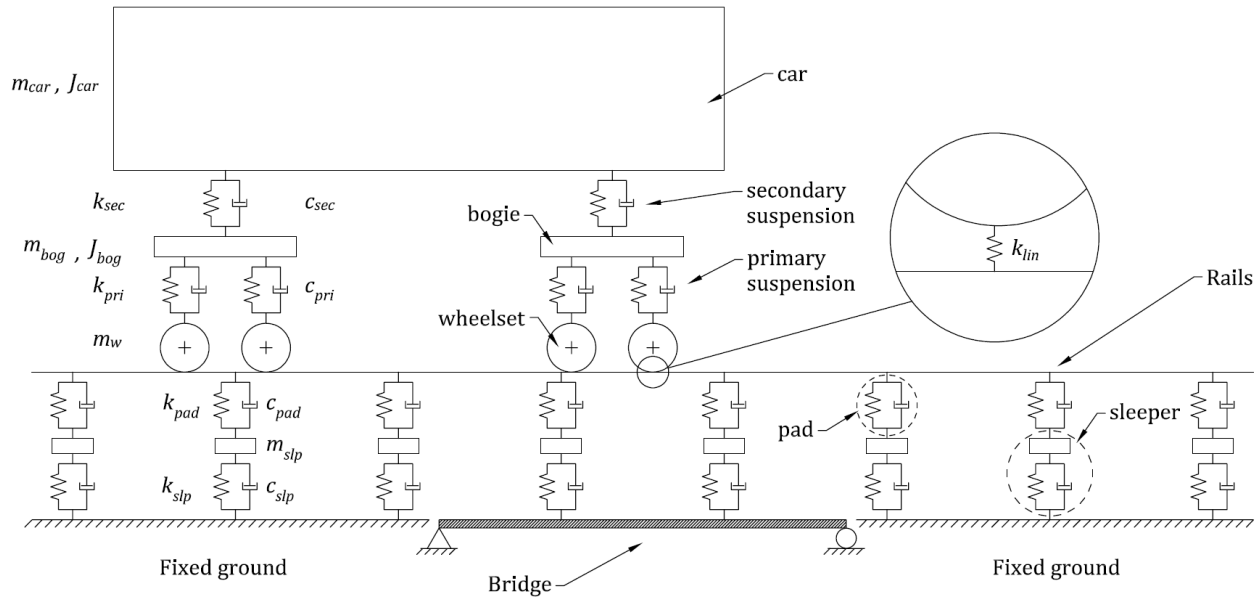


Figure 4.1: A schematic view of the final assembled model with dynamic components and properties highlighted.

4.1 ABAQUS model

At this stage, enough dynamic parameters has been evaluated in order to create an accurate bridge-vehicle interaction model in ABAQUS. Due to the complexity of each model, a scripting approach was chosen where input data could be specified and the model would be automatically created. The analysis algorithm used in this chapter is based on the one presented in Figure 3.6.

For a train with fifteen trailers and two locomotives traversing a bridge with a few short spans, the model would become over 900 m long. In order to illustrate the details of the model a few zoomed in views are presented. Figure 4.3 shows the assembled part. Bottom layer is the bridge deck, upper layer is the rail and each reference point represents a discrete sleeper. All boundary conditions are indicated by triangles. It is clear that the span is located just right of the origin where there are no boundary conditions applied. Each sleeper is locked in x-direction and is assumed to only be able to move vertically. Figure 4.4 visualizes all interactions and inertias active in the model. Line connections represent a discrete spring-

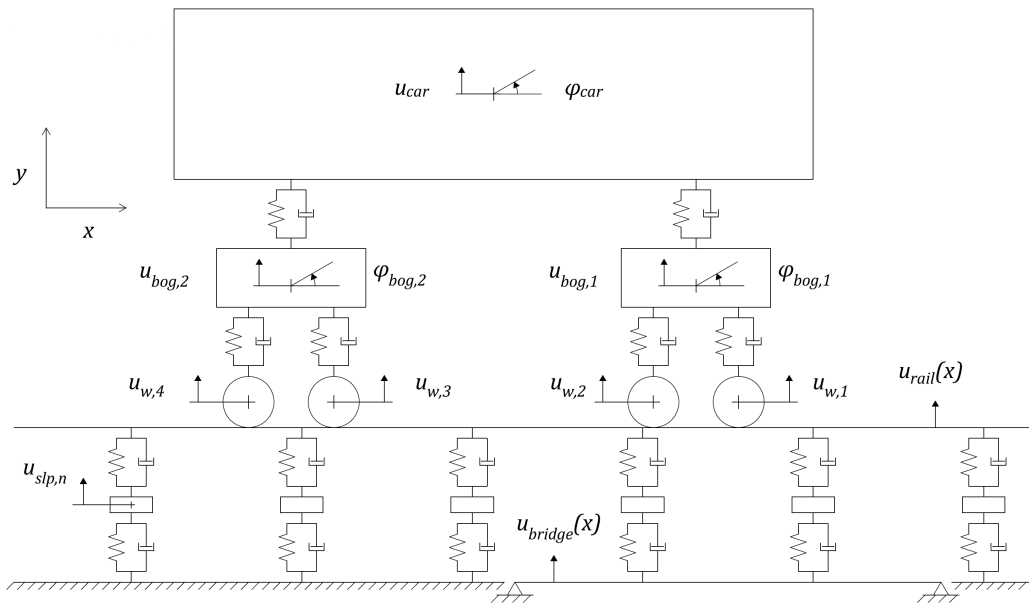


Figure 4.2: A schematic view of the final assembled model with degrees of freedom visualized.

dashpot connection. Solid boxes in each reference point represents points with a specified mass and rotary inertia. The hollow boxes along the rail represents a contact definition between the wheels and rails.

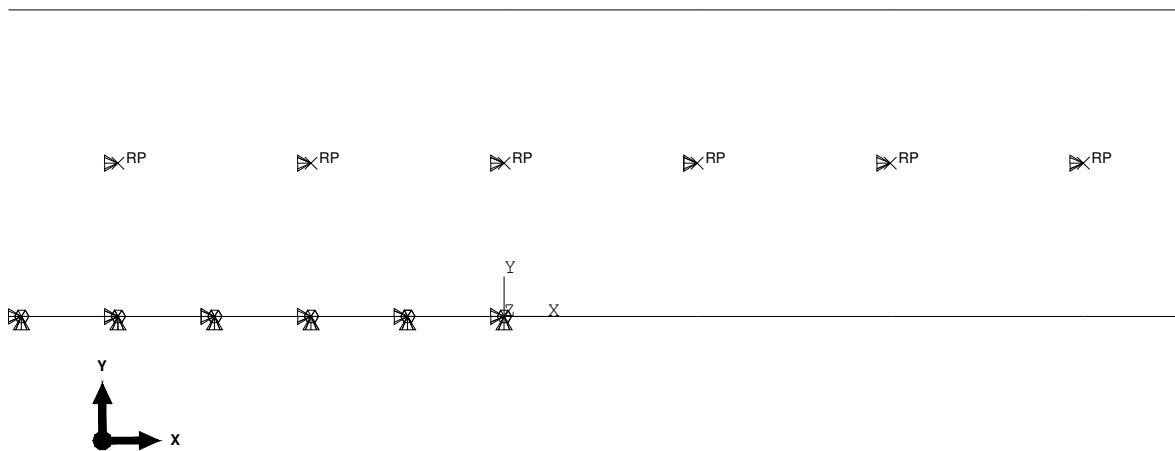


Figure 4.3: Small region of bridge deck with boundary conditions applied.

Figure 4.5 shows the assembly for a region of the model including a single motorcar. The vehicles are placed on a stiff ground layer and not the dynamic rail model as an optimization. This change in rail-model has been evaluated does not influence the dynamic behaviour on the bridge. Gravity is applied in the

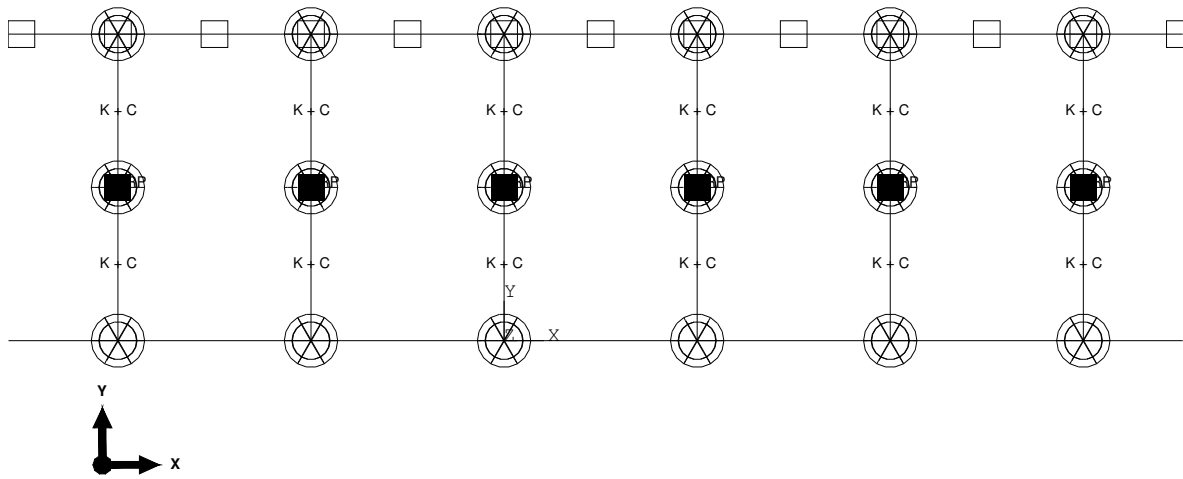


Figure 4.4: Small region of bridge deck with interactions and inertias.

centre of each vehicle part. Boundary conditions are also applied on these reference points with a prescribed horizontal motion at a specified velocity. The vehicle is free to move vertically and rotate around the z-axis. Finally Figures 4.7 and 4.6 shows the internal suspension and inertias applied in the centre of each rigid part. The hollow boxes on the wheels represents the contact surface that collides with the rail.

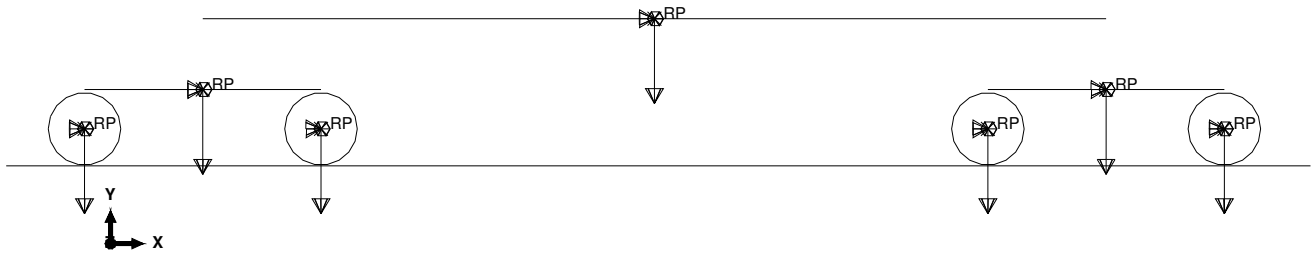


Figure 4.5: Boundary conditions and loads acting on the vehicle.

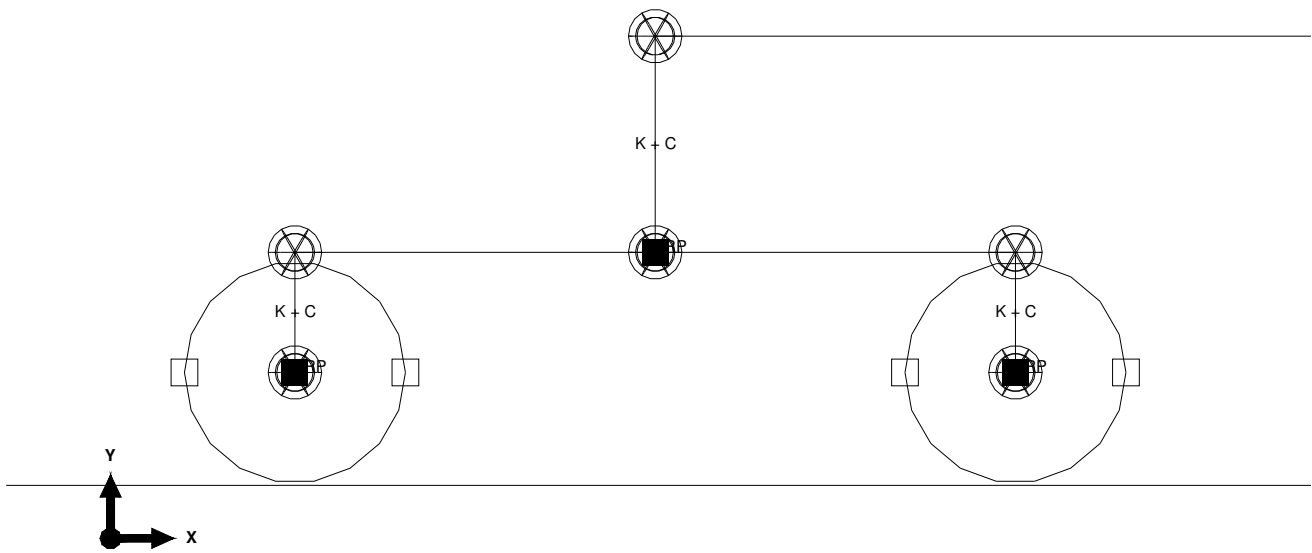


Figure 4.6: Detail of interaction system of a single motorcar bogie.

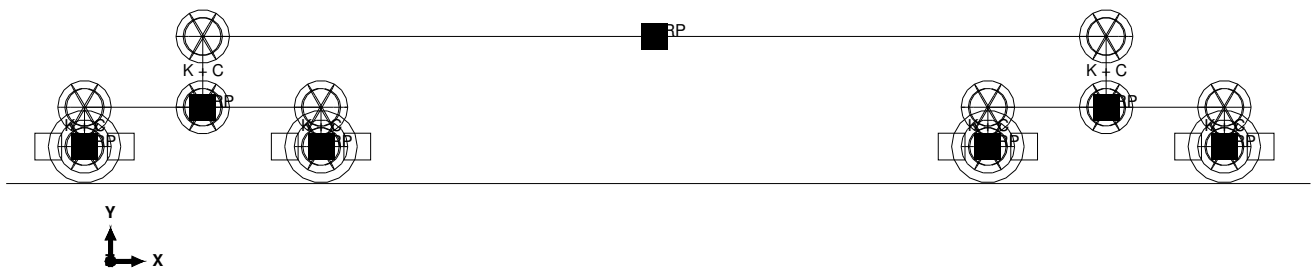


Figure 4.7: Spring-dashpot and contact interactions in a vehicle.

4.2 Convergence study

As stated in Section 2.3.3, Eurocode standards require dynamic models to include a sufficient amount of vehicles to cause maximum load effect in the longest span. One important aspect to consider in the final model is therefore the amount of train cars to include in the bulk of analyses forming the basis for the study as a whole. The bridges used for the convergence studies with respect to number of vehicles spans all have span length 24.57 m and 3 spans. The convergence studies shown in Figure 4.8 and Figure 4.9 were made at a speed of 287.5 km/h, corresponding to an apparent resonance speed according to preliminary results. There is an interest to know how the model behaves for a passenger car amount less than and greater than the exact value of 14, as presented in Section 2.1.2. Therefore, an analysis performed with 30 vehicles is taken as the exact value for comparison.

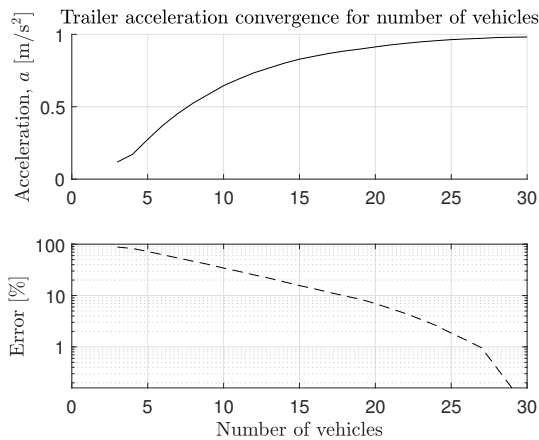


Figure 4.8: Convergence of trailer accelerations with regard to number of vehicles used in the analysis.

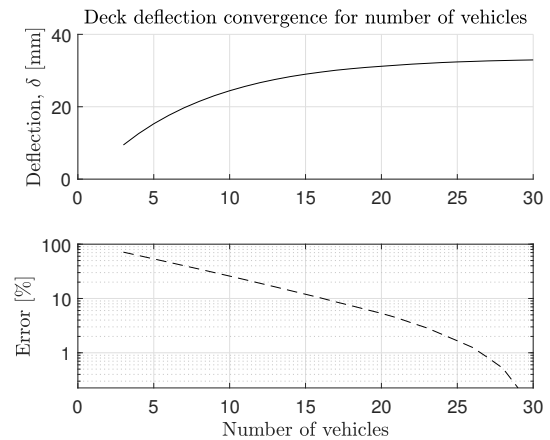


Figure 4.9: Convergence of bridge deflection with regard to number of vehicles used in the analysis.

A convergence study was made also for the same span length but at a speed that did not constitute a resonance peak; 320km/h. This was done in order to examine whether a more favorable convergence behaviour was present in the regions of the speed-span space outside of the resonance areas. As these make up the most part of the analyzed data, analyses based on this convergence study would still yield good results for a majority of the data set while potentially saving computing power. The results of this study is shown in Figure 4.10 and Figure 4.11. When the obtained results displayed a relative error less than 1 %, the number of cars was deemed sufficient. For a non-resonant peak this would correspond to 11 cars however for resonant peaks the convergence is not as apparent. Thus, the chosen number of vehicles was henceforth taken as the full train length consisting of 2 motorcars and 14 passenger trailers.

Bridges used for the convergence studies seen in Figure 4.12 and Figure 4.13 are of span length 24.57 m and are analyzed with 11 vehicles. These studies were also performed at the apparent resonance speed of 287.5 km/h. An analysis performed with 20 spans was taken as the exact value for comparison. As these studies showed convergence for a relatively low set of spans, it was deemed unnecessary to perform a second convergence study for a non-resonance speed for the sake of attaining faster convergence and in

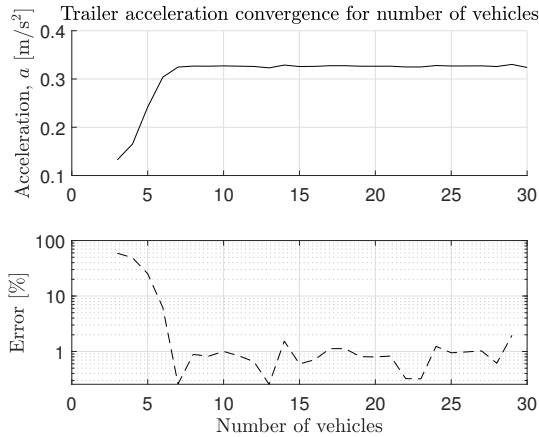


Figure 4.10: Convergence of trailer accelerations with regard to number of vehicles used in the analysis.

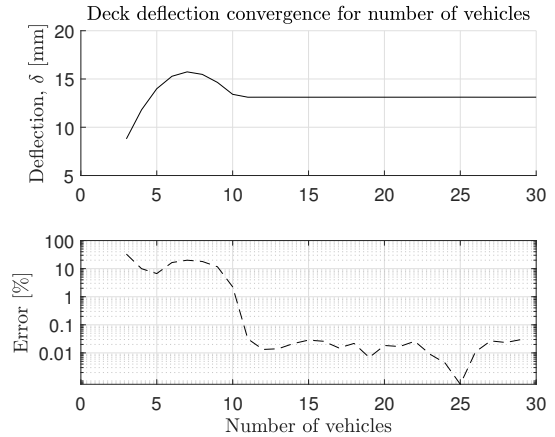


Figure 4.11: Convergence of bridge deck deflection with regard to number of vehicles used in the analysis.

turn cutting analysis times. The sufficient number of spans in order to obtain a low relative error should be 5 according to Figure 4.12, however analyses with more than 3 spans were excluded as an option for the main batch of analyses, as they were found to be to time consuming with the available FE-software.

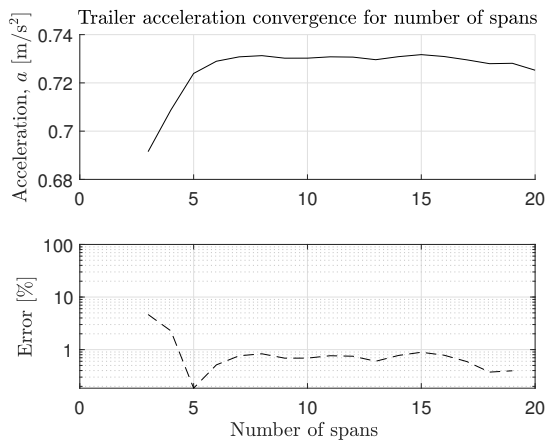


Figure 4.12: Convergence of trailer accelerations with regard to number of spans used in the analysis.

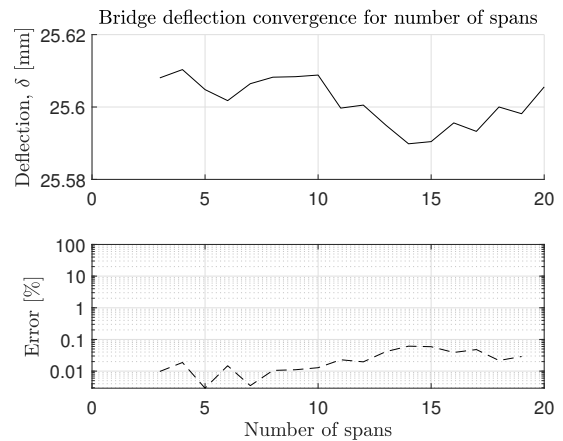


Figure 4.13: Convergence of bridge deck deflection with regard to number of spans used in the analysis.

A convergence study of the data sampling rate has been performed where some vehicle and bridge results has been evaluated, as seen in Figures 4.14, 4.15, 4.16 and 4.17. Ideally a very few data points should be extracted to optimize the performance of the model however this would sometimes yield poor results. When evaluating the dynamic vehicle response a sampling time interval of $2^{-7} \text{ s} = 0.00781 \text{ s}$ was chosen since this results in an minor error of $\sim 0.008\%$. This statement also holds for the deflection of the deck. However when evaluating the deck accelerations it is critical that sufficient number of data points are sampled in order for the second order Butterworth filter to function as intended. The filter could not be

applied for sample increments less than 2^{-6} which explains the diverging behaviour in Figure 4.16. This was because the amount of data points were too few according to the Nyquist Theorem, Section 2.6.4. In order to achieve good acceleration data the sampling time interval was chosen to 2^{-10} s \approx 0.00098 s.

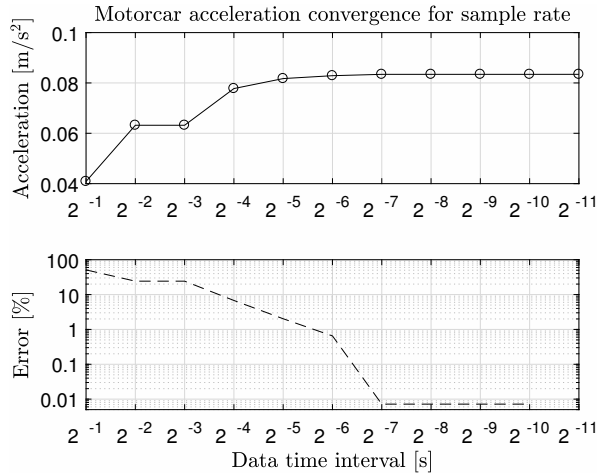


Figure 4.14: Convergence of motorcar accelerations with regards to sample rate.

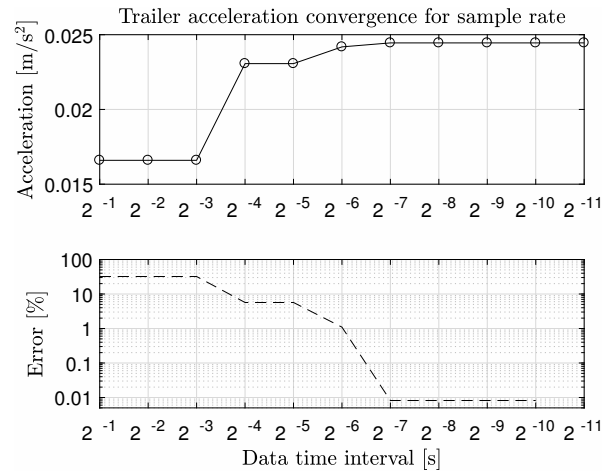


Figure 4.15: Convergence of trailer accelerations with regards to sample rate.

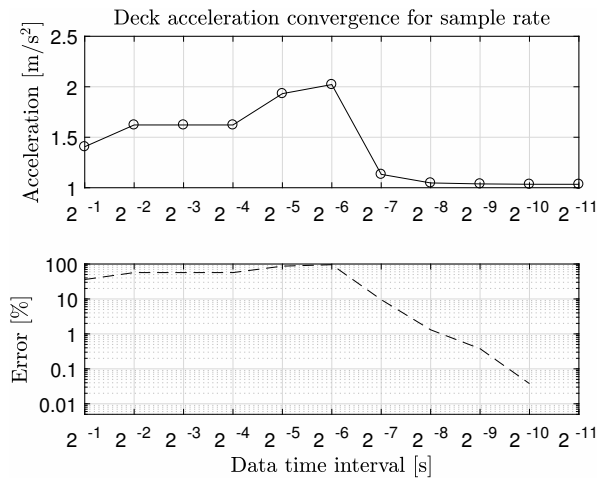


Figure 4.16: Convergence of deck accelerations with regards to sample rate.

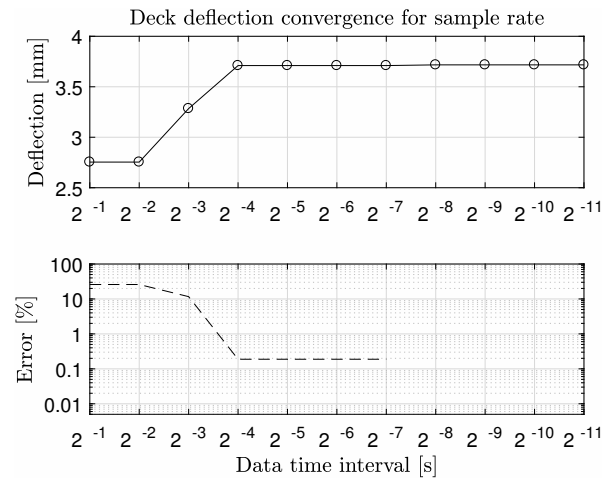





Figure 4.17: Convergence of deck deflections with regards to sample rate.

4.3 Bridge frequency analysis

In order to find resonant peaks it is important to be able to evaluate the eigenfrequency of the bridge system. Section 2.4.4 presents basic theory for the evaluation of eigenfrequencies for simple beams. Table 4.1 compares the results of that approach with the actual behaviour evaluated in ABAQUS for the first three eigenmodes.

Table 4.1: Eigenfrequency comparison between analytic solution and two-layer FE-model for a simply supported single 19.53 m span bridge.

Eigenmode	Eigenfrequency ABAQUS [Hz]	Eigenfrequency Analytic including sleepers and rail [Hz]	Eigenfrequency Analytic without sleepers and rail [Hz]	Mode shape
1	3.93	3.96	4.04	
2	15.55	15.84	16.16	
3	34.17	35.64	36.36	

The eigenfrequencies obtained in the ABAQUS-model are consistently lower than the analytic solution. This could be due to the partial restraint of the rail present only in the two-layer model. Furthermore, this comparison seems to indicate that somewhat a realistic behaviour is obtained if the additional nonstructural mass from sleepers and rail is included in the analytic frequency analysis. However the best approach in order to find the eigenfrequency seems to be a frequency analysis in ABAQUS. This correlation seems to hold for all span lengths in thesis scope according to Figure 4.18. The error seems to increase for shorter bridges and higher modes.

A similar frequency analysis was performed for continuous double and triple span bridges. Tables 4.2 and 4.3 evaluate the case where the span lengths are 19.53 m. Figures 4.19 and 4.20 present the eigenvalues for various bridges with span lengths in the range of interest.

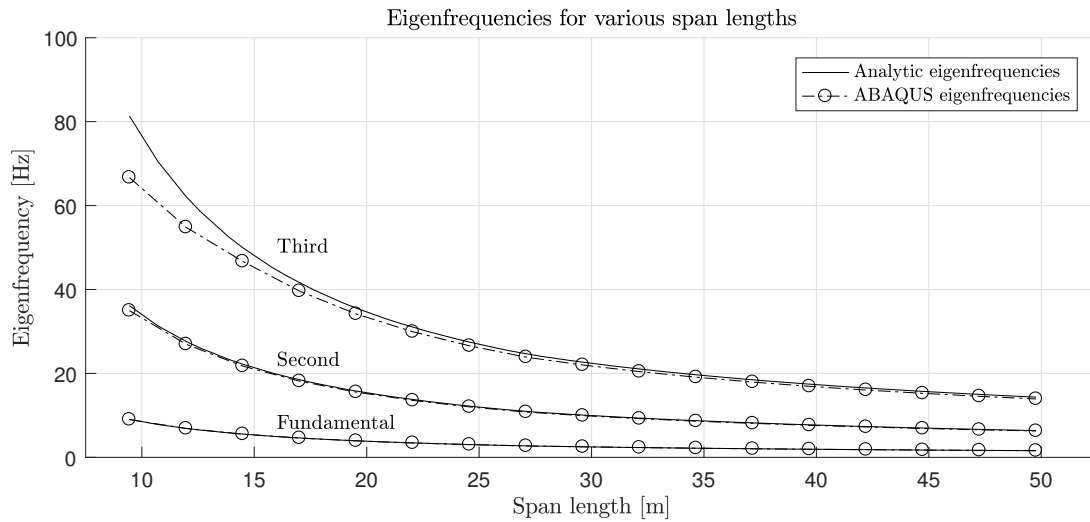


Figure 4.18: Eigenfrequencies from ABAQUS and Analytic solutions for various span lengths for a simply supported bridge of one span.

Table 4.2: Eigenfrequency comparison between analytic solution and two-layer FE-model for a continuous double 19.53 m span bridge.

Eigenmode	Eigenfrequency ABAQUS [Hz]	Eigenfrequency Analytic including sleepers and rail [Hz]	Mode shape
1	3.10	3.11	
2	4.83	4.87	
3	12.30	12.45	
4	15.49	15.76	

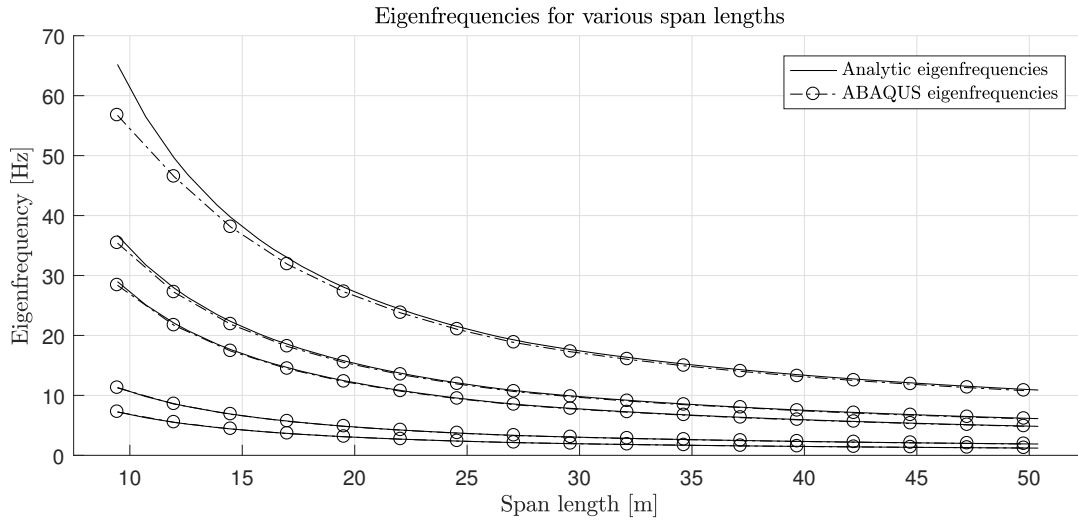


Figure 4.19: Eigenfrequencies from ABAQUS and Analytic solutions for various span lengths for a continuous double span bridge.

Table 4.3: Eigenfrequency comparison between analytic solution and two-layer FE-model for a continuous triple 19.53 m span bridge.

Eigenmode	Eigenfrequency ABAQUS [Hz]	Eigenfrequency Analytic including sleepers and rail [Hz]	Mode shape
1	3.52	3.53	
2	4.50	4.51	
3	6.54	6.64	
4	13.94	14.14	

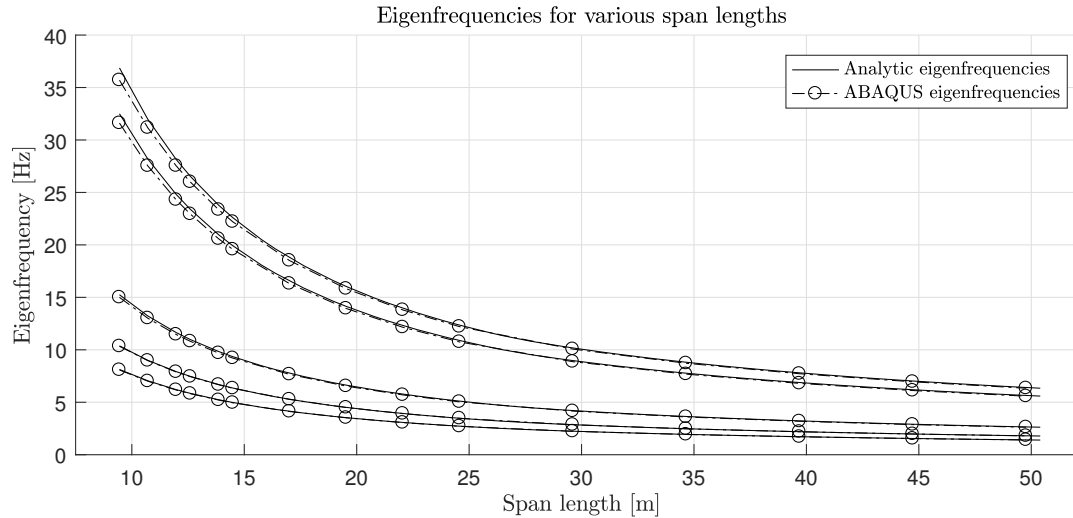


Figure 4.20: Eigenfrequencies from ABAQUS and Analytic solutions for various span lengths for a continuous triple span bridge.

4.4 Vehicle frequency analysis

When evaluating the resonant behaviour of this model it is critical to understand the dynamic properties for the motorcars and the trailers, therefore a frequency analysis was performed. The frequency study was performed in ABAQUS using the vehicles presented in Section 4.1. In this reduced model the assumption was made that the wheels are fixed to the ground, apart from that all properties of the model are identical to the full model. The undeformed shape of the trailer is presented in Figure 4.21 along with its corresponding mode shapes in Table 4.4. The modes for the motorcar is presented in Figure 4.22 along with its modes in Table 4.5. All eigenfrequencies up to the threshold of 100 Hz was studied since this is well above the limit for bridge modes as stated presented in Section 2.3.1.

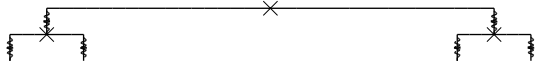


Figure 4.21: Undeformed trailer in frequency analysis.

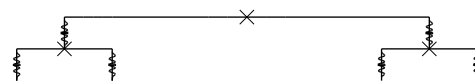


Figure 4.22: Undeformed motorcar in frequency analysis.

The first eigenmodes for both vehicles are modes corresponding to the translation and rotation of the car body. These modes eigenmodes occupy an eigenfrequency range of 0.6 to 1.0 Hz. The following modes are related to translation of the bogies at 5.5 Hz for the motorcar and 7.0 Hz for the trailer. Finally rotational eigenmodes of the bogies occur at 22.5 Hz for the motorcar and 23.7 Hz for the trailer. Different vehicle modes will be critical for various bridge modes.

Table 4.4: Eigenfrequencies and corresponding mode shapes for trailer vehicle.

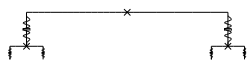

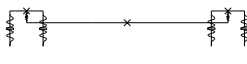
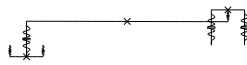
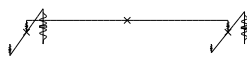
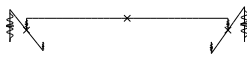

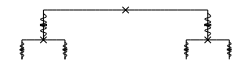
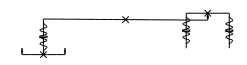
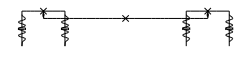
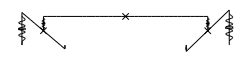
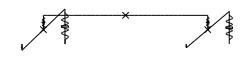
Eigenmode	Eigenfrequency [Hz]	Mode shape
1	0.58	
2	0.68	
3	6.99	
4	6.99	
5	23.69	
6	23.69	

Table 4.5: Eigenfrequencies and corresponding mode shapes for motorcar vehicle.

Eigenmode	Eigenfrequency [Hz]	Mode shape
1	0.79	
2	0.99	
3	5.50	
4	5.52	
5	22.47	
6	22.47	

4.5 Analysis scope

There are five different bridge configurations that has been evaluated. For each one of these configurations the span lengths has been varied and designed using the simplified approach for the design speed of 350 km/h. Each one of these bridges has then been evaluated at multiple speed in an envelope from the lower limit of 120 km/h to the maximum of 350 km/h. The five configurations are:

- Simply supported, Single span bridges
- Simply supported, Double span bridges
- Simply supported, Triple span bridges
- Continuous, Double span bridges
- Continuous, Triple span bridges

For each bridge configuration the height of the deck section has been adjusted to comply with the vehicle acceleration limit. Some examples of calculated heights is presented in Table 4.6.

Table 4.6: Example of sectional heights for the simply supported single span bridges designed for the maximum speed of 350 km/h.

Span length, L [m]	Deck height, h [m]
9.45	0.485
10.08	0.512
⋮	⋮
49.77	2.301

5 Results

This chapter presents results from the dynamic bridge-vehicle interaction models. Each section contains vehicle acceleration data from a large set of different bridges. All bridges analyzed should comply with the acceleration criteria which means the vertical acceleration in the vehicles should never exceed 1 m/s^2 . All vehicles in the model has been evaluated to find the maximum acceleration for a particular analysis. Due to the difference in vehicle suspension and mass properties, data has been extracted separately for these two vehicle types.

Firstly, Section 5.1 presents results extracted for the case where simply supported bridges designed using the simplified comfort acceleration analysis for the maximum speed of 350 km/h, are evaluated. These results are then complemented with Section 5.2 which presents the continuous cases.

5.1 Simply supported bridges

These results are based on bridges designed for a maximum speed of 350 km/h using Figure 2.8. This implies that all speeds from the lower limit of 120 km/h up to 350 km/h should be included in the evaluation envelope. In order to obtain as accurate results as possible for the resonant peaks, the full train with 14 passenger cars and 2 motorcars was used for these evaluations. Increments in speed were set to 5 km/h, however the data density was increased near resonant peaks.

5.1.1 Single Span

Figure 5.1 presents trailer acceleration envelopes for simply supported single span bridges with various span lengths designed using the simplified comfort approach for speeds up to 350 km/h. Figure 5.2 shows the corresponding results for the motorcar. Each line represents results from a single unique bridge. In order to better visualize these results, contour plots of this data are presented in Figures 5.3 and 5.4.

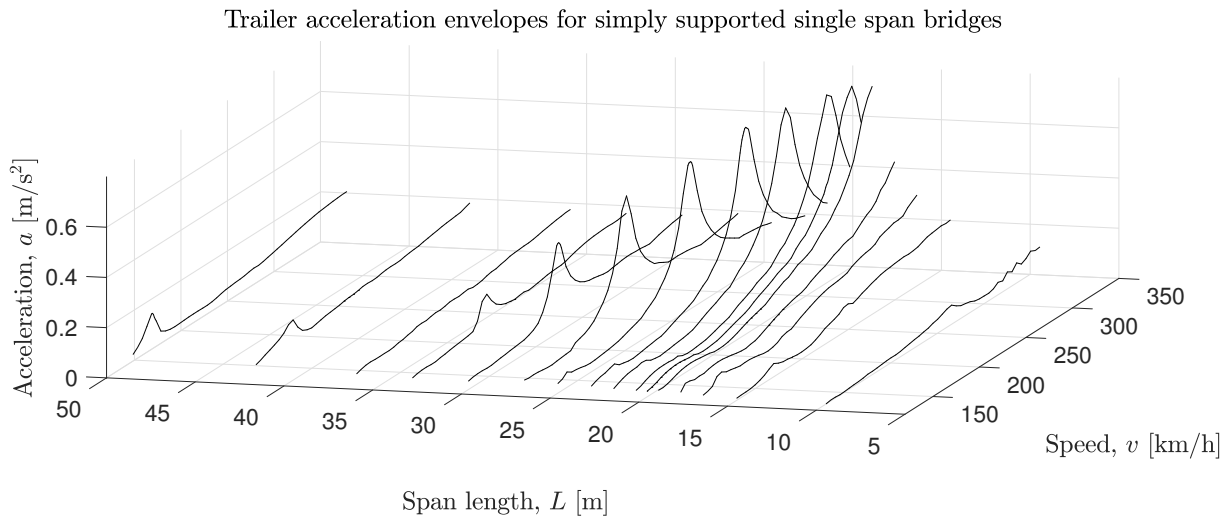


Figure 5.1: Vertical trailer acceleration envelopes for simply supported single span bridges designed for speeds up to 350 km/h.

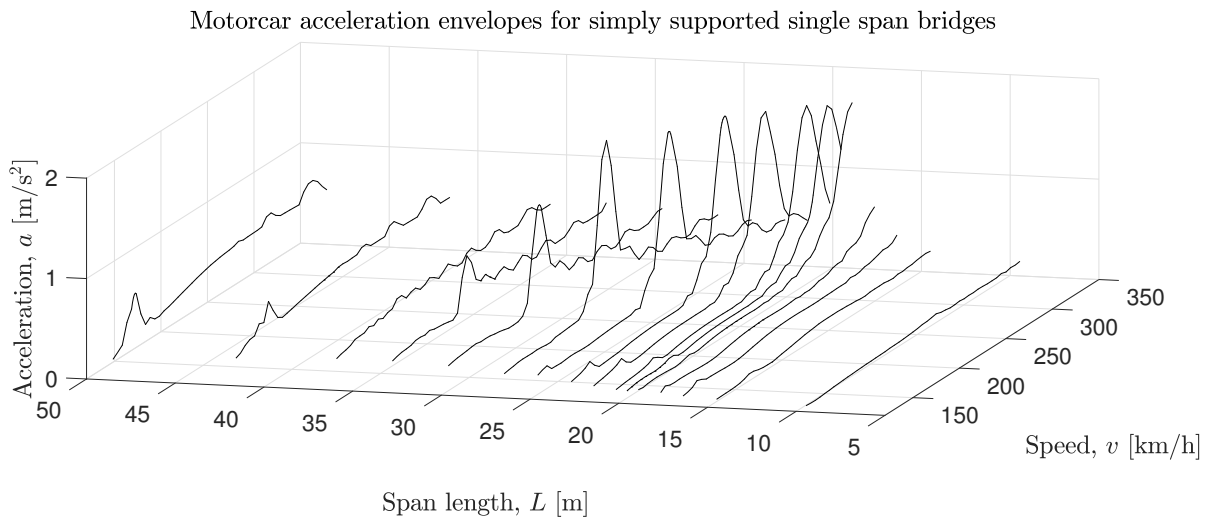


Figure 5.2: Vertical motorcar acceleration envelopes for simply supported single span bridges designed for speeds up to 350 km/h.

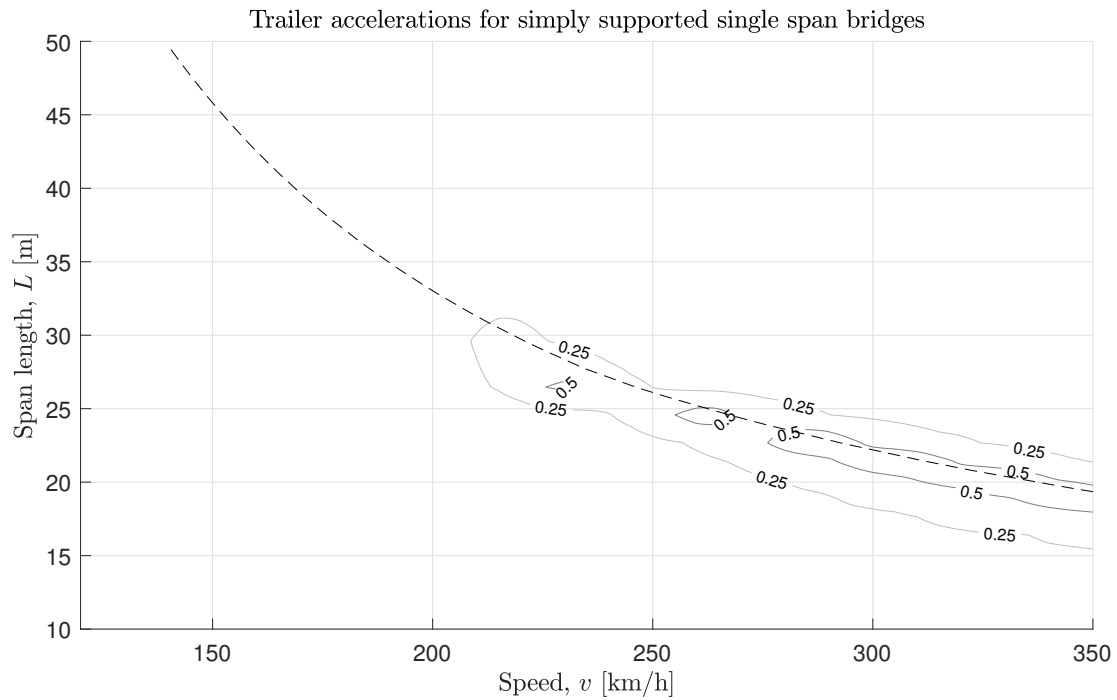


Figure 5.3: Contour plot of trailer acceleration envelopes for simple supported single span bridges.

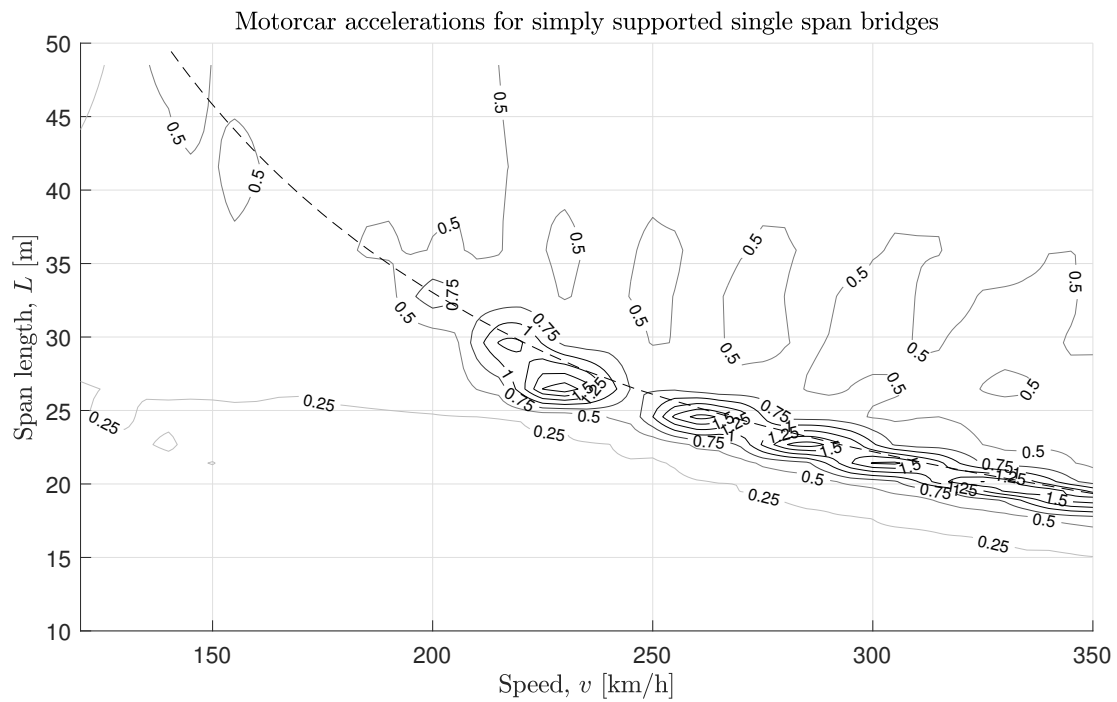


Figure 5.4: Contour plot of motorcar acceleration envelopes for simple supported single span bridges. Resonant velocities for each span length is indicated with dashed line.

The maximum envelope response for bridges with various span lengths can be visualized in Figure 5.5. The limit of 1 m/s^2 is indicated with a dotted line. Results seem to indicate that trailer accelerations never exceed the upper acceleration limit, this however does not hold for the motorcar. Figure 5.6 compares the resonant peaks from the acceleration envelopes in Figure 5.1 and 5.2 with the analytic resonant speed based on the length of the trailer. These results seem to indicate that the large passenger trailer response is obtained near the analytic resonant speed corresponding to the fundamental eigenfrequency of the bridge. Maximum trailer accelerations occur near the span length of 20 m where the design speed intersects the first resonant speed.

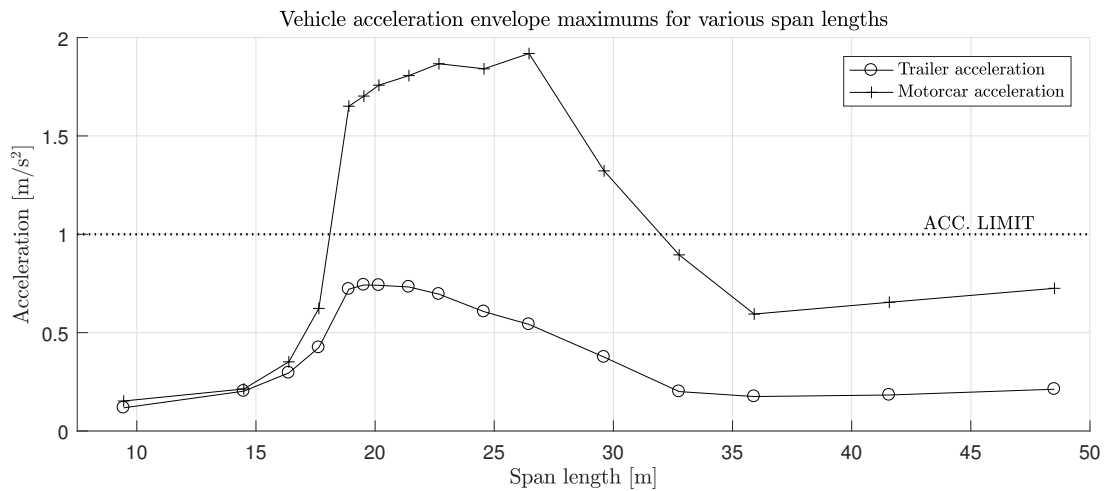


Figure 5.5: Maximum vertical vehicle acceleration from each envelope for simply supported single span bridges. Each envelope is represented by a single point in the figure.

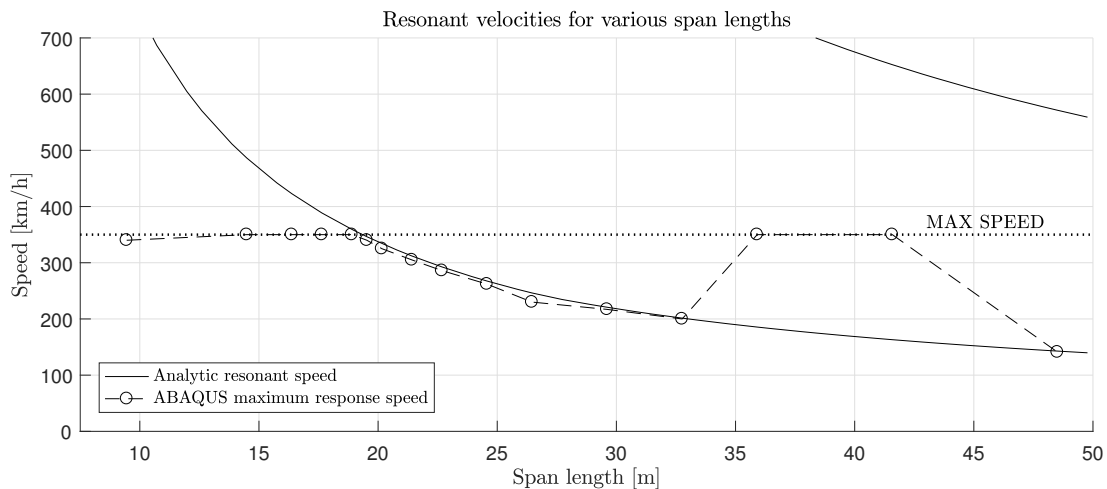


Figure 5.6: The speed at which the maximum trailer acceleration is reached is plotted versus the analytic resonant speed and the maximum speed in the analysis.

5.1.2 Double Span

This section contains the results obtained for the analyzed simply supported double span bridges. The envelopes of motorcar and trailer accelerations for all span lengths included in the analysis are presented in Figures 5.7 and 5.8. Moreover, Figures 5.9 and 5.10 present the same results though visualized from above in contour plots. These plots are overlaid with dashed lines representing the analytical resonant speeds for each mode of each bridge calculated according to Section 2.4.7.

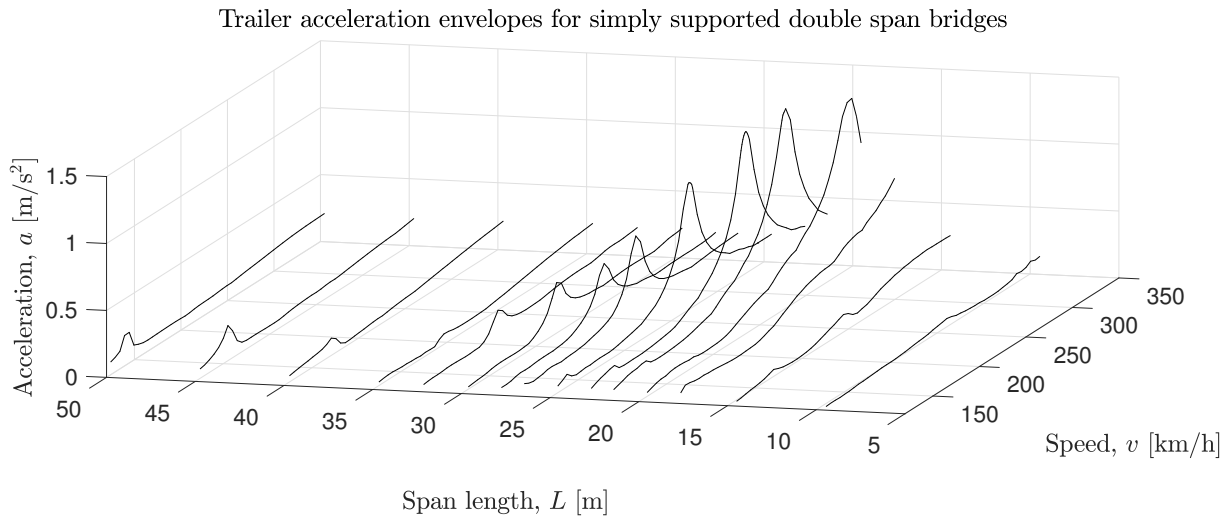


Figure 5.7: Trailer acceleration envelopes for various simply supported double span bridges. Each line represents a single unique bridge.

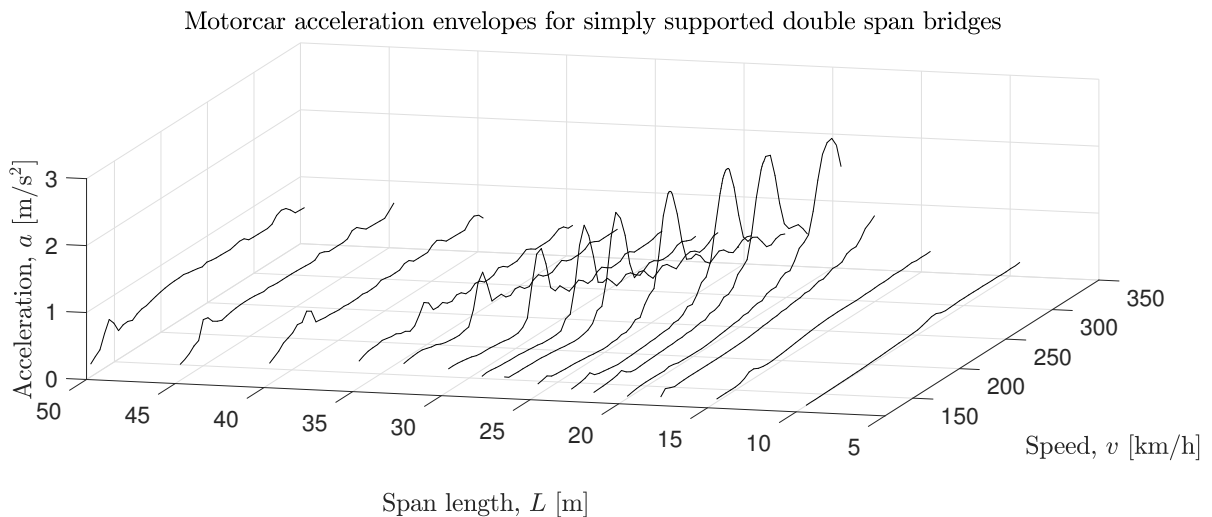


Figure 5.8: Motorcar acceleration envelopes for various simply supported double span bridges.

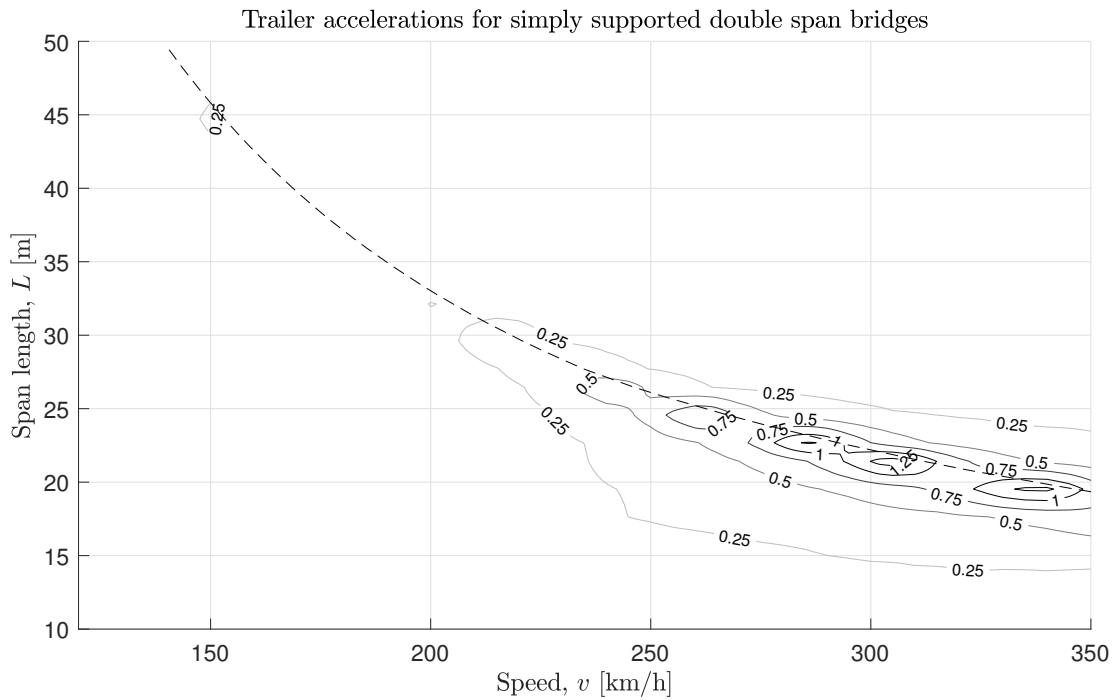


Figure 5.9: Trailer acceleration contour plots for various simply supported double span bridges. Fundamental resonant speeds are indicated with dashed line.

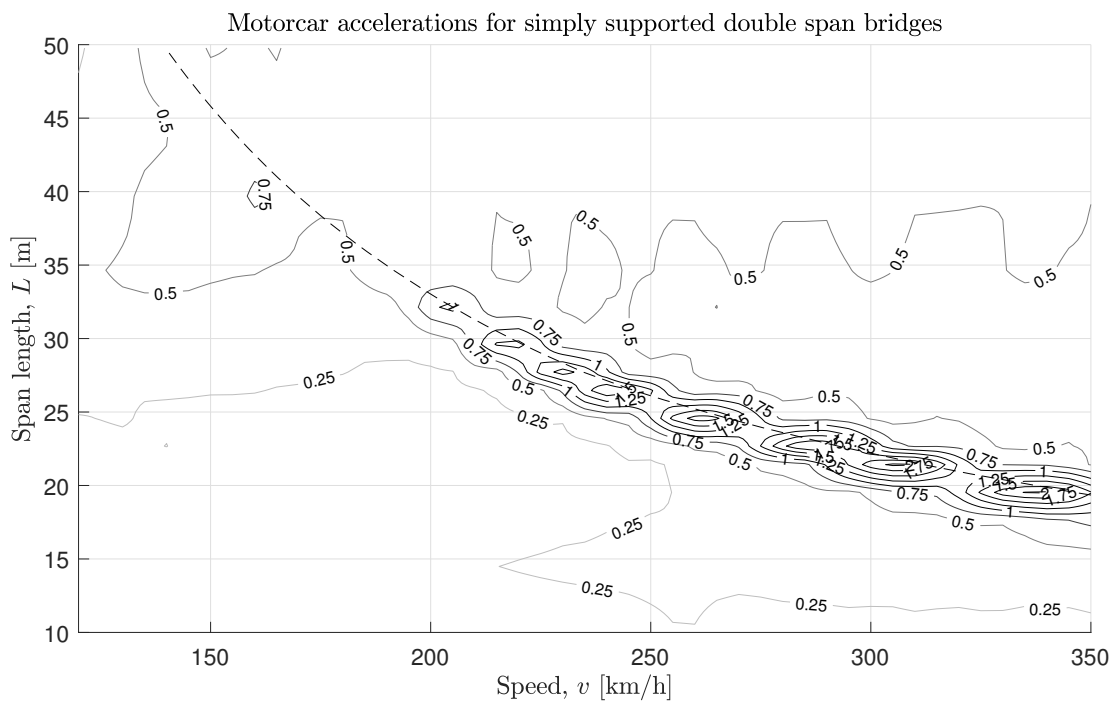


Figure 5.10: Motorcar acceleration contour plots for various simply supported double span bridges.

The maximum accelerations of each speed envelope obtained for each span configuration are seen in Figure 5.11. The corresponding speeds for which the accelerations were obtained are displayed in Figure 5.12. In both of these plots, critical trailer acceleration values exceeding the predefined limit of 1 m/s^2 are marked with red squares.

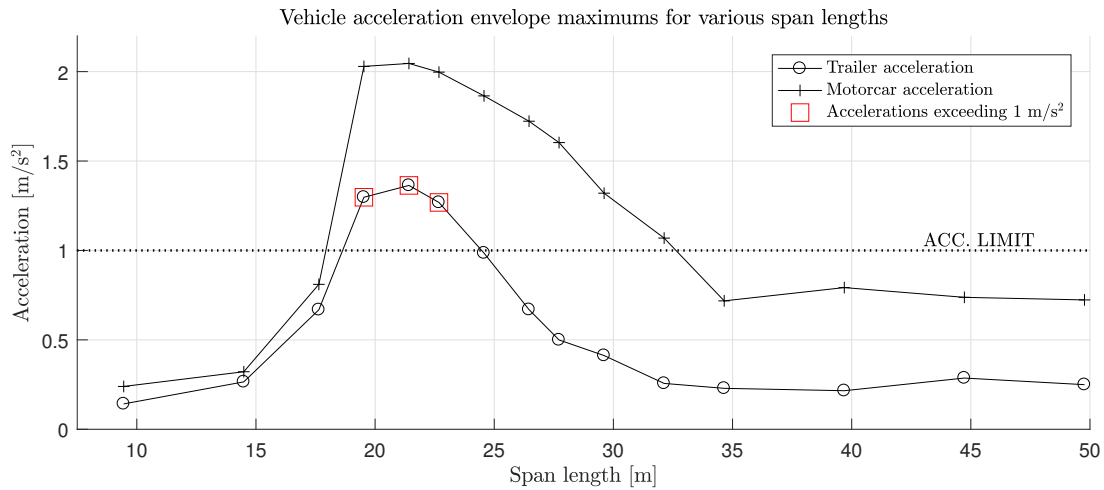


Figure 5.11: The maximum values of each envelope for various simply supported double span bridges are plotted against the acceleration limit of 1 m/s^2 . Cases exceeding this comfort limit are indicated with a red box.

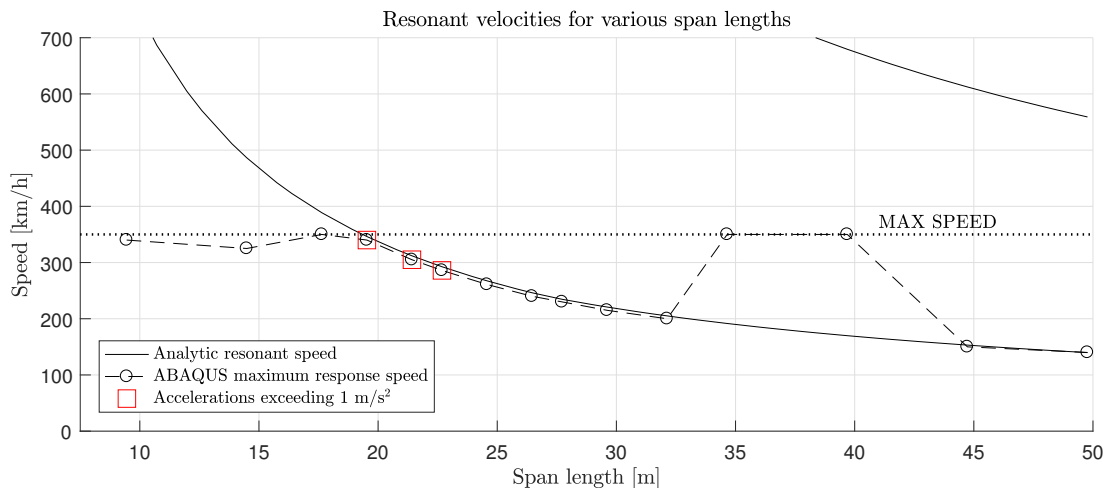


Figure 5.12: The speed at which maximum response is obtained are visualized for simply supported double span bridges. Resonant speeds for various spans are indicated and correlation is prominent.

5.1.3 Triple Span

This section contains results corresponding to simply supported triple span bridges with various span lengths. Envelopes are presented in Figures 5.13 and 5.14, contours with resonant velocity curves are presented in Figures 5.15 and 5.16, maximum values are visualized in Figure 5.17 and finally the resonant peaks are indicated in Figure 5.18.

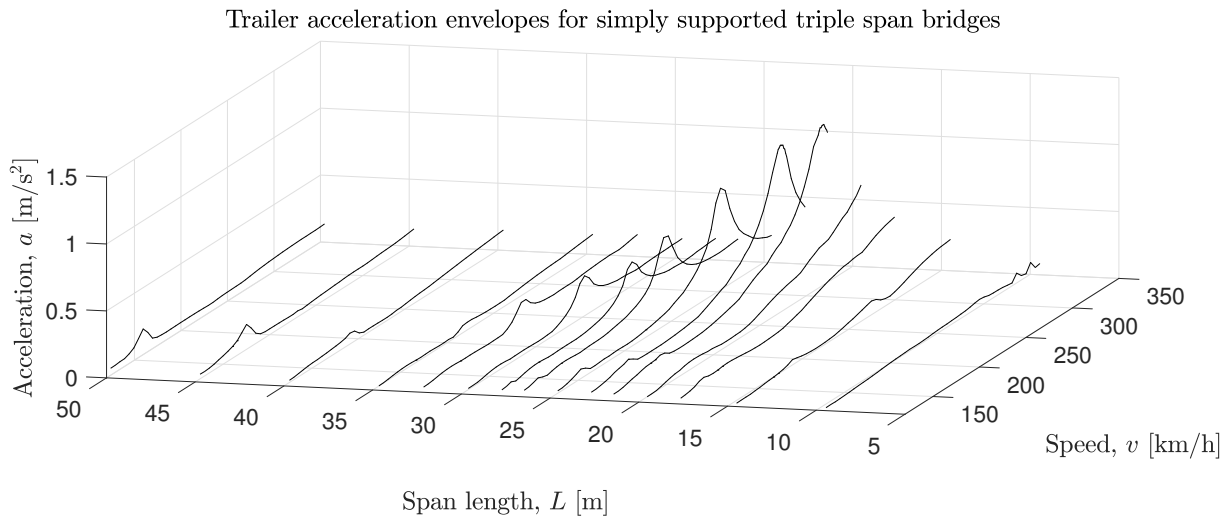


Figure 5.13: Trailer acceleration envelopes for various simply supported triple span bridges. Each line represents a single unique bridge.

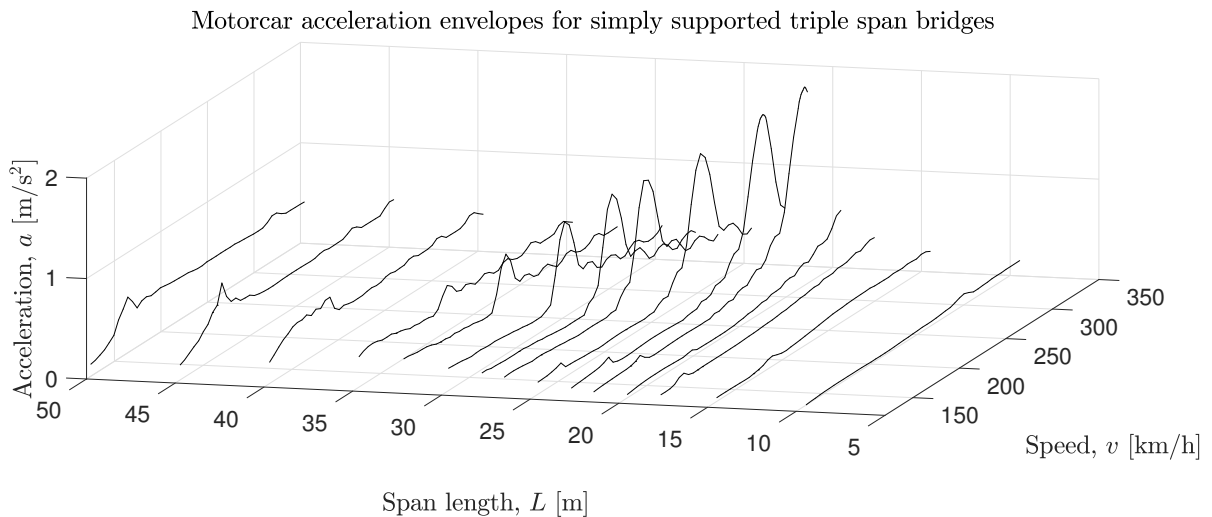


Figure 5.14: Motorcar acceleration envelopes for various simply supported triple span bridges.

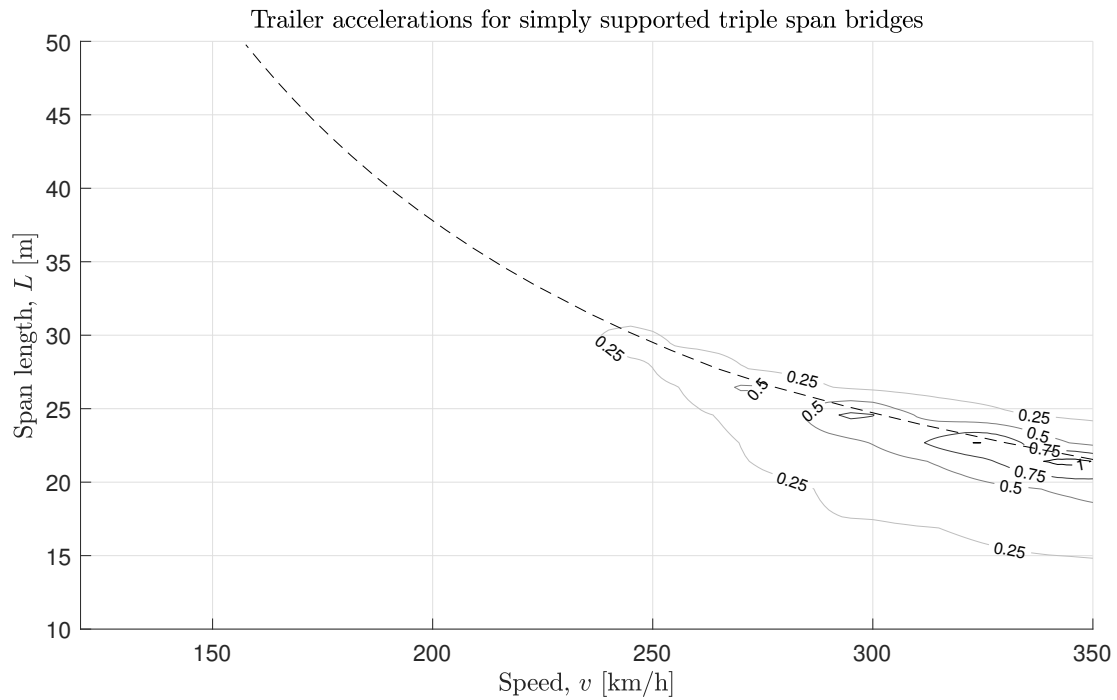


Figure 5.15: Trailer acceleration contour plots for various simply supported triple span bridges. Fundamental resonant speeds are indicated with dashed line.

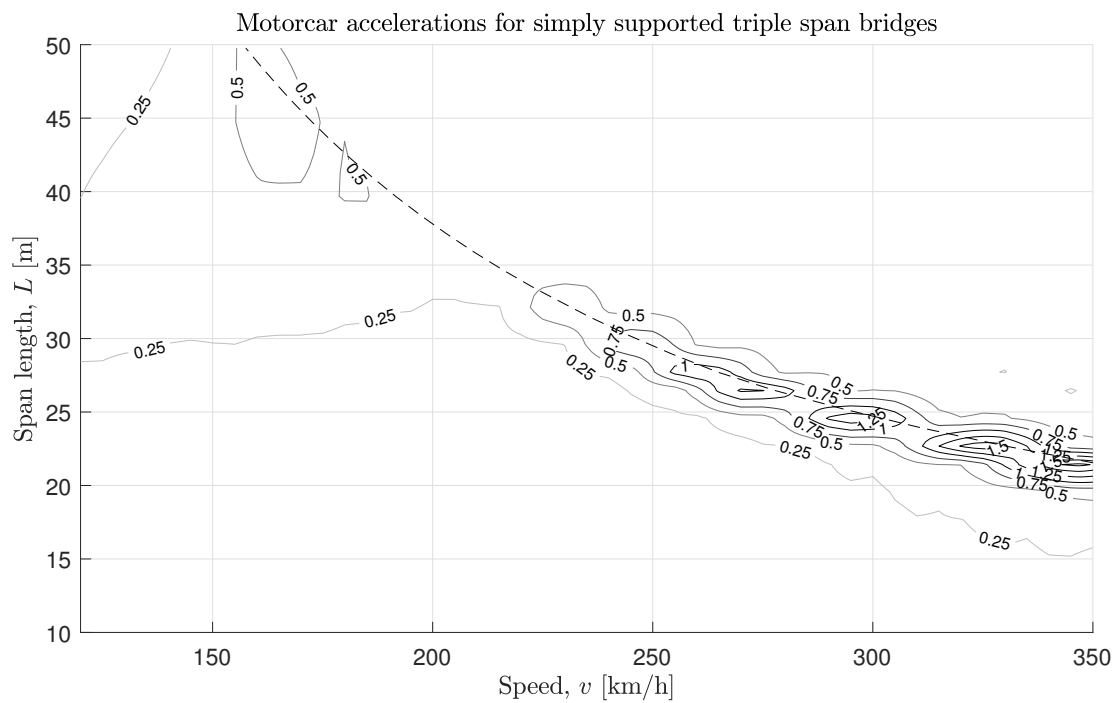


Figure 5.16: Motorcar acceleration contour plots for various simply supported triple span bridges.

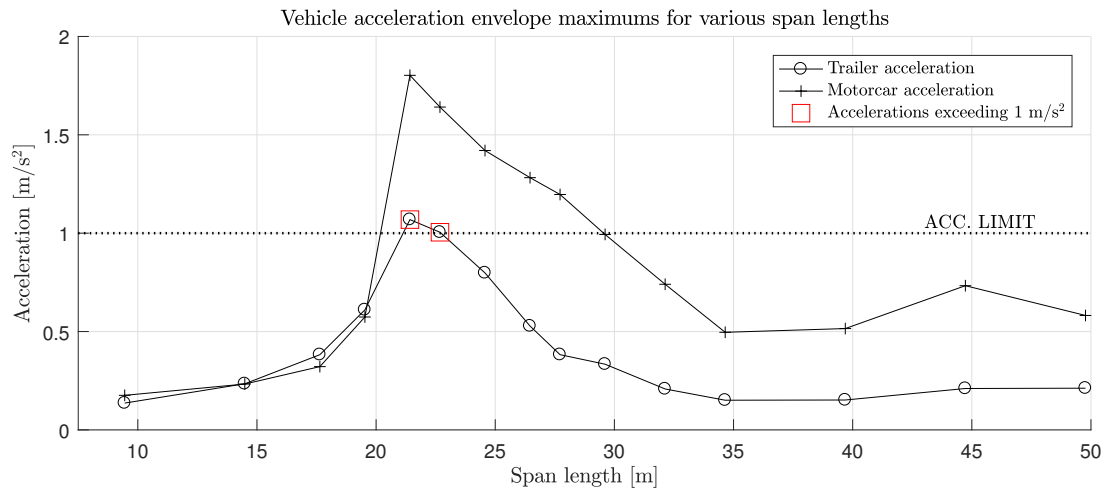


Figure 5.17: The maximum values of each envelope for various simply supported triple span bridges are plotted against the acceleration limit of 1 m/s^2 . Cases exceeding this comfort limit are indicated with a red box.

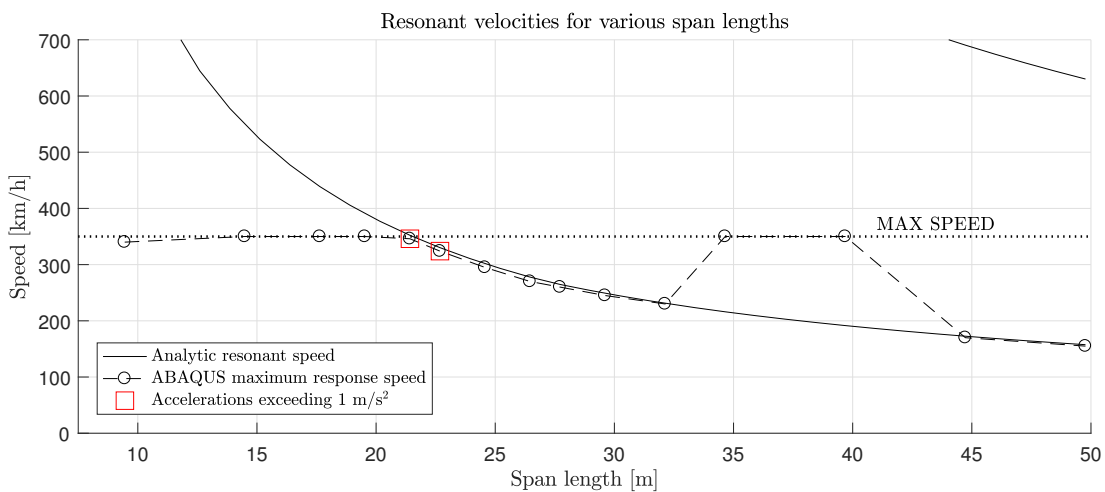


Figure 5.18: The speed at which maximum response is obtained are visualized for simply supported triple span bridges. Resonant speeds for various spans are indicated and correlation is prominent.

5.2 Continuous bridges

This section contains results for continuous bridges with two and three spans. Section 5.2.1 presents results from double span bridges and Section 5.2.2 presents the corresponding data for the triple span bridges.

5.2.1 Double Span

Results for bridges with continuous double spans are presented in this section. Figures 5.19, 5.20, 5.21 and 5.22 visualize envelopes and contours of the trailer and motorcar accelerations.

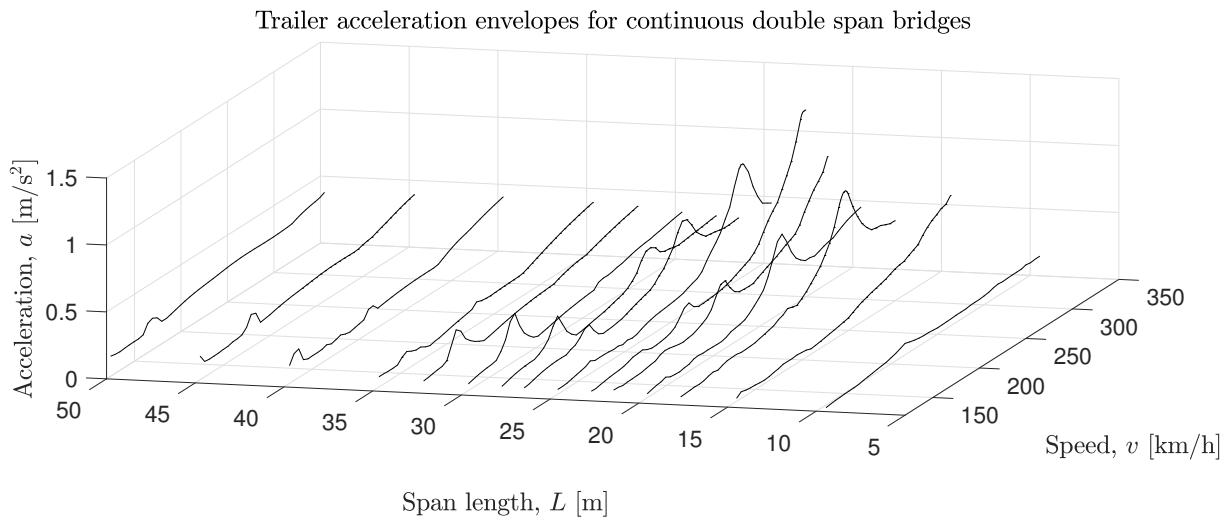


Figure 5.19: Trailer acceleration envelopes for various continuous double span bridges. Each line represents a single unique bridge.

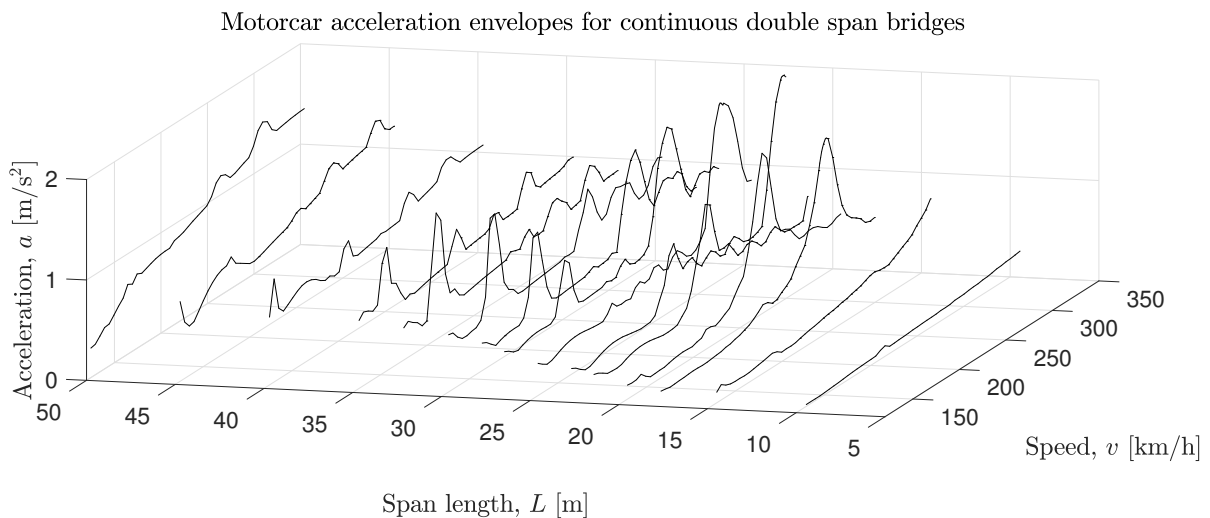


Figure 5.20: Motorcar acceleration envelopes for various continuous double span bridges.

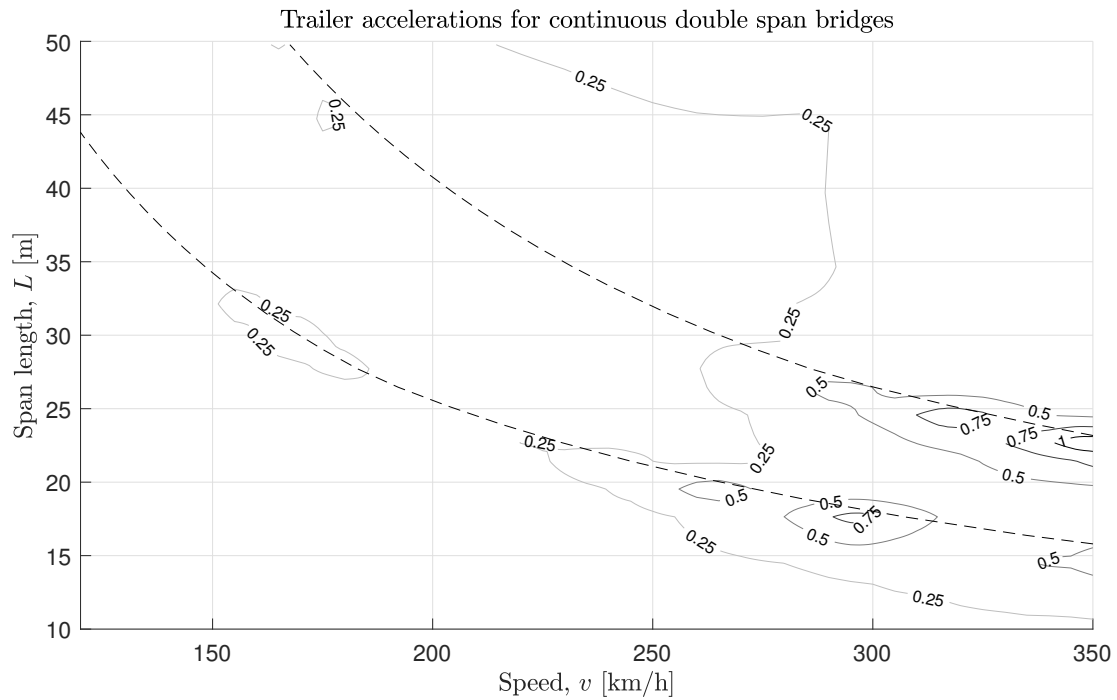


Figure 5.21: Trailer acceleration contour plots for various continuous double span bridges. Fundamental and second resonant speeds are indicated with dashed line.

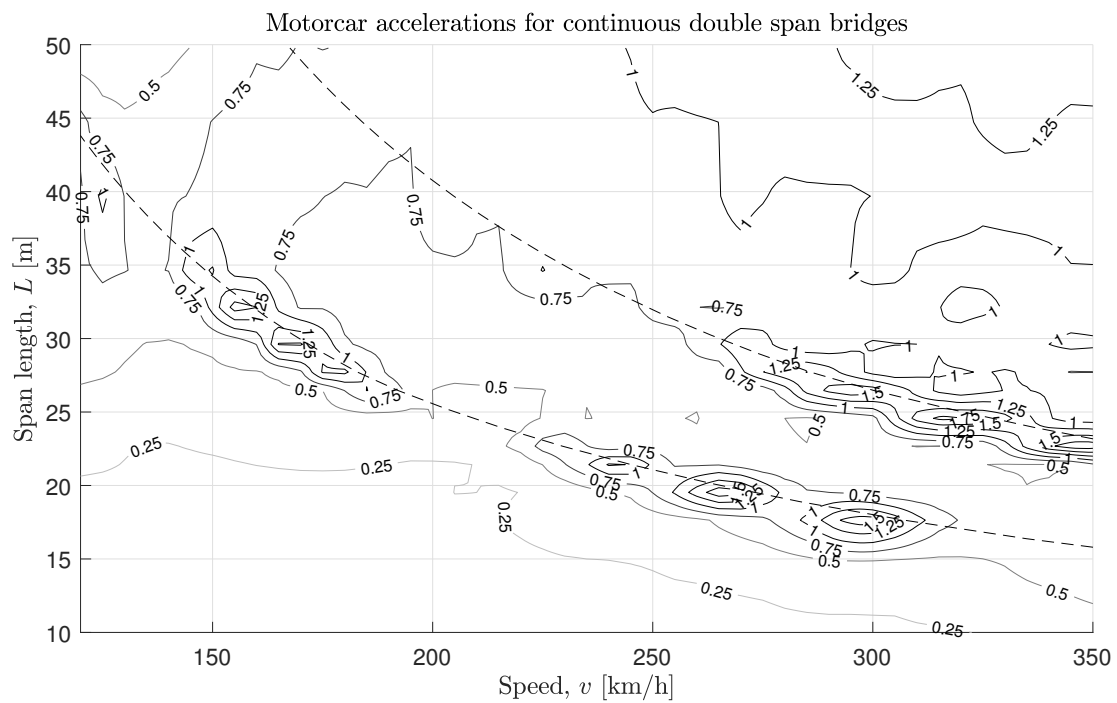


Figure 5.22: Motorcar acceleration contour plots for various continuous double span bridges.

Figures 5.23 and 5.24 capture the critical cases and visualize correspondence with analytic resonant peaks. These results differ to the simply supported structures in the way that additional mode shapes are introduced in critical regions within the speed envelope. This is also very clear in Figure 5.22 where it seems like the second eigenmode results in a more critical response than for the fundamental eigenfrequency.

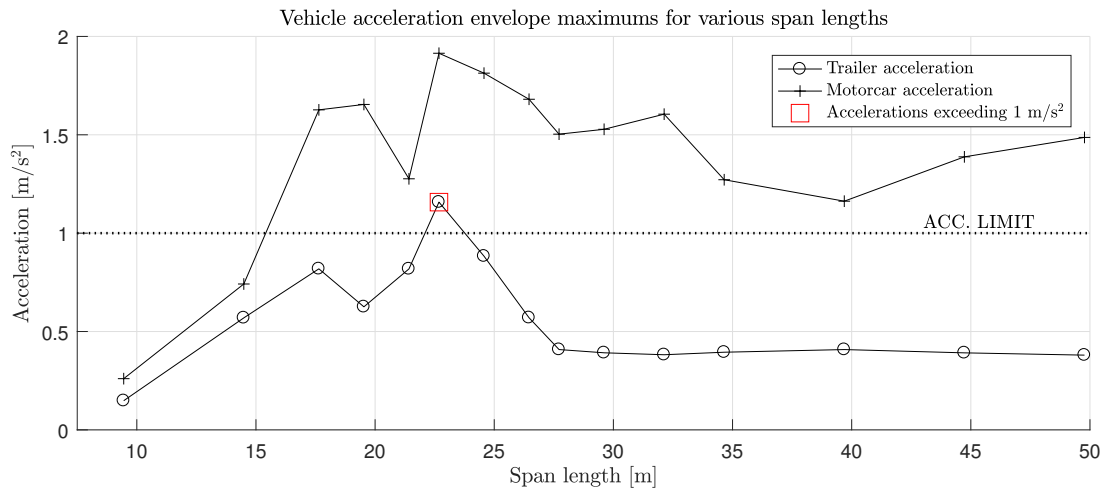


Figure 5.23: The maximum values of each envelope for various continuous double span bridges are plotted against the acceleration limit of 1 m/s^2 . Cases exceeding this comfort limit are indicated with a red box.

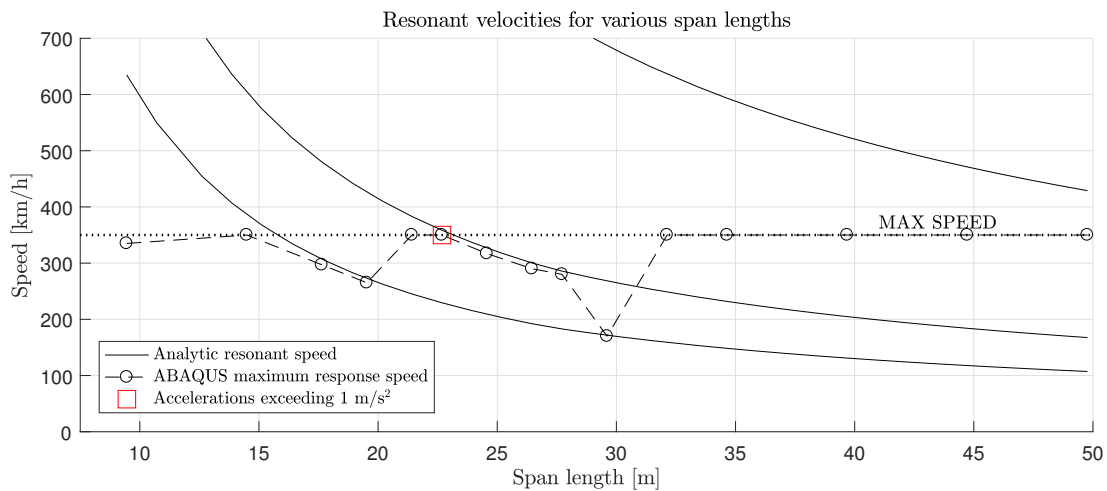


Figure 5.24: The speed at which maximum response is obtained are visualized for continuous double span bridges. Resonant speeds corresponding to the fundamental and second eigenmode for various spans are indicated and correlation is prominent.

5.2.2 Triple Span

Results for bridges with continuous triple spans are presented in this section. Figure 5.25, 5.26, 5.27 and 5.28 visualize envelopes and contours of the trailer and motorcar accelerations while Figures 5.29 and 5.30 capture the critical cases and visualize correspondence with analytic resonant peaks.

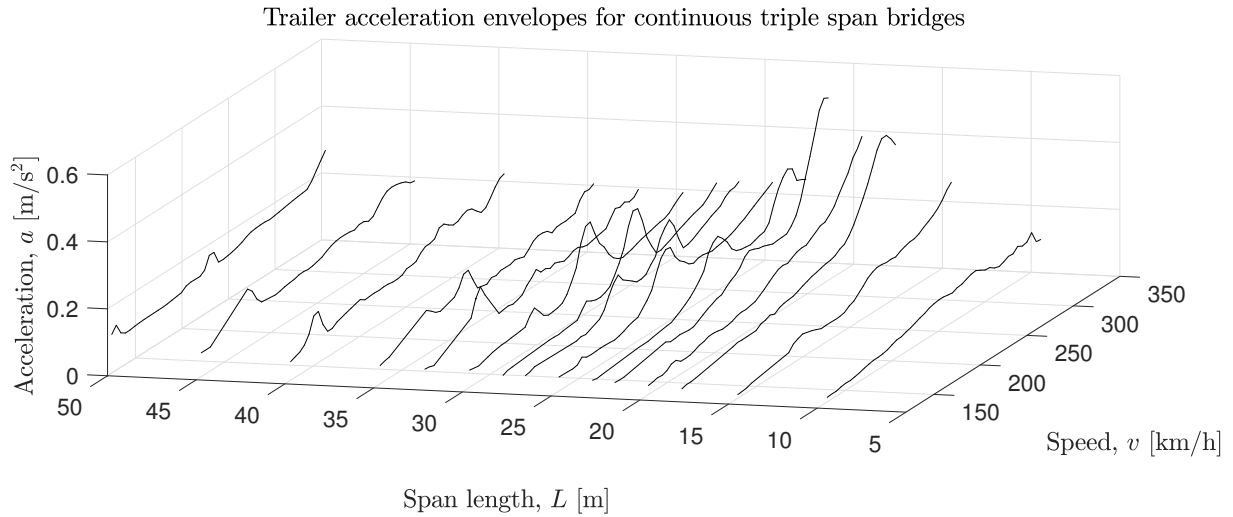


Figure 5.25: Trailer acceleration envelopes for various continuous triple span bridges. Each line represents a single unique bridge.

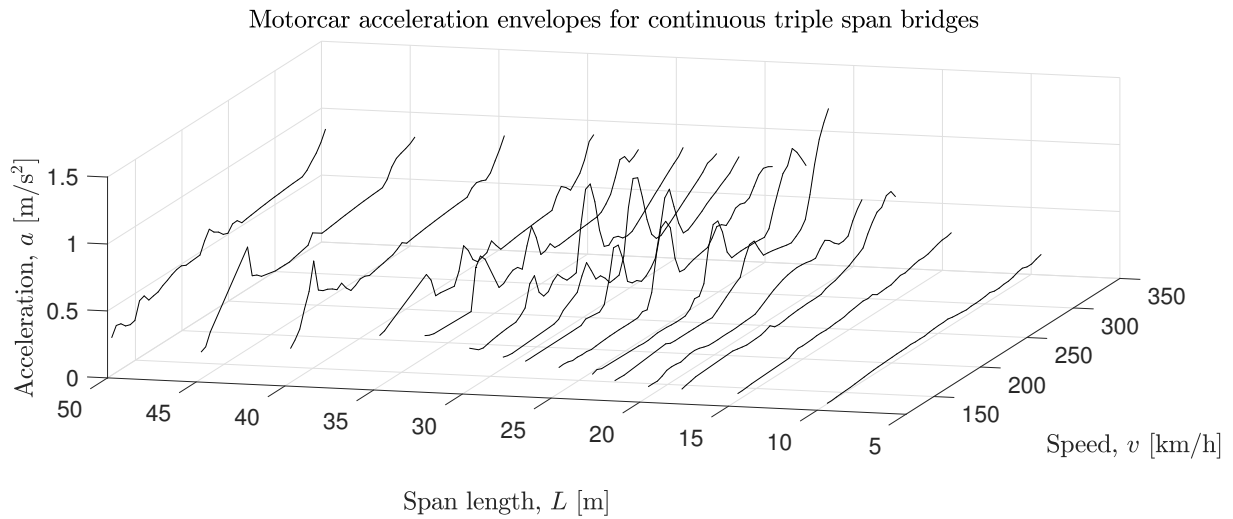


Figure 5.26: Motorcar acceleration envelopes for various continuous triple span bridges.

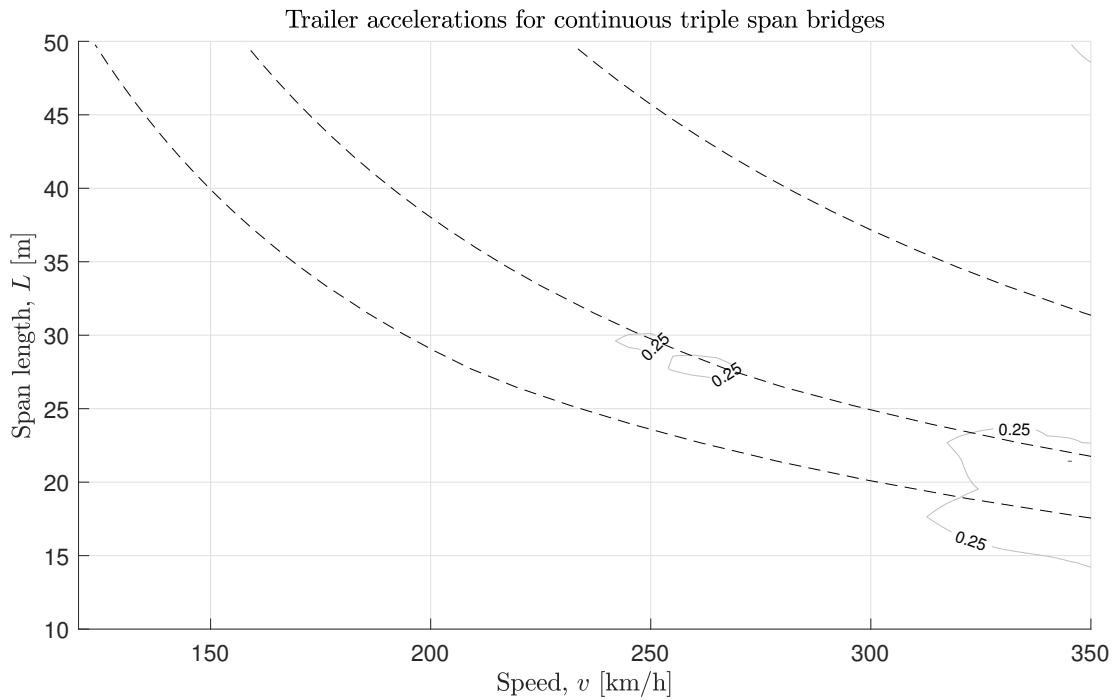


Figure 5.27: Trailer acceleration contour plots for various continuous triple span bridges. Fundamental, second and third resonant speeds are indicated with dashed line.

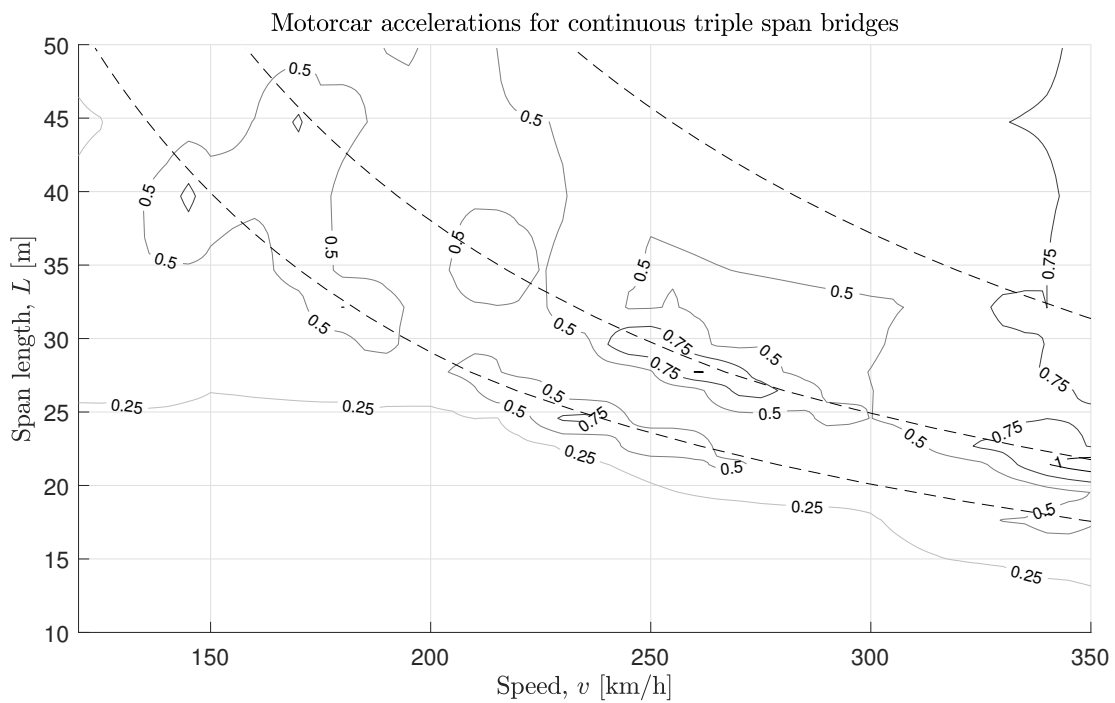


Figure 5.28: Motorcar acceleration contour plots for various continuous triple span bridges.

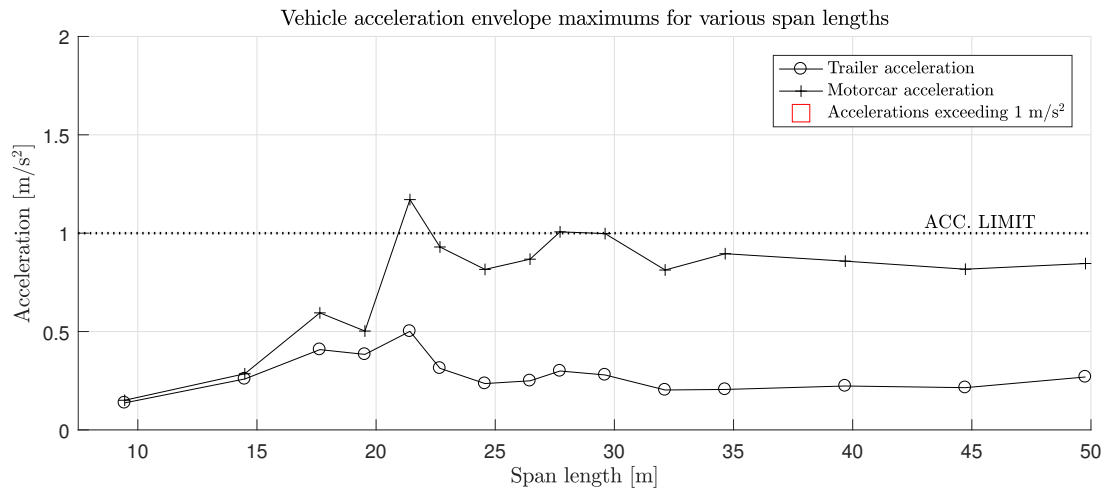


Figure 5.29: The maximum values of each envelope for various continuous triple span bridges are plotted against the acceleration limit of 1 m/s^2 . Cases exceeding this comfort limit are indicated with a red box.

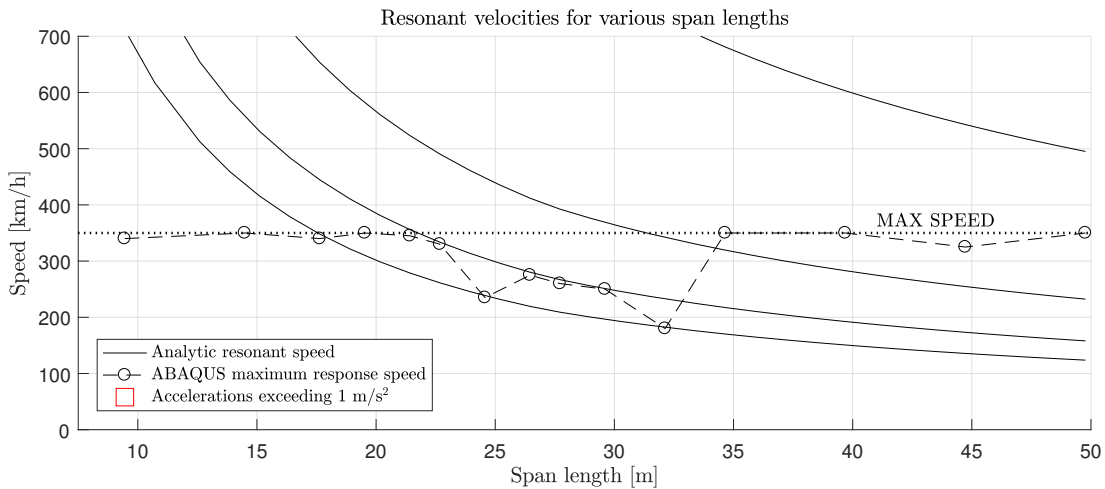


Figure 5.30: The speed at which maximum response is obtained are visualized for continuous double span bridges. Resonant speeds corresponding to the fundamental, second and third eigenmode for various spans are indicated and correlation is prominent.

6 Discussion

During the course of this study, a number of points of discussions have arisen. For instance, a variety of choices have been made in terms of setting the thesis' scope, method and modelling procedure. Some phenomena have been recognized but neglected due to time or software constraints. These are among the areas discussed in the continuation of this chapter. Furthermore, possible sources of error or insecurity are brought to light and reflected upon as well.

6.1 Evaluation of results

The results indicate that the vertical accelerations in the motorcar exceeds the same measurements in the passenger trailers for the analyzed train. This is expected since the vehicle properties of these two vehicles differ significantly. As seen in Table 2.2, the stiffness of the secondary suspension located between the bogie and the car, is much higher for the motorcar compared to the passenger trailer. This along with an increased mass for the motorcar is the main reason for the amplified behaviour. However, since passenger comfort is the main focus of this thesis and passengers are not likely to be located in the motorcars, the main vehicle that should be investigated is the passenger trailers. Furthermore, newer models of ICE-trains seems to have more similar dynamic properties for all cars instead of heavier designated motorcars. However even while neglecting the higher results from the motorcars, the limit of 1 m/s^2 is still exceeded for the passenger trailers in the case of bridges with two or three simply supported spans and continuous bridges with two spans. This indicates that the simplified approach presented in Section 2.3.2 does not result in conservative bridge designs for all configurations using the ICE 2 vehicle analyzed in this thesis.

The critical resonant peaks are obtained at speeds near the analytic resonant speed calculated from the eigenfrequencies of the bridge multiplied with the spacing equal to the length of a passenger trailer. For simply supported structures it seems like the fundamental mode is critical within the specified range of spans and speeds, however for continuous bridges additional mode shapes are introduced. For instance results from continuous double span bridges, as presented in Section 5.2.1, seems to indicate that the second mode shape is even more critical with regards to vertical vehicle accelerations.

The main problem region seems to be located at around bridges with span lengths of 20-25 m. It would seem that these span lengths are critical because they are very close to the car lengths and thus the effective spacing between the sequential loads. The results of this thesis seems to correspond well with analyses of Mao and Lu (2013) which indicated that cases where the car length to span length ratio was close to an integer were the ones where bridge resonance response was most prominent.

6.2 Thesis scope

In this thesis, rectangular reinforced concrete slab sections were evaluated for a specified range of spans and speeds. Multiple-span bridges were also evaluated, however all bridges were assumed to have uniform span lengths. This assumption works well with bridges with a single span or two spans,

however it might not be realistic for continuous bridges with three spans or more. Ideally a more detailed evaluation of bridges with varying span lengths would be performed however this is beyond the scope of this thesis. In design of a real project it is essential that the actual span configuration is analyzed.

All bridges evaluated are assumed to have a track which is non-ballasted. Hjelm and Karlsson (2016) concluded in their thesis that this is a suitable choice for high speed railway on heavy concrete structures since the track alignment accuracy is increased and low maintenance is required. If a ballasted railway-bridge is to be analyzed it is important to adjust the model to capture this behaviour.

Bridges with more than three spans was not included in this thesis. Of course for bridges with multiple spans it is important to model a sufficient number of spans in order to capture the resonant behaviour, as stated by Eurocode. Figure 4.12 seems to indicate that for bridges with multiple spans there is convergence at around 5 spans with an error less than 1%. During bridge design this convergence should be verified since this might not hold true for all bridges.

6.3 Method choice

The main objective of this thesis is to evaluate the simplified comfort criteria method in Eurocode using a dynamic model. There are multiple approaches to solve this task. The method applied in this thesis is designing sections based on the simplified approach for a certain bridge and maximum speed, taking the designed section, performing dynamic bridge-vehicle analysis and then comparing the vehicle acceleration results. If the results are less or equal to 1 m/s^2 then the method is on the safe side, otherwise it is on the unsafe side. This method is efficient since it does not require any iteration of the FE-model. The results are clear, either the model is safe or it is unsafe. However it does not say how the bridge should be designed to actually get a maximum vehicle acceleration of 1 m/s^2 .

Another approach would be to iterate the dynamic vehicle-bridge FE-model until the maximum vehicle acceleration of 1 m/s^2 is achieved. When this section is found, it could be compared to the simplified approach and show how the real deflection limits should be set in Figure 2.8. Since the FE-analysis is the main time constraint in the work-flow, this method would be much slower to use. However if the focus were to find new simplified design curves for a specific train, this approach would be optimal. An algorithm for this alternative approach is proposed in Figure 6.1.

Alternative Abaqus Algorithm
Optimization of the simplified method

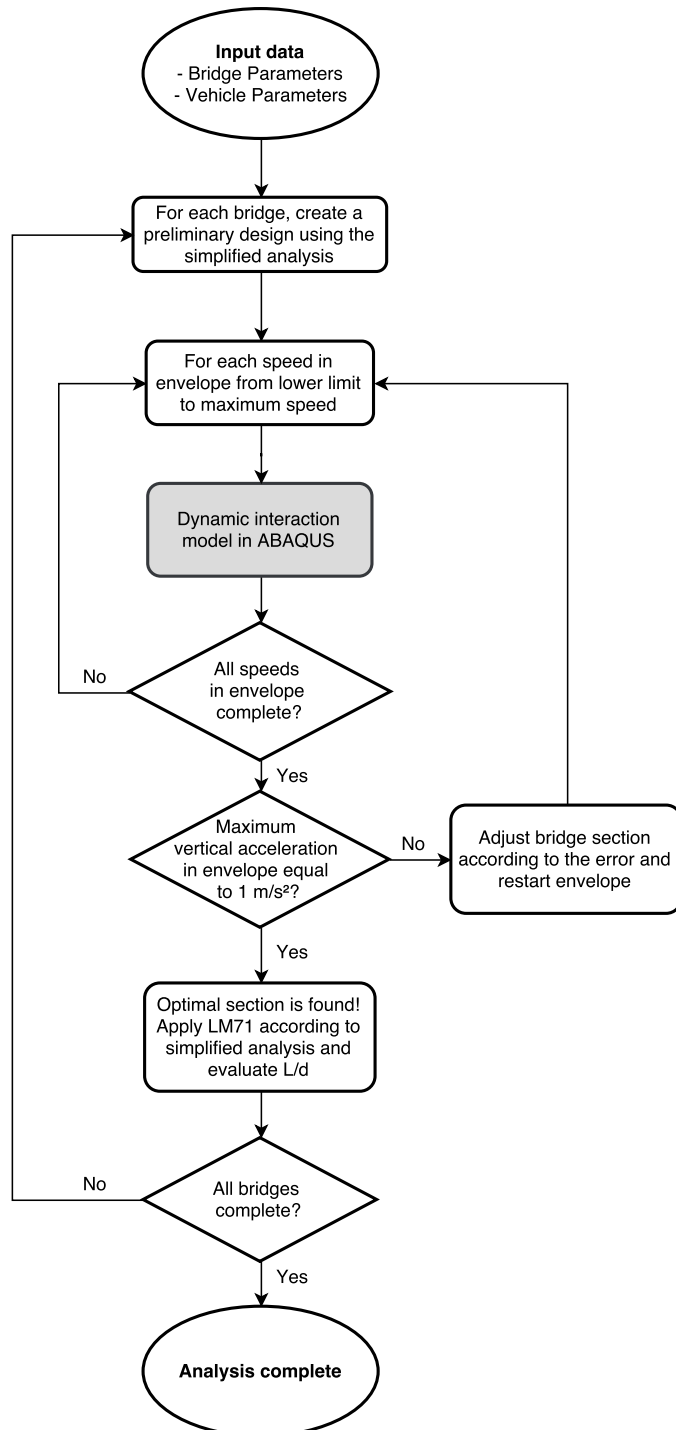


Figure 6.1: Alternative ABAQUS/Explicit algorithm for optimization of simplified comfort analysis.

6.3.1 Preliminary study

Before attempting to solve the main objective of the thesis, a secondary objective was formed. It was to study and understand the influence of certain modelling choices for increasingly more complex vehicle and bridge models. This step was performed in order to achieve an accurate and realistic final model. An alternative approach would be to disregard any preliminary studies and directly construct the final evaluation model from a set of assumptions regarding the model behaviour. In the case of this thesis there were uncertainties regarding the influence of these parameters, therefore the preliminary study was performed.

The preliminary study functioned as a basis for validation as higher level of complexities was added. However ideally the preliminary study should have been expanded to include multiple vehicles to better resemble the final model. The effect of some parameters that was evaluated might be much larger in a vehicle assembly that could cause resonance in the bridge model. The choice to model simple single vehicles in the preliminary study was made in order to compare ABAQUS results with the analytic point load solution. The main reason that final modeling was performed in ABAQUS was due the flexibility in the model assembly and contact formulation as opposed to the MATLAB model. If the final model was build directly without any preliminary evaluations it would have been very difficult to verify the validity.

It is important to take into account that the preliminary study was only performed for a simply supported single span bridge with fixed sectional parameters. Furthermore only single point vehicles was evaluated as opposed to multiple point vehicles. Ideally additional complexities would be evaluated however that was not possible within the time frame of the thesis. The main application of this comparison was therefore validation of the modelling complexities when moving the analysis model from MATLAB to ABAQUS.

6.3.2 Search method

In the first phase of the final study envelopes were chosen with an increment in span length of 5 m for all configurations evaluated. When results where gathered and resonant regions were discovered, a more detailed study was performed in these areas. Additional envelopes were introduced and the data density was refined over resonant peaks. This method allowed for a high degree of flexibility and was critical with regards to computational limitations, as is expanded upon in Section 6.5.4.

6.3.3 Section design method

All bridge sections has been designed using the simplified vehicle comfort acceleration limit specified in Section 2.3.2. No further design has been performed neither has the bridges been designed for ULS. This simplification hold under the assumption that the sections remain uncracked and that the entire concrete section contributes to the stiffness of the structure. In a real design however it is critical that a complete design is performed for all bridges.

6.4 Input parameters

This section will discuss the accuracy and impact of the input data chosen in this thesis. Ideally multiple sets of parameters should be evaluated to find accurate and critical data. This comparison lied beyond the scope, however models were created so that input-data easily could be swapped if other trains and track were to be evaluated.

6.4.1 Train parameters

Train parameters were based on data presented by Lei (2017). Even though the book is very recent, there are some uncertainties regarding this data. Firstly it does not explicitly state which train model the parameters are from. Therefore it is difficult to determine a realistic motorcar and passenger trailer configuration. This thesis assumes that an ICE 2 train is used which consists of two motorcars and 14 passenger trailers. However to be on the safe side, trains with additional passenger trailers were also evaluated in Section 4.2.

6.5 Modelling choices

The decision was made to model the system in 2D. This was an efficient approach since behaviour could be verified using analytic models. Apart from being much more computationally costly, a 3D model could introduce unexpected behaviour which could be difficult to verify and evaluate. By modelling in 2D certain effects are neglected such as plate-eigenmodes. However these are not as prominent in concrete slab bridges which is the main focus of this thesis, compared to other types such as girder or box sections. Furthermore the effect of lateral instability is not accounted for, see Section 6.5.3.

6.5.1 Analysis method

A finite element formulation was used in both preliminary and the final evaluation model. This approach was flexible and allowed for easy troubleshooting during development. The models are also very efficient visualization tools for presentation and explanation in the thesis. Another approach to solve for a dynamic bridge-vehicle interaction system would be to apply an analytic solution using a Fourier transformation approach as presented by Lei (2017). This method would be very difficult for a complex model as the one studied in this thesis. Furthermore, it would also be difficult to troubleshoot and fix unexpected behaviour in such a model.

6.5.2 Number of cars

Convergence study presented in Section 4.2 indicated that it was critical to model the whole train including two motorcars and 14 passenger trailers, especially we evaluating the response at resonant peaks. Ideally it would be more efficient to model fewer vehicles with regards to computational time and the fact that convergence was reached much earlier for non-resonant peaks, however the error on resonant peaks was too large.

6.5.3 Vehicle lateral instability

As a train travels along the railway, it may experience what is known as Hunting oscillation. This phenomenon causes bogies to oscillate sideways whilst twisting slightly along their vertical axes as explained by Möller (2017). This behaviour stems from the conical shape of the wheel tread, which increases in diameter closer to the wheel flange. As speeds get higher, these effects tend to get more prominent and a critical speed may be defined over which a risk for derailment is considerable. In order to prevent these effects, modern trains have introduced stabilizing struts connecting bogies to the car. A negative consequence of this system is that it effectively shortcuts the secondary suspension system of the train to some extent in that it provides an alternative, more direct path for the vibrations to propagate. Since modelling is only taking place in 2D-space this effect has been neglected. In order to visualize this effect a more complex model is required which lies beyond the scope of this thesis.

6.5.4 Computational limitations

As the model is presented in Chapter 4, a single analysis would take about 5 minutes for trains with high speeds traversing short bridges. However for low speeds and long bridges analysis could take up to 30 minutes. These limitations affect how many cases that can be studied. Ideally we would study all speeds and spans in the specified range with a very small increment. This was not possible within the time-frame specified for this thesis, therefore a decision was made to study speeds with the increment 5 km/h and span lengths with increment 5 m. In regions where resonant behaviour was captured the speed and span increments were refined. Multiple measures were implemented in order to reduce the time required. Firstly multithreading capabilities in ABAQUS were utilized which allowed the model to run faster. This feature was also required to avoid internal ABAQUS-errors that would occur randomly when only a single thread was used. The second improvement was to run multiple instances of ABAQUS on the available octacore-CPU workstations. With these improvements it only took about two weeks to run all analyses.

The ideal solution would be to use all cores on one single instance instead of using multiple instances. This approach would be easier to manage and more efficient. When this was attempted however, ABAQUS failed with obscure errors which could not be handled. The use of Chalmers cluster was examined but was not applicable for this case since a large number of smaller jobs had to be performed. The cluster is mainly to be used for heavy projects where single jobs are much more demanding. An alternative approach would be to implement a custom clustering solution which would dynamically run all configurations. This would be a good idea if many more bridges were to be evaluated but it was beyond the scope of this thesis. Due to these computational limitations it would be sub-optimal to model this system using any element except 2D-beam elements.

7 Conclusions

The simplified vehicle comfort analysis presented in Eurocode could yield bridges that have a vehicle response above the allowed limit for the ICE 2 train evaluated. An improved version of the simplified analysis should be investigated in order to find accurate correlation with modern high-speed trains. Ideally, a connection should be drawn to the dynamic HSLM models as these might prove a better indicator of vehicle comfort than a static load model such as LM71.

The mass and stiffness properties of the vehicles greatly influence the amplitude of the response. That is apparent when evaluating the results from the motorcar as opposed to the trailers. The motorcars have a consistently higher response for all configurations analyzed. However, the location of resonant peaks is dependent on the trailer length and the fundamental frequencies of the bridge. This is because the length between trailers corresponds to the main forcing frequency of the system and will be critical when evaluating the resonant response.

Critical vehicle response was found for bridges where the resonant speed were close to the design speed in the envelope. This is especially true in the region where the ratio L_{car} / L_{span} is close to 1. It seems like when there are trains moving at high speed and a lot of the energy can be transferred into a specific eigenmode of the bridge, a critical response is reached.

The fundamental eigenmode was critical for simply supported bridges and the second eigenmode was critical for the continuous double span bridge. For the simply supported bridges other eigenmodes corresponded to resonant velocities well above the maximum speed of 350 km/h, therefore there was no excitation of these modes.

8 Further studies

It would be of interest to compare the results of this thesis to an identical train using a point load model or HSLM. This could be performed in BRIGADE, however it was found from preliminary testing that dynamic track components could not be incorporated in such a model. Instead the influence of rail and sleepers would only be as a non-structural mass component. Perhaps a custom model could be created to model a more complex track behaviour. A comparison of these results could help the development of a more refined vehicle comfort approximation. It would make more sense to use a high-speed load-model such as HSLM to model this behaviour instead of the static load-model, LM71.

This thesis only includes reinforced concrete slab bridges in its scope, however there are many other types of bridges that could be evaluated. Box-sections and girder bridges are some examples, for these however it could be important to model in 3D in order to capture plate-buckling modes which are much more prominent for these structures. In addition to this it would be interesting to evaluate bridges with non-uniform span configurations. This comparison was not performed in this thesis in order to reduce the amount of free variables in the project. However in real life, these structures occur frequently.

Other trains could easily be evaluated using the same method as presented in this thesis by replacing existing input-data with new data. It would be interesting to evaluate the performance of newer models of ICE-trains as well as the french Train à Grande Vitesse (TGV) since these are likely to be used in the East Link project. Finding accurate and up-to-date data on these trains would be the main challenge of such a project. In addition to traditional railway it would also be interesting to evaluate the vehicle response of magnetic levitation trains traversing bridges. This analysis would require another bridge-vehicle interaction model since the train layout and behaviour is quite different to the vehicle in this thesis.

Bridges analyzed in this thesis are assumed to remain uncracked which means that the stiffness of the section can be approximated without reinforcement. Ideally all bridges analyzed would be designed with account to reinforcement and tensile concrete limits should be verified.

References

- Abaqus, i. (2005). Overview of abaqus/explicit. Retrieved March 2, 2017, from <http://imechanica.org/files/0-overview%5C%20Explicit.pdf>. (Cited on pages 27, 32)
- Arvidsson, T. (2014). *Train–bridge interaction: Literature review and parameter screening* (Doctoral dissertation, KTH Royal Institute of Technology). (Cited on pages 13, 36).
- ASCE 7-05. (2005). *Asce chapter 12 - seismic design requirements for building structures*. American Society of Civil Engineers. (Cited on page 26).
- Bogacz, R. & Kowalska, Z. (2001). Computer simulation of the interaction between a wheel and a corrugated rail. *European Journal of Mechanics - A/Solids*, 20. (Cited on page 34).
- CALFEM. (2004). Calfem: A finite element toolbox, version 3.4. Retrieved March 2, 2017, from http://www.solid.lth.se/fileadmin/hallfasthetslara/utbildning/kurser/FHL064_FEM/calfem34.pdf. (Cited on pages 28, 30, 46)
- CEN. (2006). *SS-EN-1990 A2: Basis of structural design - Annex A2*. EUROPEAN COMMITTEE FOR STANDARDIZATION. (Cited on pages 12, 13).
- CEN. (2010a). *SS-EN-1990: Basis of structural design*. EUROPEAN COMMITTEE FOR STANDARDIZATION. (Cited on page 1).
- CEN. (2010b). *SS-EN-1991-2: Actions on structures – Part 2: Traffic loads on bridges*. EUROPEAN COMMITTEE FOR STANDARDIZATION. (Cited on pages 11, 13).
- Chatterjee, A. (1997). *Rigid body collisions: Some general considerations, new collision laws, and some experimental data* (Doctoral dissertation, Cornell University). (Cited on page 33).
- Craig Jr., R. R. & Kurdila, A. J. (2006). *Fundamentals of structural dynamics*. John Wiley & Sons, New York. (Cited on pages 14, 18, 24, 26, 31).
- DASSAULT SYSTEMS. (2017). Abaqus unified fea: Complete solutions for realistic simulation. Retrieved March 3, 2017, from <https://www.3ds.com/products-services/simulia/products/abaqus/abaqusexplicit/>. (Cited on pages 4, 30)
- Diehl, T., Carroll, D., & Nagaraj, B. (1999). *Using digital signal processing (dsp) to significantly improve the interpretation of abaqus/explicit results*. ABAQUS Users' Conference. (Cited on page 32).
- Esveld, C. (2001). *Modern railway track - second edition*. MRT-Productions. (Cited on page 33).
- Eurail. (2017). Ice high-speed train. Retrieved February 3, 2016, from <http://www.eurail.com/europe-by-train/high-speed-trains/ice>. (Cited on page 5)
- Grassie, S. L. (2012). Rail irregularities, corrugation and acoustic roughness: Characteristics, significance and effects of reprofiling. *Proc IMechE Part F: J Rail and Rapid Transit*, 226, 542–557. (Cited on page 34).
- Hertz, H. (1881). Über die berührung fest elastischer körper. *Journal für die reine und angewandte Mathematik*, 92, 156–171. (Cited on pages xiv, 33).
- Hjelm, M. & Karlsson, N. (2016). *Dynamic response of railway bridges subjected to high speed trains* (Master's thesis, Chalmers University of Technology, Division of Structural Engineering). (Cited on pages 1, 9, 84).
- Lei, X. (2017). *High speed railway track dynamics. Models, Algorithms and Applications*. Science Press, Beijing / Springer Nature Singapore Pte. Ltd. (Cited on pages 5–8, 46, 87).
- Lundh, H. (2007). *Grundläggande hållfasthetslära*. Instant Book AB. (Cited on page 9).

- Mackertich, S. (1990). Moving load on a timoshenko beam. *Journal of the Acoustical Society of America*, 88. (Cited on page 24).
- Mao, L. & Lu, Y. (2013). Critical speed and resonance criteria of railway bridge response to moving trains. *Journal of Bridge Engineering*, 18(2), 131–141. (Cited on pages 25, 83).
- MATLAB. (2016a). Design of experiments (doe). Retrieved February 3, 2016, from <http://se.mathworks.com/help/stats/design-of-experiments-1.html?refresh=true>. (Cited on page 4)
- MATLAB. (2016b). Signal processing toolbox. Retrieved March 2, 2017, from https://se.mathworks.com/help/pdf_doc/signal/signal_gs.pdf. (Cited on page 32)
- MATLAB. (2017). Mathworks: Matlab. Retrieved March 2, 2017, from <https://se.mathworks.com/>. (Cited on pages 30, 46)
- Möller, P. (2017, May 2). personal communication. (Cited on page 88).
- Nielsen, J., Ekberg, A., & Lundén, R. (2005). Influence of short-pitch wheel/rail corrugation on rolling contact fatigue of railway wheels. *Proc. IMechE Part F: J. Rail and Rapid Transit*, 219, 177–187. (Cited on pages 5, 34).
- Nielsen, J. & Igeland, A. (1995). Vertical dynamic interaction between train and track influence of wheel and track imperfections. *Journal of Sound and Vibration*, 187, 825–839. (Cited on pages 8, 34, 35, 47).
- Nielsen, J., Pieringer, A., & Kropp, W. (2014). The influence of contact modelling on simulated wheel/rail interaction due to wheel flats. *Wear (0043-1648)*, 314, 273–281. (Cited on page 33).
- Nyquist, H. (1928). Certain topics in telegraph transmission theory. *PROCEEDINGS OF THE IEEE*, 90, 280–305. (Cited on page 32).
- Ottosen, N. S. & Petersson, H. (1992). *Introduction to the finite element method*. Prentice Hall. (Cited on pages 28, 46).
- Qin, Q. & Lou, L. (2000). *Effects of non proportional damping on the seismic responses of suspension bridges*. Dept. of Civil Engineering, Tsinghua University, Haidian, Beijing, China. (Cited on page 26).
- Scanscot. (2017). Brigade/plus: Complete tool-box for analysis and design of bridges and civil structures. Retrieved March 3, 2017, from <https://scanscot.com/products/bridge-design/brigade-plus/>. (Cited on page 30)
- Siemens. (2017). High speed trainset ice 2, germany. Retrieved May 12, 2017, from <https://www.mobility.siemens.com/apps/references/index.cfm?z=1&do=app.detail&referenceID=383&IID=1>. (Cited on page 5)
- Talukdar, S. (2016). *Vibration of continuous systems*, Indian Institute of Technology Guwahati. Department of Civil Engineering. (Cited on pages 22, 93).
- Timoshenko, S. (1922). On the transverse vibrations of bars of uniform cross-section. *Philosophical Magazine, Series 6*. (Cited on page 24).
- Trafikverket. (2011). *Trvk bro 11*. TRV publ. 2011:085. TRAFIKVERKET. (Cited on page 11).
- Wanming Zhai, K. W. C. C. (2009). Fundamentals of vehicle-track coupled dynamics. *Vehicle System Dynamics*, 47:11, 1349–1376. (Cited on page 6).
- Wu, Y., Yau, J., & Yang, Y. (2004). *Vehicle-bridge interaction dynamics*. With Application to High-speed Railways. World Scientific Publishing Company. (Cited on page 23).
- Zhou, Y. (2011). A theoretical model of collision between soft-spheres with hertz elastic loading and nonlinear plastic unloading. *Theoretical and Applied Mechanics Letters*, 1. (Cited on page 33).

A Mode Shapes for Continuous Beams

The shape functions for a continuous bridge with multiple spans of equal length have been established by Talukdar (2016) and are presented in full in Eqs. (A.1) - (A.5). The mode shape functions ϕ_{nr} correspond to a certain mode number, n and span number, r .

$$\phi_{nr}(x) = \begin{cases} \sin(\beta_{nr}x_r) - \frac{\sin(\beta_{nr}l)}{\sinh(\beta_{nr}l)} \sinh(\beta_{nr}x_r) & r = 1 \\ P_r M_r(x_r) + Q_r N_r(x_r) & r = 2, 3, \dots, N \end{cases} \quad (\text{A.1})$$

$$P_r = \frac{[\cosh(\beta_{nr}l) - \cos(\beta_{nr}l)][\sinh(\beta_{nr}l) \sin(\beta_{nr}l)] - \sin(\beta_{nr}l)[\sinh(\beta_{nr}l) \cos(\beta_{nr}l) - \sin(\beta_{nr}l) \cosh(\beta_{nr}l)]}{\sinh(\beta_{nr}l) ([\cos(\beta_{nr}l) - \cosh(\beta_{nr}l)][\sinh(\beta_{nr}l) - \sin(\beta_{nr}l)])} \quad (\text{A.2})$$

$$Q_r = \frac{[\cosh(\beta_{nr}l) - \cos(\beta_{nr}l)][\sinh(\beta_{nr}l) \sin(\beta_{nr}l)] + \sin(\beta_{nr}l)[\sinh(\beta_{nr}l) \cos(\beta_{nr}l) - \sin(\beta_{nr}l) \cosh(\beta_{nr}l)]}{\sinh(\beta_{nr}l) ([\cos(\beta_{nr}l) - \cosh(\beta_{nr}l)][\sinh(\beta_{nr}l) - \sin(\beta_{nr}l)])} \quad (\text{A.3})$$

$$M_r(x_r) = [\cos(\beta_{nr}l) - \cosh(\beta_{nr}l)] \sinh(\beta_{nr}x) + \sinh(\beta_{nr}l)[\cosh(\beta_{nr}x) - \cos(\beta_{nr}x)] \quad (\text{A.4})$$

$$N_r(x_r) = [\cos(\beta_{nr}l) - \cosh(\beta_{nr}l)] \sin(\beta_{nr}x) + \sin(\beta_{nr}l)[\cosh(\beta_{nr}x) - \cos(\beta_{nr}x)] \quad (\text{A.5})$$

where:

r	is number of spans [-].
β_{nr}	is the frequency parameter for mode number r [-].
l	is the span length r [m] .
x_r	is the length coordinate in span r [m] .

The frequency parameter β_{nr} for bridges with up to three spans is presented in table A.1.

Table A.1: Frequency parameter β_{nr} for different span and mode numbers.

Number of spans, r	$n = 1$	$n = 2$	$n = 3$	$n = 4$	$n = 5$
1	π	2π	3π	4π	5π
2	3.1416	3.9272	6.2832	7.0686	9.4248
3	3.1416	3.5500	4.3040	6.2832	6.6920